Algorithmic studies of compact lattice QED with Wilson fermions

D I S S E R T A T I O N

zur Erlangung des akademischen Grades
doctor rerum naturalium
(Dr. rer. nat.)
im Fach Physik

eingereicht an der
Mathematisch-Naturwissenschaftlichen Fakultät I
Humboldt-Universität zu Berlin

von
Herr Dipl.-Phys. Nikolai Zverev
geboren am 14.12.1971 in Moskau, UdSSR

Präsident der Humboldt-Universität zu Berlin:
Prof. Dr. J. Mlynek

Dekan der Mathematisch-Naturwissenschaftlichen Fakultät I:
Prof. Dr. B. Ronacher

Gutachter:

1. Prof. Dr. M. Müller-Preussker
2. Prof. Dr. I. Montvay
3. Prof. Dr. U. Wolff

eingereicht am: 27. September 2001
Tag der mündlichen Prüfung: 18. Dezember 2001

Abstract

We investigate numerically and in part analytically the compact lattice quantum electrodynamics with Wilson fermions. We studied the following particular tasks of the theory: the problem of the zero-momentum gauge field modes in the Coulomb phase and the performance of different Monte Carlo algorithms in the presence of dynamical fermions.

We show that the influence of the zero-momentum modes on the gauge dependent lattice observables like photon and fermion correlators within the Coulomb phase leads to a behaviour of these observables different from standard perturbation theory. These modes are responsible also for the screening of the critical behaviour of the gauge invariant fermion values near the chiral limit line. Within the Coulomb phase the elimination of these zero-momentum modes from gauge configurations leads to the perturbatively expected behaviour of gauge dependent observables. The critical properties of gauge invariant fermion observables upon removing the zero-momentum modes are restored. The critical hopping-parameter obtained from the invariant fermion observables coincides with that extracted from gauge dependent values.

We implement the two-step multiboson algorithm for numerical investigations in the U(1) lattice model with even dynamical Wilson fermion flavours. We discuss the scheme of an appropriate choice of technical parameters for both two-step multiboson and hybrid Monte Carlo algorithms. We give the theoretical estimates of the performance of such simulation methods. We show both numerically and theoretically that the two-step multiboson algorithm is a good alternative and at least competitive with the hybrid Monte Carlo method. We argue that an improvement of efficiency of the two-step multiboson algorithm can be achieved by increasing the number of local update sweeps and also by decreasing the orders of first and second polynomials corrected for by the reweighting step.

Keywords:

Compact lattice QED, Wilson fermions, zero-momentum modes, Monte Carlo simulation, dynamical fermions

Zusammenfassung

Wir untersuchen numerisch und teilweise analytisch die kompakte Quantenelektrodynamik auf dem Gitter mit Wilson-Fermionen. Dabei konzentrieren wir uns auf zwei wesentliche Teilprobleme der Theorie: der Einfluß von Eichfeld-Moden mit verschwindendem Impuls in der Coulomb-Phase und die Effizienz von verschiedenen Monte-Carlo-Algorithmen unter Berücksichtigung dynamischer Fermionen.

Wir zeigen, daß der Einfluß der Null-Impuls-Moden auf die eichabhängigen Gitter-Observablen wie Photon- und Fermion-Korrelatoren nahe der kritischen chiralen Grenzlinie innerhalb der Coulomb Phase zu einem Verhalten führt, das vom naiv erwarteten gitter-störungstheoretischen Verhalten abweicht. Diese Moden sind auch für die Abschirmung des kritischen Verhaltens der eichinvarianten Fermion-Observablen nahe der chiralen Grenzlinie verantwortlich. Eine Entfernung dieser Null-Impuls-Moden aus den Eichfeld-Konfigurationen führt innerhalb der Coulomb-Phase zum störungstheoretisch erwarteten Verhalten der eichabhängigen Observablen. Die kritischen Eigenschaften der eichinvarianten Fermion-Observablen in der Coulomb-Phase werden nach dem Beseitigen der Null-Impuls-Moden sichtbar. Der kritische Hopping-Parameter, den man aus den invarianten Fermion-Observablen erhält, stimmt gut mit demjenigen überein, der aus den eichabhängigen Observablen extrahiert werden kann.

Wir führen den zweistufigen Multiboson-Algorithmus für numerische Untersuchungen im U(1)-Gittermodell mit einer geraden Anzahl von dynamischen Fermion-Flavour-Freiheitsgraden ein. Wir diskutieren die geeignete Wahl der technischen Parameter sowohl für den zweistufigen Multiboson-Algorithmus als auch für den hybriden Monte-Carlo-Algorithmus. Wir geben theoretische Abschätzungen für die Effizienz dieser Simulationsmethoden. Wir zeigen numerisch und theoretisch, daß der zweistufige Multiboson-Algorithmus eine gute Alternative darstellt und zumindestens mit der hybriden Monte-Carlo-Methode konkurrieren kann. Wir argumentieren, daß eine weitere Verbesserung der Effizienz des zweistufigen Multiboson-Algorithmus durch eine Vergrößerung der Zahl lokaler Update-Schleifen und auch durch die Reduktion der Ordnungen der ersten und zweiten Polynome zu Lasten des sogenannten 'Reweighting' erzielt werden kann.

Schlagwörter:
Kompakte Gitter–QED, Wilson–Fermionen, Moden verschwindenden Impulses, Monte-Carlo-Simulation, dynamische Fermionen

Contents

Chapter 1

Introduction

Quantum electrodynamics (QED) is the theory of electromagnetic interactions between electrically charged particles like electrons or muons. In principle, QED explains their behaviour with high accuracy in the framework of renormalizable continuum perturbation theory [1] – [3]. This is due to the small coupling constant of electromagnetic interactions at low energies. Hence, the nonperturbative lattice study of QED is motivated neither by so far unexplained phenomena nor by an absence of a computational method. One is studying lattice QED for reasons which can be briefly formulated as follows: the problem of mathematical consistency of the quantum electrodynamics [4, 5] and various physical and technical questions in models of a Grand Unification which can be studied by an appropriate reduction to the simple (compact) Abelian theory represented by lattice QED [6, 7].

An apparent mathematical inconsistency in QED contrary to quantum chromodynamics (QCD) is the existence of the so-called energetical 'Landau pole' in the perturbative behaviour of the renormalized coupling constant [4, 5]. Such a problem is absent only if the electrical charge asymptotically vanishes (trivial electrodynamics). The spurious pole might not appear if QED has an ultraviolet stable fixed point for the running coupling which lies outside the perturbative region. That is why the lattice regularization [8] – [10] of QED could be the best way to study the 'Landau pole' problem. The problem of the existence of a possible ultraviolet stable fixed point in QED was intensively studied both by the continuum mean field method [11] and in the framework of noncompact lattice QED with staggered fermions describing $N_f = 4$ flavours [12] – [16]. A detailed inspection of the renormalized coupling constant within this lattice approach provided a strong indication for the absence of the 'Landau pole' in QED: a singular

behaviour can never be reached and noncompact QED with staggered fermions seems to have a trivial continuum limit when approaching the end point of the chiral phase transition line [16].

But there are problems left. First of all, a lattice discretization scheme requires a careful study of the continuum limit (see [15]). Second, the absence of the 'Landau pole' should be independent of the number of fermion flavours. And finally, the noncompact lattice formulation is a matter of discussions from both mathematical and physical points of view. On the one hand, its action requires gauge fixing and the results should be independent of various fixing procedures [14]. On the other hand, the noncompact theory can not explain the discrete electrical charge values and can not be embedded into a lattice discretized non-Abelian gauge theory which requires a compactification of the gauge potential [8] (see also [6, 7]).

The latter problems do not occur in compact lattice QED. This way to discretize quantum electrodynamics leads to the occurence of several phases separated by phase transition lines at strong coupling [17, 18]. In particular, there is a phase compatible with the continuum QED – the Coulomb phase. The topical task to understand the 'Landau pole' phenomenon within the framework of compact lattice QED requires a thorough investigation of the phase structure of the theory and of the possible existence of (tri-) critical points to which one can approach from the Coulomb phase. A corresponding ultra-violet fixed point - if it exists here - should be determined by studying the flow of lines of constant physics obtained from non-perturbatively renormalized lattice observables. Such an investigation can be carried out by various methods, e.g. within the framework of the Schrödinger functional approach [19, 20]. In any case one has to achieve agreement of both lattice perturbation theory and numerical simulation results obtained for a finite lattice volume with those of continuum perturbation theory. The comparison requires an appropriate selection or tuning of physical and technical parameters on the lattice and of boundary conditions for the boson and fermion fields (see [20]). Compact lattice QED from this point of view remained purely understood over the years.

Let us come to a second point of the lattice QED destination – studies for QCD as well as for the electro-weak theory. Compact lattice QED is the simplest (Abelian) gauge theory i.e. the prototype for all compact gauge theories on the lattice. Theoretical as well as numerical questions and methods can be nicely tested first in the U(1) gauge theory. From the theoretical point of view, there

are two problems which require the use of the compact Abelian theory: the quark confinement phenomenon and the chiral symmetry breaking effect.

The lattice gauge theory appears to be the easiest way to display the quark confinement, when the static quark potential infinitely grows with increasing distance between quarks [8, 9]. Confinement can be reproduced by every standard compact lattice formulation including the U(1) lattice model. Theoretical arguments [6, 7] and numerical studies [17, 18] of pure U(1) lattice gauge theory have shown that confinement is caused mainly by the influence of the monopole-antimonopole pairs. It is worthwhile to note that the lattice approach in QED gives a mathematically rigorous way of describing topologically nontrivial gauge configurations such as magnetic monopoles [6, 7, 17]. Moreover, it was indicated both theoretically [21] – [24] and numerically [25] – [27] that the confinement phenomenon in QCD can be understood in terms of Abelian degrees of freedom of the SU(3) gauge theory. Next, the confinement mechanism has a deep connection to the chiral symmetry breaking effect [28]. And again, analytical [29, 30] and numerical [31, 32] studies of the latter effect detected the existence of a parity-flavour breaking (or Aoki) phase with a similar behaviour of pseudofermion composite particles in both non-Abelian [30, 31] and U(1) [32] gauge groups. These results mean that in order to study the quark confinement as well as the chiral symmetry violation effects, one should first turn to the investigation of corresponding phenomena in an Abelian model. Here, the U(1) theory can be viewed as an Abelian projection of a more general gauge theory [21] – [23].

Another aspect is the algorithmic problem in investigations of different lattice fermion models of QCD. It is well-known [9, 10] that the inclusion of the fermion loops (dynamical fermions) is much more complicated than simulations in the case of pure gauge theory. However, as it was shown in [33], the critical behaviour of lattice observables in lattice QCD with dynamical fermions resembles to the dynamical fermion U(1) case at strong coupling. This would mean that since numerical investigations of Abelian models are much easier and faster than for other more complicate gauge groups, studies of the U(1) model with dynamical fermions might give useful results applicable to more general theories.

The main purpose of this thesis are some numerical and also analytical investigations of the lattice compact 4-dimensional (4d) QED theory with Wilson fermions required as an intermediate step to future lattice QED investigations. In chapter 2 we give an introduction to the lattice QED, describe the approximation

methods used for investigation of lattice models and present the phase structure of the U(1) gauge theory. In chapter 3 we discuss the problem of gauge fixing for a lattice study of gauge dependent observables. In chapter 4 we investigate the particular problem of the physical Coulomb phase in compact lattice QED – the influence of constant or zero-momentum gauge modes on gauge dependent and gauge invariant fermion observables. Chapter 5 is devoted to a detailed study of various simulation algorithms in the U(1) lattice model, mainly the dynamical fermion ones. Finally in chapter 6 we present an itemized conclusion of our investigation and give an outlook to the further study of lattice QED.

It will be shown that the disagreement of gauge dependent photon and fermion zero-momentum correlators within the physical weakly interacting Coulomb phase in comparison with standard lattice perturbation theory is caused by constant (or zero-momentum) modes which are the gauge copies of the Lorentz gauge fixing prescription in the pure gauge theory. Secondly, these constant modes hide also the critical behaviour of the gauge invariant fermion observables in the vicinity of the chiral limit. We discuss various methods of eliminating the zero-momentum modes. Our numerical studies of the Coulomb phase show that as soon as one removes these constant modes from gauge configurations, the correct behaviour of both gauge dependent and gauge invariant lattice correlation functions is restored [34, 35].

We have adapted the two-step multiboson algorithm (TSMB) [36] – [38] to numerical investigations in the U(1) lattice model with even number of dynamical fermion flavours. For this purpose, the simulation methods for the pure gauge theory and for the evaluation of lattice fermion observables were carefully studied. In order to investigate the performance of the TSMB in comparison with the well-known hybrid Monte Carlo (HMC) method [39, 40] in the framework of the U(1) lattice model, we give the prescription of an appropriate choice of technical parameters for these dynamical fermion algorithms. Theoretical estimates of the performance of these simulation methods are presented. Our numerical results as well as theoretical arguments show that the TSMB algorithm is at least competitive with the HMC one [41]. We also propose ways to improve the performance of the TSMB algorithm.

Finally, we discuss proposals for further studies of compact lattice QED with odd number of fermion flavours.

Chapter 2

Formulation of lattice QED

2.1 Continuum theory

The QED action in the continuum Euclidean theory [1] – [3]:

$$S_{\rm QED} = S_G + S_F, \tag{2.1}$$

consists of the pure gauge action S_G and the fermion one S_F:

$$S_G = \frac{1}{4e_0^2}\int {\rm d}^4x \sum_{\substack{\mu,\nu \\ \mu<\nu}} F_{x,\mu\nu}^2, \tag{2.2}$$

$$S_F = \int {\rm d}^4x \left\{ \frac{1}{2}\sum_{\mu} \left(\overline{\psi}_x \gamma_\mu \mathcal{D}_\mu \psi_x - \overline{\mathcal{D}_\mu \psi}_x \gamma_\mu \psi_x \right) + m_0 \overline{\psi}_x \psi_x \right\}. \tag{2.3}$$

Here the $F_{x,\mu\nu} = \partial A_{x,\nu}/\partial x_\mu - \partial A_{x,\mu}/\partial x_\nu$ is the Abelian gauge field strength tensor, the $A_{x,\mu}$ is the gauge potential, $\mathcal{D}_\mu = \partial/\partial x_\mu + {\rm i}A_{x,\mu}$ denotes the gauge covariant derivative. The e_0 and m_0 stand for the bare electric charge (or coupling constant) and bare fermion mass, respectively. The ψ, $\overline{\psi}$ are anticommuting (Grassmann) variables and γ_μ are the 4×4 Dirac matrices satisfying to the algebra:

$$\begin{aligned} \gamma_\mu\gamma_\nu + \gamma_\nu\gamma_\mu = 2\delta_{\mu\nu}\cdot\mathbf{1}, \qquad & \gamma_5 = \gamma_1\gamma_2\gamma_3\gamma_4, \\ \gamma_5\gamma_\mu + \gamma_\mu\gamma_5 = \mathbf{0}, \qquad & \mu,\nu = 1,\ldots,4. \end{aligned}$$

The action (2.1) is invariant under local Abelian gauge transformations:

$$\begin{aligned} \psi_x \longrightarrow \psi_x^g = g_x\psi_x, \qquad & \overline{\psi}_x \longrightarrow \overline{\psi}_x^g = \overline{\psi}_x g_x^\dagger, \\ A_{x,\mu} \longrightarrow A_{x,\mu}^g = A_{x,\mu} - \partial\alpha_x/\partial x_\mu, \qquad & g_x = {\rm e}^{{\rm i}\alpha_x}, \end{aligned} \tag{2.4}$$

and for $m_0 = 0$ under global chiral rotations:

$$\psi_x \longrightarrow \mathrm{e}^{\mathrm{i}\gamma_5\lambda}\psi_x, \qquad \overline{\psi}_x \longrightarrow \overline{\psi}_x \mathrm{e}^{\mathrm{i}\gamma_5\lambda}. \tag{2.5}$$

Quantization with path integral of the theory described by the action (2.1) requires gauge fixing and a regularization with subsequent renormalization [2, 3]. The quantum corrections violate the classical chiral invariance (2.5) and lead to the Abelian chiral anomaly [42, 43]. In order to study the mathematically correct theory, one has to introduce a suitable regularization. Such a regularization widely used for the numerical nonperturbative investigations is just the *lattice theory* [9, 10]. Below we describe its basic principles.

2.2 Lattice theory

2.2.1 Discretization steps

To go from the continuum theory to the discrete lattice version, it is necessary to perform the following steps. First of all, the continuum 4-dimensional coordinates x are replaced with discrete points called lattice sites:

$$x = a(n_1, n_2, n_3, n_4), \qquad n_\mu = 0, \pm 1, \pm 2, \ldots,$$

where a is a discrete 4-dimensional space-time size called lattice spacing. Then the integration over 4-dimensional space is replaced with the sum over all lattice points:

$$\int \mathrm{d}^4 x \longrightarrow a^4 \sum_x = a^4 \sum_{n_1,\ldots,n_4} .$$

The Fourier transformation on the lattice looks like:

$$\tilde{f}_p = \sum_x \mathrm{e}^{\mathrm{i}px} f_x, \qquad f_x = \int\limits_{-\pi/a}^{\pi/a} \frac{\mathrm{d}^4 p}{(2\pi)^4} \mathrm{e}^{-\mathrm{i}px} \tilde{f}_p$$

Note that the lattice discretization introduces the ultraviolet cut-off: $|p_\mu| \leq \pi/a$.

In many practical cases such as numerical simulations, the number of lattice points x must be finite. In other words, one has to consider a finite lattice:

$$n_\mu = -N_\mu/2 + 1, \ldots, N_\mu/2, \qquad N_\mu \text{ is even},$$

and therefore to replace the integration measure and momentum in the infinite Fourier transformation as follows:

$$\int\limits_{-\pi/a}^{\pi/a} \frac{\mathrm{d}^4 p}{(2\pi)^4} \longrightarrow \frac{1}{a^4 V} \sum_l, \qquad p_\mu = \frac{2\pi}{a N_\mu} l_\mu, \qquad l_\mu = -N_\mu/2 + 1, \ldots, N_\mu/2,$$

where $V = N_1 \ldots N_4$ is the dimensionless lattice volume. Therefore, the finite lattice determines the infrared cut-off: $|p_\mu| \geq 2\pi/aN_\mu$ if $p_\mu \neq 0$.

To remove these cut-offs, one takes first the *thermodynamic limit* when the lattice volume $V \to \infty$ at fixed spacing a, then the *continuum limit* when $a \to 0$ at infinite volume V. Of course, the lattice discretization breaks the continuum relativistic invariance. But such invariance is expected to be restored in the continuum limit.

Further, the continuum derivative $\partial/\partial x_\mu$ has be replaced with the discrete forward ∂_μ and backward $\overline{\partial}_\mu$ derivatives:

$$\partial_\mu f_x = \frac{f_{x+a\hat{\mu}} - f_x}{a}, \qquad \overline{\partial}_\mu f_x = \frac{f_x - f_{x-a\hat{\mu}}}{a}, \qquad \hat{\mu} = (0, \ldots, \underset{\mu}{1}, \ldots, 0). \tag{2.6}$$

Then in order to preserve the local gauge invariance (2.4) on the lattice, it is necessary to work with the compact lattice gauge (or link) variable [8]:

$$U_{x,\mu} = \mathrm{e}^{\mathrm{i}aA_{x,\mu}}, \tag{2.7}$$

which transforms under gauge rotations according to the following rule:

$$U_{x,\mu} \longrightarrow U^g_{x,\mu} = g_x U_{x,\mu} g^\dagger_{x+a\hat{\mu}}, \qquad g_x \in \mathrm{U}(1). \tag{2.8}$$

From this we can construct lattice forward ∇_μ and backward $\overline{\nabla}_\mu$ covariant derivatives as:

$$\nabla_\mu f_x = \frac{1}{a}\left\{U_{x,\mu} f_{x+a\hat{\mu}} - f_x\right\}, \qquad \overline{\nabla}_\mu f_x = \frac{1}{a}\left\{f_x - U^\dagger_{x-a\hat{\mu},\mu} f_{x-a\hat{\mu}}\right\}. \tag{2.9}$$

Note that the backward derivatives are Hermitean conjugated of the forward derivatives with respect to the lattice space. In order to work with the lattice derivatives on the finite lattice, one has to introduce boundary conditions (b.c.) which are taken usually in the following way:

$$f_{x+aN_\mu\hat{\mu}} = \pm f_x,$$

where the $+$ or $-$ sign denotes periodic or antiperiodic boundary conditions, respectively. For gauge or boson fields as well as gauge transformations g, one uses

periodic b.c. In principle, it is possible to apply these conditions to fermion fields. However, in order to avoid spurious infrared divergences in the fermion propagator which happen e.g. at the study of chiral fermion models, one usually takes for Fermi-fields antiperiodic boundary conditions.

It is possible to consider the straightforwardly discretized lattice version of the gauge action (2.2), where $A_{x,\mu}$ takes values in the $(-\infty, \infty)$ interval. Such a theory is called *noncompact* lattice QED and has been already used for study of the 'Landau pole' problem [12] – [16]. However, it is worthwhile to investigate also the *compact* lattice QED model [8]. The latter requires to use the compact link variables (2.7) where $A_{x,\mu} \in (-\pi, \pi]$, and the U(1) compactified gauge field strength tensor is called plaquette variable:

$$U_{x,\mu\nu} = U_{x,\mu} U_{x+a\hat{\mu},\nu} U^{\dagger}_{x+a\hat{\nu},\mu} U^{\dagger}_{x,\nu}, \tag{2.10}$$

which is invariant under gauge transformations (2.8). Then the compact, or plaquette, version of gauge action S_G can be written as follows:

$$S_G[U] = \beta \sum_{\substack{x,\mu,\nu \\ \mu<\nu}} (1 - \mathrm{Re}\, U_{x,\mu\nu}), \tag{2.11}$$

where $\beta = 1/e_0^2$ is the inverse squared bare coupling parameter.

The plaquette variable (2.10) in case of U(1) group is invariant also under the constant transformations:

$$U_{x,\mu} \longrightarrow U^c_{x,\mu} = c_\mu U_{x,\mu}, \qquad c_\mu \in \mathrm{U}(1). \tag{2.12}$$

Let us now discuss the difference between the infinite and finite lattice cases. For the infinite lattice, the constant transformations are a special case of the usual (2.8) ones:

$$g_x = \prod_\mu c_\mu^{\dagger\, x_\mu/a}, \qquad c_\mu \in \mathrm{U}(1). \tag{2.13}$$

But in case of finite lattice volume, the transformations (2.12) can not be reduced to (2.8) because of the impossibility to fulfill the periodic b.c. for gauge transformation g except for discrete values:

$$c_\mu = \mathrm{e}^{2\pi \mathrm{i} k_\mu / N_\mu}, \qquad k_\mu = 0, \pm 1, \pm 2, \ldots, \qquad \mu = 1, \ldots, 4.$$

The constant transformations (2.12) or (2.13) which can not be represented by ordinary gauge rotations (2.8) will be called *nonperiodic* gauge transformations but the usual (2.8) ones are named *periodic* transformations.

In the classical theory in the continuum limit $a \to 0$, the plaquette action (2.11) as well as the lattice discretized fermion action (2.3) coincide with their continuum origins. But in the case of quantum theory, one is interested first in the particle spectrum described by the given model. So, the photon propagator in the compact gauge theory (2.11) (in diagonal gauge):

$$\langle A_\mu A_\nu \rangle_p = \frac{\delta_{\mu\nu}}{\sum_\lambda (2/a)^2 \sin^2 (p_\lambda a/2)} \longrightarrow \frac{\delta_{\mu\nu}}{p^2}, \qquad a \to 0,$$

correctly reproduces the photon spectrum. But the fermion propagator of the naively discretized fermion action (2.3):

$$\left\langle \psi\overline{\psi} \right\rangle_p = \frac{-\mathrm{i} \sum_\mu \gamma_\mu \sin(p_\mu a)/a + m_0}{\sum_\mu \sin^2(p_\mu a)/a^2 + m_0^2} \longrightarrow \sum_{s=0,1} \frac{-\mathrm{i} \sum_\mu (-1)^{s_\mu} (p_\mu - \pi s_\mu/a) \gamma_\mu + m_0}{(p - \pi s/a)^2 + m_0^2},$$

in the limit $a \to 0$ describes $2^4 = 16$ fermion states instead of one in the continuum. This effect is called spectrum degeneracy and the nonphysical fermion states are called doublers.

The above result is explained by the 'no-go' theorem [44, 45] which states that if a fermion action is Hermitean, local (its momentum operator in the Fourier space is continuous) and invariant under discrete translations and global chiral rotations (2.5), it inevitably describes the chirally positive and the same number of chirally negative fermion states.

2.2.2 Wilson fermions

To cure the problem of fermion spectrum degeneracy, one can either remove the doublers or exploit them in an appropriate way. The former method, proposed by Wilson [8], requires the addition of the following mass-like term:

$$S_W = a^4 \sum_{x,\mu} \frac{ar}{2} \overline{\nabla}_\mu \overline{\psi}_x \nabla_\mu \psi_x, \qquad r > 0, \tag{2.14}$$

to the straightforwardly discretized, or naive, fermion action (2.3). Such a term vanishes in the classical theory in the continuum limit. But in the quantum case, the perturbative fermion propagator

$$\left\langle \psi\overline{\psi} \right\rangle_p = \frac{-\mathrm{i} \sum_\mu \gamma_\mu \sin(p_\mu a)/a + (2r/a) \sum_\mu \sin^2 (p_\mu a/2) + m_0}{\sum_\mu \sin^2(p_\mu a)/a^2 + \left[(2r/a) \sum_\mu \sin^2 (p_\mu a/2) + m_0 \right]^2} \longrightarrow \frac{-\mathrm{i} \not{p} + m_0}{p^2 + m_0^2}$$

correctly describes the fermion spectrum since all doublers acquire masses of order $O(a^{-1})$ and therefore do not propagate. At the same time, the Wilson term (2.14) breaks the global chiral symmetry (2.5). Perturbative investigations of the lattice Wilson fermion model have shown [46] that in the continuum limit the well-known expression for the chiral abelian anomaly [42, 43] is reproduced.

The total lattice Wilson fermion action can be rewritten as follows:

$$S_{WF}[U,\overline{\psi},\psi] = a^4 \sum_{x,y} \overline{\psi}_x \mathcal{M}[U]_{xy} \psi_y, \tag{2.15}$$

where $\mathcal{M}$ is Wilson fermion matrix:

$$\mathcal{M}[U]_{xy} = \left(\frac{4r}{a} + m_0\right)\delta_{xy} - \frac{1}{2a}\sum_{\mu}\left\{(r-\gamma_\mu)U_{x,\mu}\delta_{x+a\hat{\mu},y} + \right. \\ \left. +(r+\gamma_\mu)U^{\dagger}_{y,\mu}\delta_{y+a\hat{\mu},x}\right\}. \tag{2.16}$$

Introducing the so-called hopping-parameter κ:

$$\kappa = \frac{1}{2(4r + am_0)}, \tag{2.17}$$

and rescaling the fermion fields by the coefficient $\sqrt{2\kappa/a^3}$, one rewrites the Wilson fermion matrix $\mathcal{M}$ in the following way:

$$\mathcal{M}[U]_{xy} = \delta_{xy} - \kappa\sum_{\mu}\left\{(r-\gamma_\mu)U_{x,\mu}\delta_{x+a\hat{\mu},y} + \right. \\ \left. +(r+\gamma_\mu)U^{\dagger}_{y,\mu}\delta_{y+a\hat{\mu},x}\right\}. \tag{2.18}$$

The fermion matrix (2.16) or (2.18) is covariant under the gauge transformations (2.8):

$$\mathcal{M}[U^g]_{xy} = g_x \mathcal{M}[U]_{xy} g^{\dagger}_y, \tag{2.19}$$

and is γ_5-Hermitean:

$$\mathcal{M}^{\dagger} = \gamma_5 \mathcal{M} \gamma_5, \tag{2.20}$$

where the complex conjugation is taken with respect to all coordinate and spinor indices. The parameter r is expected to be irrelevant at the renormalization or finite tuning of lattice observables. Hence and also for convenience (see [9]), we will take it equal to $r = 1$.

Another method to handle the fermion spectrum degeneracy was proposed by Kogut and Susskind [47]. In this method, the fermion doublers are transformed to the $2^{4/2} = 4$ fermion flavours by means of the spin diagonalization of the naive

lattice fermion action (2.3) and retaining only one spinor component in the transformed action. Such a theory, called *staggered fermions*, is invariant under global chiral rotations (2.5) but the flavour symmetry is broken. In the framework of the staggered fermion model the 'Landau pole' problem was investigated [12] – [16]. However the staggered fermions describe 4 mass degenerate flavours. In order to study the case of a small number of fermion flavours, one takes a fermion model like the Wilson one (2.15).

At the same time, the Wilson fermion method requires more additional fine tuning of lattice observables in the continuum limit than for staggered fermions since the Wilson mass term (2.14) brings the lattice corrections of order $\mathrm{O}(a)$ to the continuum fermion action (2.3) whereas in case of the staggered fermions, such corrections have order $\mathrm{O}(a^2)$. To get the lattice computed observables closer to the continuum ones, the Wilson fermion action requires $\mathrm{O}(a)$ improvement. At the present moment, there are many improved actions based on the original Wilson (2.15) one. Let us mention the model with perturbatively improving *clover term* [48, 49], the nonperturbatively improved *overlap fermions* [50] – [52] and the exact *Ginsparg-Wilson fermions* [53] – [55], and also the *approximate Ginsparg-Wilson fermions* [56] – [58] generalizing the perturbative clover improvement. In this thesis we will not touch the problem of the Wilson action improvement since it complicates the numerical lattice simulations. We note only that the influence of the Wilson term is reflected in the phase structure of the compact Wilson lattice QED.

2.3 Gauge invariant observables on the lattice

The standard action of compact lattice QED [8] consists of pure compact gauge action (2.11) and Wilson fermion one (2.15):

$$S_{\mathrm{QED}}[U,\overline{\psi},\psi] = S_G[U] + S_{WF}[U,\overline{\psi},\psi] \tag{2.21}$$

Then the average value of a lattice observable can be computed according to the equation:

$$\langle\mathcal{O}\rangle = \frac{1}{Z}\int[\mathrm{d}U][\mathrm{d}\bar{\psi}\mathrm{d}\psi]\mathcal{O}[U,\overline{\psi},\psi]\exp(-S_{\mathrm{QED}}[U,\overline{\psi},\psi]), \tag{2.22}$$

where the normalization constant

$$Z = \int[\mathrm{d}U][\mathrm{d}\overline{\psi}\mathrm{d}\psi]\exp(-S_{\mathrm{QED}}[U,\overline{\psi},\psi]) \tag{2.23}$$

also depends on the bare lattice parameters β, κ. The integration with respect to the gauge field is taken over a compact space. And therefore, in contrast to continuum and lattice noncompact theory cases, one is not forced to fix a gauge in compact lattice models.

For practical evaluation of fermion observables, it is convenient to perform the following trick. Let us add to the action (2.21) the auxiliary fermion source term:

$$S_{\overline{\eta}\eta} = -\sum_x \left(\overline{\psi}_x \eta_x + \overline{\eta}_x \psi_x\right),$$

where $\overline{\eta}$, η are external anticommuting variables. Then substituting it to the equation (2.22) and integrating out the $\overline{\psi}$, ψ variables in case of N_f fermion flavours, the equation for average observables can be represented as follows:

$$\langle \mathcal{O} \rangle = \frac{1}{Z} \int [\mathrm{d}U] \mathcal{O}\left[U, \frac{\overleftarrow{\partial}}{\partial \eta}, \frac{\partial}{\partial \overline{\eta}}\right] \exp\left(-S_G[U] + \overline{\eta} \mathcal{M}^{-1}[U] \eta\right)\Big|_{\overline{\eta},\ \eta=0} \det{}^{N_f} \mathcal{M}[U], \tag{2.24}$$

where $\frac{\overleftarrow{\partial}}{\partial \eta}$ denotes the left acting derivative with respect to η. Note that the fermion determinant $\det \mathcal{M}$ is gauge invariant and real as it follows from the properties (2.19) and (2.20), respectively.

The equation (2.24) is the standard quantization formula for the investigation of the gauge invariant observables $\mathcal{O}$:

$$\mathcal{O}[U^g, \overline{\psi}^g, \psi^g] = \mathcal{O}[U, \overline{\psi}, \psi]. \tag{2.25}$$

Without loss of generality we will restrict ourselves to invariant observables (2.25) which depend only on the gauge field U: $\mathcal{O} = \mathcal{O}[U]$. The reason is that the average values of fermion observables are expressed in terms of elements of the inverse fermion matrix $\mathcal{M}^{-1}[U]$ as it follows from equation (2.24).

Let us present some gauge invariant observables which are very important in the investigation of lattice theory. In this thesis, we will study the mean gauge energy $\langle E_G \rangle$ [9], the scalar condensate $\langle \overline{\psi}\psi \rangle$ and the pion norm $\langle \Pi \rangle$ [18]:

$$\langle E_G \rangle = \langle \frac{1}{6V} \sum_{\substack{x,\mu,\nu \\ \mu<\nu}} (1 - \operatorname{Re} U_{x,\mu\nu}) \rangle, \tag{2.26}$$

$$\langle \overline{\psi}\psi \rangle = \langle \frac{1}{4V} \sum_x \overline{\psi}_x \psi_x \rangle = \langle \frac{1}{4V} \operatorname{Tr} \mathcal{M}^{-1} \rangle, \tag{2.27}$$

$$\langle \Pi \rangle = \langle \frac{1}{4V} \sum_x (\overline{\psi}_x \gamma_5 \psi_x)^2 \rangle = \langle \frac{1}{4V} \operatorname{Tr} \gamma_5 \mathcal{M}^{-1} \gamma_5 \mathcal{M}^{-1} \rangle. \tag{2.28}$$

where the trace is taken over coordinate and spinor indices. Note also that the fermion observables are independent of the choice of boundary conditions for Fermi-fields as it follows from invariance of the integral (2.22) under nonperiodic gauge transformations (2.12). The mean gauge energy (2.26) is proportional to the $\partial \ln Z/\partial\beta$, where Z is defined according to equation (2.23). The scalar condensate (2.27) and the pion norm (2.28) are represented via sums of inverse eigenvalues of the $\mathcal{M}$ and $\mathcal{M}^\dagger\mathcal{M}$ operators, respectively. And therefore, these fermion values (especially pion norm) can serve for an identification of the critical zero eigenvalue behaviour of the Wilson fermion matrix (2.18).

Hence, the gauge invariant observables (2.26) – (2.28) are widely used for studying of the phase structure of lattice fermion models (see [18]).

2.4 Quenched and dynamical fermion approximations

In both analytical and numerical studies of a lattice theory, the investigation of the fermion determinant $\det \mathcal{M}$ is very difficult. Traditional methods of computing the determinant directly fail to extract numerical as well as physical information about the contribution of fermion loops to the theory.

Nevertheless, one can enormously simplify the consideration of lattice models by taking into account the smallness of the hopping-parameter κ. From its definition (2.17) it follows that κ satisfies the inequality $\kappa < 1$ for $r = 1$ or more concretely, κ is of order $1/8$. This in case of large fermion mass allows us to perform an expansion in powers of κ of the Wilson fermion matrix (2.18) in the fermion determinant. In the leading order:

$$\det \mathcal{M} = \text{const.}$$

One retains often only this order of the determinant in the integral (2.24) [59] – [61]. But higher orders can be considered as corrections to the average observable value.

This approximation known as *quenched* approximation, corresponds to:

$$N_f = 0. \tag{2.29}$$

In other words, one neglects the contribution of the fermion loops to the weight

function. One then simply averages lattice observables with the weight factor $\exp(-S_G[U])$ which facilitates numerical as well as analytical lattice investigations.

However, the approximation (2.29) and the hopping-parameter expansion are not valid in case of very large condition number ζ:

$$\ln \zeta \gg 1, \qquad \zeta = \frac{\lambda_{\max}}{\lambda_{\min}}, \tag{2.30}$$

where $\lambda_{\max}$ and $\lambda_{\min}$ are the maximal and minimal eigenvalues of the $\mathcal{M}^\dagger\mathcal{M}$ matrix, respectively. Then one has to take into account the whole determinant in (2.24). This case, when one does not neglect the influence of the fermion loops, is called the *dynamical fermion* case [10].

The evaluation of the fermion determinant requires much more computer resources than a numerical simulation of a pure gauge theory described by action $S_G[U]$ (2.11). Another difficulty is the sign problem of the fermion determinant which may lead to a pathological result for physical observables. However, if the number of fermion flavours

$$N_f = \text{even}, \tag{2.31}$$

the simulations of the determinant can be facilitated due to its parametrization by an auxiliary complex spinor field [60]. The calculation of lattice observables then does not need the knowledge of the sign of the determinant.

We consider in this thesis compact lattice QED in both the quenched approximation (2.29) and in the dynamical (2.31) $N_f = 2$ case. But we will discuss also the problem of the odd fermion flavour investigation.

2.5 The phase structure of compact lattice QED

Let us remember that the lattice gauge theory is only a *regularization* for the investigation of the continuum field theory. The results obtained by means of lattice caluclations, make physical sense only in the continuum limit $a \to 0$. At the same time, the continuum renormalized parameters such as masses or running couplings, must take finite values. Hence in order to go to the continuum limit, one has to require that the couplings β and κ depend on the lattice spacing a (see [9, 10]).

It is necessary to know which lines in the (β, κ) plane correspond to constant physics in the limit $a \to 0$. One of such lines is obtained by means of the study of

lattice renormalized masses. They can be extracted from corresponding correlators in the following way [62]:

$$\Gamma_\Phi(\tau) = \sum_{\vec{x}} \langle \Phi_0 \Phi_x \rangle \propto \exp(-m_\Phi \tau), \qquad x = (\vec{x}, \tau), \qquad a \to 0. \tag{2.32}$$

For example, the operator for the extraction of the pseudoscalar 'pion' mass m_π is $\Phi_x^{(\pi)} = \overline{\psi}_x \gamma_5 \psi_x$.

Keeping with $\tau = a n_4$ the integer value n_4 in the (2.32) finite, one can formulate the condition for the bare lattice parameters in the continuum limit:

$$a m_{\rm phys} \to 0, \qquad a \to 0. \tag{2.33}$$

where $m_{\rm phys} = m_{\rm phys}(\beta, \kappa)$ are masses of physical particles or energies of their ground states extracted according to (2.32).

Equation (2.33) determines the critical line $\kappa = \kappa_c(\beta)$ where the fermion particles in a units have zero masses [63] – [65]. It means that along this line known as the chiral limit line, the chiral symmetry broken by the Wilson mass term (2.14) is partially restored. On the other hand, since the powers of the $1/a m_{\rm phys}$ contribute to fermion observables like (2.27) or (2.28) and the masses $m_{\rm phys}$ are finite, the chiral limit line in the language of the thermodynamics must be a line of at least second order phase transition. Instead of the bare fermion mass m_0, one can define the naive lattice fermion mass m_q [63] as

$$a m_q = \frac{1}{2} \left(\frac{1}{\kappa} - \frac{1}{\kappa_c(\beta)} \right). \tag{2.34}$$

Studies of the 4-dimensional U(1) model with Wilson fermions have shown (see e.g. [6, 7], [17, 18], [63] – [70]) that such a theory has a nontrivial phase structure (Figure 2.1). It consists of at least 4 phases in the (β, κ) plane separated by different order phase transition lines. But there is a difference between the quenched approximation and $N_f = 2$ dynamical fermions. While in the quenched case the critical line separating Coulomb and confinement phase has the same β value equal to 1.01(1) (Figure 2.1a), in the dynamical case it coincides partially with the chiral limit line (Figure 2.1b) [70]. This line $\kappa = \kappa_c(\beta)$ connects the points $\kappa_c(0) = 1/4$ and $\kappa_c(\infty) = 1/8$ at the Wilson coefficient $r = 1$ [63]. The deviation of $\kappa_c(\beta)$ from the exact perturbative value 1/8 can be explained as an influence of the chirally noninvariant Wilson mass-like term (2.14).

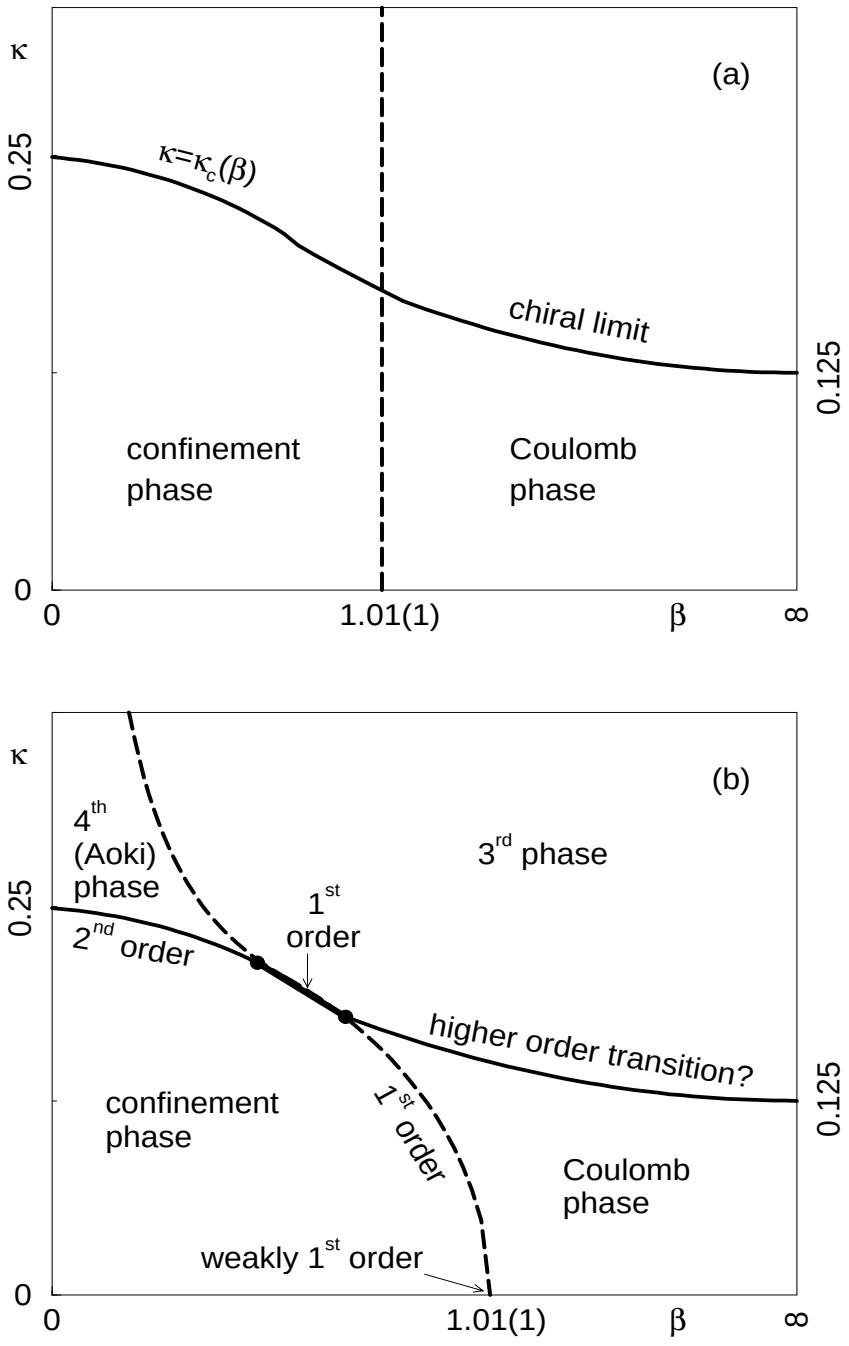

Figure 2.1: Phase structure of compact lattice QED in the quenched approximation (a) and with $N_f = 2$ dynamical fermions [70] (b).

We are interested mostly in the Coulomb phase because it describes the usual static Coulomb potential and the vanishing photon mass. It is characterized by the suppression of magnetic monopoles [17]. However, it is worth to discuss also the confinement phase having many similarities with QCD one. In this phase in quenched approximation, the static potential for charged particles is directly proportional to the distance between them [8], the corresponding gauge bosons acquire a non-zero mass and one detects a condensation of monopole-antimonopole pairs [17].

These phases are separated by the line of the first order phase transition [17], [71] – [73] (see Figure 2.1). It means that one has to search for the continuum limit points $(\beta^\star, \kappa^\star)$ outside this line. According to the above presented arguments, these points should lie on the curve $\kappa = \kappa_c(\beta)$ in the Coulomb phase. The precise numerical value for the $\beta^\star$ point is unknown so far in spite of numerous efforts in this direction (see e.g. [74] – [76]). We will not touch this problem but note that it requires a very careful study of the renormalized masses and coupling constant [13] – [16].

At the same time, the investigation [77] of the confinement phase near the chiral limit and also the 4th (Aoki) phase [29] (see Figure 2.1b) is complicated because the well-known method for such purposes, the hybrid Monte Carlo algorithm [39, 40], does not work well in the case of large condition numbers ζ (2.30) (see also [33, 78]). To decrease this number, in case of $N_f = 2$ one can introduce the following twisted mass term [30, 31]:

$$h\overline{\psi}\gamma_5 \otimes \tau_3\psi, \tag{2.35}$$

and then at the evaluation of desired observables take the limit $h \to 0$. The investigation of the Aoki phase led to the conclusion that there the composite pseudoscalar fermion masses are equal to 0 and the combined parity-flavour symmetry is broken [29] – [32]. But in order to better understand the properties of this phase, one should use an alternative to the hybrid Monte Carlo algorithm. And moreover, presently the studies of the lattice compact QED were done in the framework of the quenched approximation or for even dynamical fermion flavours [77]. It would be interesting to investigate also the dynamical models with odd fermion flavours. The problems of such investigation will be discussed later together with the consideration of the dynamical fermion algorithms.

In the following let us use the convention $a = 1$ for the lattice spacing. If it

is necessary, dimensions can be easily re-inserted. The lattice size will be $V = N_s^3 \times N_4$, with $N_4 \geq N_s$ in order to compute masses from correlators as (2.32).

Chapter 3

Gauge fixing on the lattice

3.1 Motivation

As it was already mentioned, studying the gauge invariant observables on the lattice in the framework of compact gauge models [8] does not require a gauge fixing (see [9]). Nevertheless, applying the Faddeev-Popov trick [79] to the integral (2.24) by inserting the unity:

$$1 = \Delta_{\mathrm{FP}}[U] \int [\mathrm{d}g] \delta \left(F[U^g] \right),$$

where $\Delta_{\mathrm{FP}}[U]$ is the so-called Faddeev-Popov determinant, and by integrating out the gauge transformation field g, we get the following expression for the averaged gauge invariant operator $\mathcal{O}$ (2.25):

$$\langle \mathcal{O} \rangle = \frac{1}{Z} \int [\mathrm{d}U] \Delta_{\mathrm{FP}}[U] \delta \left(F[U] \right) \mathcal{O}[U] \mathrm{e}^{-S_G[U]} \det{}^{N_f} \mathcal{M}[U], \tag{3.1}$$

similar to the continuum field theory case.

However, in the case of perturbative study of a lattice model [46], one has to introduce a gauge fixing term just as in the continuum theory. Moreover, the evaluation of such gauge invariant objects as Wilson loops is very simple e.g. in 2-dimensional gauge models when an additional gauge fixing method is employed [9].

We note that usual gauge invariant values describe either composite particles or bounded states of quantum fields e.g. mesons or glueballs [10]. At the same time, studies of gauge dependent observables like photon or fermion propagator can give us more detailed and natural information about quantum objects such as

behaviour of renormalized Green functions [14]. But the straightforward averaging of gauge dependent operators over gauge field without any gauge fixing term leads, according to group symmetry properties, to zero. For instance, in the case of fermion propagator one has:

$$\langle \psi_x \overline{\psi}_y \rangle = \frac{1}{Z} \int [\mathrm{d}U] \left(\mathcal{M}^{-1}[U] \right)_{xy} \mathrm{e}^{-S_G[U]} \det{}^{N_f} \mathcal{M}[U] = \delta_{xy} \langle \psi \overline{\psi} \rangle,$$

as it follows from the covariance property (2.19) of the Wilson matrix, and where the translational invariance of the theory has been used. Hence, to consider on the lattice the gauge dependent objects, one has to use a gauge fixing procedure. And the expression (3.1) can serve as a definition for the average value of a gauge dependent observable.

In our case, studying the 'Landau pole' problem in the compact lattice QED requires an investigation of the renormalized coupling constant and fermion mass [15, 16]. They can be extracted in the best way from the gauge dependent photon (link) and fermion correlators by the method analogous to (2.32) (see [13, 14]). That is why we are interested in the study of gauge dependent objects in the U(1) theory on the lattice.

3.2 Methods of gauge fixing

One of the very popular methods of gauge fixing in quantum theory is the Lorentz (or Landau) gauge fixing condition. For the U(1) gauge theory it looks as follows [80, 81]:

$$F_x[U] = \sum_\mu \overline{\partial}_\mu A_{x,\mu} = 0 \mod 2\pi, \qquad \forall x, \tag{3.2}$$

where the backward derivative $\overline{\partial}_\mu$ is defined according to (2.6). However for practical reasons, it is convenient to consider the *nonlinear* lattice version of the Lorentz gauge fixing [82, 83]:

$$F_x[U] = \sum_\mu \overline{\partial}_\mu \operatorname{Im} U_{x,\mu} = 0, \qquad \forall x, \tag{3.3}$$

which can be reached in numerical calculations demanding the maximization of the following functional $G_{\max}[U]$ with respect to all periodic gauge transformations (2.8):

$$G_{\max}[U] = \frac{1}{4V} \sum_{x,\mu} \operatorname{Re} U_{x,\mu}, \qquad G_{\max}[U^g] \xrightarrow{g} \max. \tag{3.4}$$

The maximization of this functional can be realized as follows. One performs successive for every lattice point x, or cyclic, rotations (2.8) of the gauge links U according to the rule:

$$\begin{aligned} U_{x,\mu} \to g_x U_{x,\mu}, \qquad U_{x-\hat{\mu},\mu} \to U_{x-\hat{\mu},\mu} g_x^\dagger, \qquad \forall \mu = 1, \ldots, 4, \\ g_x = (K_x/|K_x|)^{-\omega}, \qquad K_x = \sum_\mu \left\{ U_{x,\mu} + U_{x-\hat{\mu},\mu}^\dagger \right\}, \qquad \forall x, \end{aligned} \tag{3.5}$$

where the remaining components of the transformation g are put equal to 1 and all other links are kept fixed. Here ω is the overrelaxation parameter. In case of $\omega = 1$, the transformations (3.5) maximize the functional (3.4) step by step, whereas if the $\omega = 2$, the $G_{\max}$ is kept unchanged. But for the best convergence of the (3.5) prescription, the parameter ω should be taken somewhere in the $1 < \omega < 2$ interval (see [84]), e.g. we choose $\omega = 1.7$. These updates are continued until both the mean and the local maximal absolute values of the l.h.s. in equation (3.3) become less than some small given numbers ε_1 and ε_2, respectively:

$$\frac{1}{V} \sum_x |F_x[U]| < \varepsilon_1, \qquad \max_x |F_x[U]| < \varepsilon_2.$$

For instance, in our case $\varepsilon_1 = 10^{-6}$ and $\varepsilon_2 = 10^{-5}$.

Now let us describe another method of gauge fixing on the lattice which is very popular in the study of confinement phenomena – Laplacian gauge fixing [85]. In this method in the case of the U(1) gauge group, the gauge field U is fixed in such a way that each component of the eigenvector $\phi^{(\min)}$ corresponding to the smallest eigenvalue $\lambda_{\min}$ of the covariant Laplacian $\Delta[U]$,

$$\Delta[U]\phi^{(\min)} = \lambda_{\min}\phi^{(\min)}, \qquad \Delta[U] = \sum_\mu \overline{\nabla}_\mu[U]\nabla_\mu[U], \tag{3.6}$$

is real and non-negative:

$$\phi_x^{(\min)} \geq 0, \qquad \forall x. \tag{3.7}$$

Here the covariant derivatives ∇_μ and $\overline{\nabla}_\mu$ are defined according to (2.9). Due to the covariance property of the Laplacian $\Delta[U]$:

$$\Delta[U^g] = g\Delta[U]g^\dagger,$$

to reach the condition (3.7), one searches first for a eigenvector $\phi^{(\min)}$ satisfying to the equation (3.6) and then performs the periodic gauge transformation (2.8)

with the function g equal to:

$$g_x = {\phi_x^{(\min)}}^\dagger / \|\phi^{(\min)}\|, \quad \forall x; \qquad \|\phi^{(\min)}\| = \left(\sum_x |\phi_x^{(\min)}|^2 \right)^{1/2}.$$

In this thesis, we will not study the Laplacian gauge fixing procedure (3.6), (3.7). We only note that the evaluation of the smallest eigenvalue and corresponding eigenvector of the covariant Laplacian $\Delta[U]$ can be done, for instance, by various versions of the Lanczos or conjugate gradient methods (see chapter 5).

3.3 The problem of the gauge fixing ambiguites

It is well known that a gauge fixing procedure can lead to the occurence of gauge fixing ambiguities called as Gribov copies [86]. For QED this happens even in the continuum, as long as the theory is defined with toroidal boundary conditions [87]. The problem of Gribov copies is related to topology and can be explained as follows. If the smooth gauge fixing functional $F_g = F[U^g]$ on a compact space takes a zero value, it should pierce the zero line at least twice [87]. Otherwise the Faddeev-Popov determinant $\Delta_{\rm FP}[U]$ will be degenerated.

At the same time, contrary to the gauge invariant objects, the average values of gauge dependent operators depend on the gauge fixing condition $F[U] = 0$. Hence one has to find a gauge fixing procedure which allows us to get configurations providing the best agreement of the gauge dependent observables computed according to (3.1) with the lattice perturbative ones.

The standard iterative way to fix the Lorentz gauge for compact U(1) lattice gauge theory has been shown to lead to serious Gribov copy effects [81, 83, 88, 89]. As a consequence, the transverse non-zero momentum photon correlator does not reproduce the perturbatively expected zero-mass behaviour. For the fermion correlator, a strong dependence on the achieved gauge copies has been also reported [81]. The standard fermion mass determination becomes badly defined. Careful numerical [83], [89] – [91] and analytical [92, 93] studies have shown that the main gauge field excitations, responsible for the occurence of disturbing gauge copies, are *double Dirac sheets* (DDS) and *zero-momentum modes* (ZMM).

DDS are identified as follows. Let us write the following decomposition for the plaquette angle i.e. the gauge field strength tensor in case of U(1) lattice theory

[6, 7, 17]:

$$\partial_\mu A_{x,\nu} - \partial_\nu A_{x,\mu} = \overline{F}_{x,\mu\nu} + 2\pi n_{x,\mu\nu}. \tag{3.8}$$

Here ∂_μ, ∂_ν are the forward lattice derivatives defined in (2.6). The gauge potential $A_{x,\mu} \in (-\pi, \pi]$ determines the compact gauge field (2.7). The value $\overline{F}_{x,\mu\nu} \in (-\pi, \pi]$ due to the definition of the compact plaquette (2.10) can be interpreted as physical gauge invariant electromagnetic flux. The discrete gauge dependent term $2\pi n_{x,\mu\nu}$, $n_{x,\mu\nu} = 0, \pm 1, \pm 2$ represents a Dirac string passing through the given plaquette in case of $n_{x,\mu\nu} \neq 0$ (the Dirac plaquette). A set of Dirac plaquettes providing a world sheet of a Dirac string on the space orthogonal to this plaquette is called Dirac sheet. Double Dirac sheets consist of two sheets with opposite flux orientation which cover the whole lattice and are closed by periodic boundary conditions. Thus, they can easily be identified by counting for every plane (μ, ν) the total number of Dirac plaquettes

$$N_{DP}^{(\mu\nu)} = \sum_x |n_{x,\mu\nu}|. \tag{3.9}$$

The necessary condition for the appearance of a DDS is that at least for one of the six planes (μ, ν) holds the following inequality:

$$N_{DP}^{(\mu\nu)} \geq 2\frac{V}{N_\mu N_\nu}. \tag{3.10}$$

Let us present an analytic expression for a DDS [92]:

$$A_{x,\mu} = \tilde{A}_{x,\mu}(\mathbf{R}^{(a)}) - \tilde{A}_{x,\mu}(\mathbf{R}^{(b)}),$$

where

$$\tilde{A}_{x,\mu}(\mathbf{R}) = \sum_{\nu=1}^{2} \epsilon_{\mu\nu} \overline{\partial}_\nu f_x(\mathbf{R}), \qquad f_x(\mathbf{R}) = \frac{2\pi}{N_1 N_2} \sum_{k,\ |k|\neq 0} \frac{e^{2\pi \mathrm{i} k(x-\mathbf{R})/N}}{K^2(k)},$$

$$k = (k_1, k_2), \quad x = (x_1, x_2), \quad \mathbf{R} = (R_1, R_2), \quad K^2(k) = \sum_{\mu=1}^{2} 4\sin^2(\pi k_\mu / N_\mu).$$

It can be transformed to the trivial potential $A_{x,\mu} = 0$ by periodic gauge rotations (2.8). It satisfies to the linear Lorentz fixing condition (3.2) and

$$\sum_{\mu,\nu=1}^{2} \epsilon_{\mu\nu} \partial_\nu A_{x,\mu} = 2\pi(\delta_{x,\mathbf{R}^{(a)}} - \delta_{x,\mathbf{R}^{(b)}}).$$

Comparing the latter result with the plaquette decomposition (3.8), we can convince ourselves that such a configuration satisfies the condition (3.10) and represents a DDS.

Double Dirac sheets can be removed, or at least be reduced – in case of the confinement phase – by decreasing the Dirac plaquettes number (3.9) [94] applying periodic gauge transformations (2.8). The latter have to be coupled to the Lorentz gauge because, as it was demonstrated in [83], the standard Lorentz fixing procedure usually does not succeed in doing this.

DDS occur quite independently of the lattice size and the chosen β. And, as it was detected in [90] – [92], they are mainly responsible for the significant deviation of the non-zero momentum transverse photon correlator from the expected zero-mass perturbative one. However, as soon as one eliminates the unwanted DDS configurations, the correct zero-mass behaviour is restored (see also next chapter).

It is a common believe (see [95, 96]) that the Gribov problem can be solved by searching for the *global maximum* of the gauge functional (3.4) providing the *best* gauge copy (or copies, in case of degeneracy). For the DDS, this functional does not reach its maximum value. It was shown [90] that in order to reach the global maximum, one has necessarily to remove both the DDS and the ZMM from the gauge fields.

We have discussed here DDS gauge copies. Other copies, ZMM, deserve special attention and will be considered in the next chapter with the study of the Coulomb phase.

Chapter 4

The problem of zero-momentum modes

4.1 Zero-momentum modes

Let us investigate now the problem of other gauge copies, zero-momentum modes, for the case of the physically interesting Coulomb phase.

The constant or zero-momentum modes of the gauge field (2.7) are defined as follows:

$$\phi_\mu[U] = \frac{1}{V}\sum_x A_{x,\mu}. \tag{4.1}$$

Let us describe their properties. First of all, they do not contribute at all to the pure gauge field action (2.11) because it is invariant under the transformation:

$$U_{x,\mu} \to U_{x,\mu} \mathrm{e}^{-\mathrm{i}\phi_\mu[U]}, \qquad \forall x, \mu.$$

And hence, these constant modes are gauge copies of a gauge fixing procedure in the quenched fermion case. However, they can not be removed by usual periodic gauge transformations (2.8). As an example, for the Lorentz gauge fixing (3.3), (3.4) with DDS suppression, we measure the probability distributions $P(\phi)$ for the space- and time-like components of ZMM evaluated according to equation (4.1). The distributions turn out to be more or less flat within some interval $\phi_\mu \in [-\phi_\mu^{\max}, \phi_\mu^{\max}]$ with effective cutoff $\phi_\mu^{\max} \sim \pi/N_\mu$ (see Figure 4.1) providing an average value:

$$\langle|\phi_\mu|\rangle \sim \frac{\pi}{2N_\mu}, \tag{4.2}$$

and to be widely independent of β.

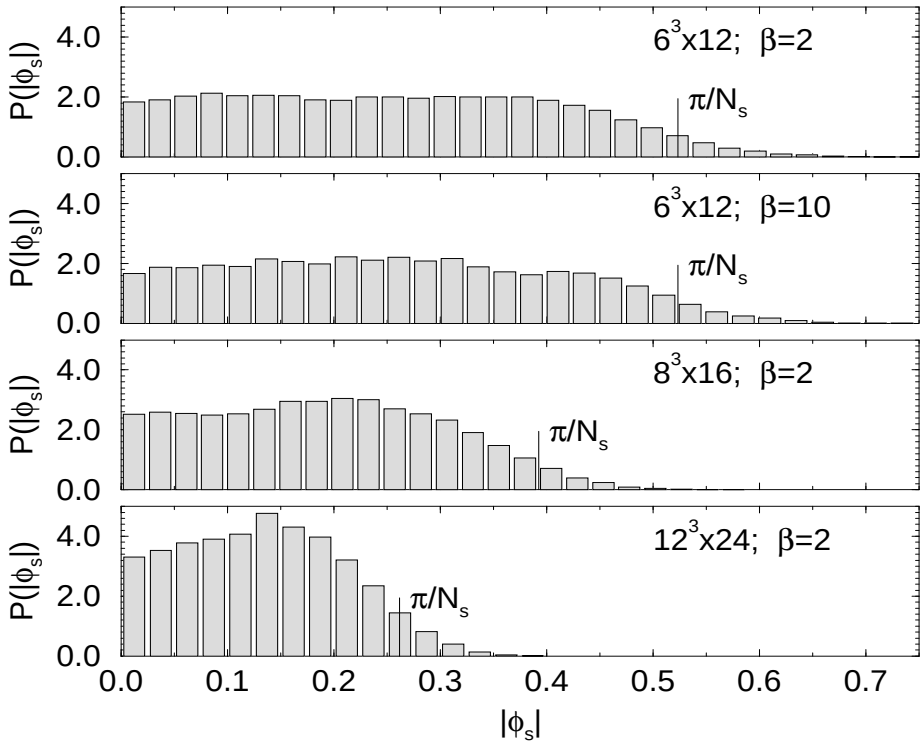

Figure 4.1: Distributions of the spacelike zero-momentum mode at different β-values and lattice sizes at the Lorentz gauge fixing. DDS excluded.

One can explain the behaviour of such constant modes as follows. For ordinary i.e periodic gauge transformations (2.8), the zero-momentum modes are changed only by values proportional to $2\pi/V$:

$$\phi_\mu[U^g] = \phi_\mu[U] + \frac{2\pi}{V} k_\mu, \qquad k_\mu = 0, \pm 1, \ldots \tag{4.3}$$

At the same time, for gauge configurations representing small fluctuations around constant modes (that takes place in the Coulomb phase):

$$A_{x,\mu} = \phi_\mu + \delta A_{x,\mu}, \qquad \sum_x \delta A_{x,\mu} = 0, \qquad |\delta A_{x,\mu}| \ll 1, \tag{4.4}$$

the Lorentz functional $G_{\max}$ (3.4) becomes larger with decreasing ϕ_μ values. And the iterative Lorentz fixing procedure (3.5) maximizing $G_{\max}$, tends to decrease also the ZMM (4.1) but obviously can not succeed in their complete elimination. Hence, in order to reach the global maximum of the Lorentz functional provided that all $\phi_\mu = 0$, one must *explicitely* remove these constant modes from the gauge field configurations.

4.2 Methods to eliminate the zero-momentum modes

In order to remove the zero-momentum modes, it was proposed [90] to use the iterative Lorentz gauge fixing procedure (3.3), (3.4) together with the suppression of the constant modes (4.1):

$$A_{x,\mu} \to A'_{x,\mu} = A_{x,\mu} - \phi_\mu[U] \mod 2\pi, \qquad \forall x, \quad \forall \mu = 1, \ldots, 4. \tag{4.5}$$

One notes that such subtraction removes the zero-momentum modes only up to values proportional to $2\pi/V$. And the proper elimination of these modes, when $\phi_\mu = 0$, can be achieved only if the Lorentz gauge fixing (3.4) is employed. Hence, the successive Lorentz gauge iteration steps (3.5) are always followed by non-periodic gauge transformations (2.12) suppressing the ZMM. Of course, we should check at the end whether the gauge field also contains the DDS. The latter can be excluded (in Coulomb phase) simply by repeating the same algorithm starting again with a random gauge transformation applied to the same gauge field configuration. We call the combined procedure (3.4), (4.5) as *zero-momentum Lorentz* (ZML) gauge. It is worth noting that the ZML gauge fixing alone removes already most of the DDS configurations. In Figure 4.2 we show how the achieved values of the gauge functional $G_{\max}$ (3.4) are correlated with the occurence of DDS which are visible as sharp peaks in the maximal number of Dirac plaquettes $N_{DP} = \max_{\mu,\nu} N_{DP}^{(\mu\nu)}$ where $N_{DP}^{(\mu\nu)}$ defined in (3.9). Whereas for Lorentz gauge strong fluctuations occur (Figure 4.2a), they disappear after ZML gauge fixing. The few DDS seen in Figure 4.2b are easily removed by restarting the procedure with random initial gauges. Random gauges can also be used in order to convince oneself that the ZML gauge prescription leads to the global maximum of the gauge functional in more than 99% of all events [90, 91].

We will now discuss an alternative method to get rid off the constant modes (4.1) of the gauge fields. In [83] it was proposed to use the nonperiodic gauge rotations (2.12) transforming the average Polyakov lines $P_\mu[U]$ into real and positive numbers:

$$P_\mu[U] = \frac{N_\mu}{V} \sum_{x_\perp} \prod_{x_\mu=1}^{N_\mu} U_{x,\mu} > 0, \qquad \forall \mu = 1, \ldots, 4. \tag{4.6}$$

where the $x_\perp$ are points in the subspace orthogonal to μ direction. The Polyakov line fixing exactly removes the constant gauge configurations $U_{x,\mu} = c_\mu$ which

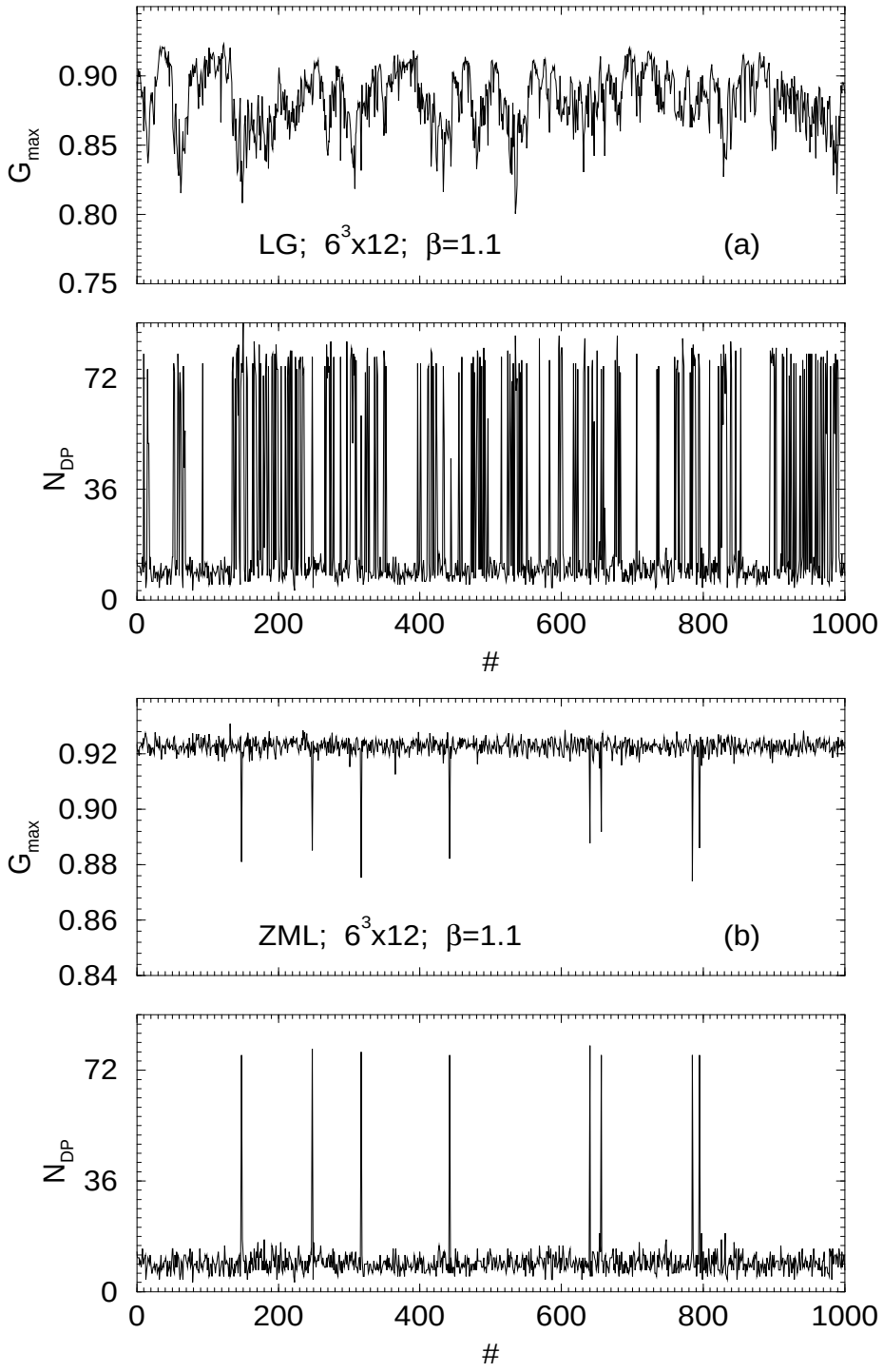

Figure 4.2: Time history of $G_{\max}$ and N_{DP} at $\beta = 1.1$ on the $6^3 \times 12$ lattice in the standard Lorentz gauge (a) and in the ZML gauge (b).

correspond to the free gauge case $\beta \to \infty$. But contrary to the ZMM (4.1), the Polyakov lines (4.6) are invariant under periodic gauge transformations (2.8). Let us defines the Polyakov phases $\phi_\mu^{(\mathrm{Pol})}[U]$ according to the equation:

$$\exp(\mathrm{i}N_\mu \phi_\mu^{(\mathrm{Pol})}[U]) = P_\mu[U], \qquad -\frac{\pi}{N_\mu} < \phi_\mu^{(\mathrm{Pol})}[U] \leq \frac{\pi}{N_\mu}. \tag{4.7}$$

Then in order to reach the $P_\mu > 0$ condition, one must take the following constant gauge transformation in (2.12):

$$c_\mu = \exp\left(\mathrm{i}\phi_\mu^{(\mathrm{Pol})}[U]\right).$$

And such transformation leads immediately to the gauge configuration with Polyakov phase $\phi_\mu^{(\mathrm{Pol})} = 0$.

At the end, let us present the integral for average gauge dependent observables in case of gauge fixing with an additional ZMM subtraction. Since the fermion matrix is not invariant under constant gauge transformations (2.12) such averages must differ from the standard ones defined by equation (3.1). Now they are evaluated as follows:

$$\langle \mathcal{O} \rangle_{\phi=0} = \frac{1}{Z} \int [\mathrm{d}U] \Delta_{\mathrm{FP}}[U^c] \delta\left(F[U^c]\right) \mathcal{O}[U^c] \Big|_{\phi[U^c]=0} \mathrm{e}^{-S_G[U]} \det{}^{N_f} \mathcal{M}[U], \tag{4.8}$$

where the U^c configuration, obtained from U by the nonperiodic transformation (2.12), satisfies the zero-momentum suppression condition $\phi_\mu[U^c] = 0$, $\forall \mu = 1, \ldots, 4$, and $\phi_\mu[U]$ is defined according to (4.1) or (4.7). Note that in case of gauge invariant observables, one can omit the Lorentz fixing condition $F[U] = 0$ and use only the Polyakov gauge fixing (4.6) in order to get rid off the contribution of zero-momentum modes.

4.3 Gauge dependent observables

4.3.1 Photon correlator

In this section we study the effects of the zero-momentum modes in case of the gauge dependent observables in the quenched approximation within the Coulomb phase.

The first gauge variant observable we are going to discuss is the transverse photon correlator at various (including non-zero) momenta [83]:

$$\Gamma_{\mathrm{ph}}(\vec{p}, \tau) = \frac{1}{N_4} \sum_{x_4=1}^{N_4} \left\langle \Phi(\vec{p}, x_4 + \tau) \Phi^\dagger(\vec{p}, x_4) \right\rangle, \qquad \tau = 0, \ldots, N_4 \tag{4.9}$$

where

$$\Phi(\vec{p}, x_4) = \sum_{\vec{x}} \exp(\mathrm{i}\vec{p}\vec{x} + \mathrm{i}p_\mu/2)\,\mathrm{Im}\,U_{x,\mu}, \qquad \mu = 1 \text{ or } 3,$$
$$\vec{p} = (0, p, 0), \quad x = (\vec{x}, x_4), \quad p = 2\pi k/N_s, \quad k = 0, 1, \ldots$$

In the free perturbative case, this photon correlator has the following behaviour (see also [83, 91]):

$$\Gamma_{\mathrm{ph}}^{(\mathrm{pert})}(\vec{p}, \tau) \propto \begin{cases} \dfrac{\cosh\left[E_{\mathrm{ph}}(\vec{p})(\tau - N_4/2)\right]}{\sinh\left[E_{\mathrm{ph}}(\vec{p})/2\right]\sinh\left[E_{\mathrm{ph}}(\vec{p})N_4/2\right]}, & \vec{p} \neq \mathbf{0} \\ \dfrac{N_4^2 - 1}{6N_4} + \tau\left(\dfrac{\tau}{N_4} - 1\right), & \vec{p} = \mathbf{0} \end{cases}, \tag{4.10}$$

where

$$\sinh^2 \frac{E_{\mathrm{ph}}(\vec{p})}{2} = \sum_{l=1}^{3} \sin^2 \frac{p_l}{2}.$$

Let us convince ourselves that the removal of the above mentioned gauge copies leads to the correct behaviour of the transverse photon correlator. First of all we consider the normalized photon correlator $\Gamma_{\mathrm{ph}}(\vec{p}, \tau)/\Gamma_{\mathrm{ph}}(\vec{p}, 0)$ for lowest non-vanishing momentum $p = 2\pi/N_s$ and for different Lorentz gauge prescriptions (see Figure 4.3a). For the standard one (open boxes) we see a clear deviation from the expected perturbative zero-mass result (4.10). On the other hand, Lorentz, as well as ZML, gauges without DDS (filled circles) provide an agreement with the perturbative result [83, 90, 91]. The given observations do not change, when β and/or the lattice size are considerably increased [91]. As it is obvious from the decomposition (4.4), in case of non-vanishing momenta p, the constant modes do not contribute to the photon correlator (4.9). Therefore application of the ZML gauge in this situation is not necessary.

But in case of the zero momentum $p = 0$ (see Figure 4.3b), there is no an agreement of this correlator in the Lorentz gauge with the perturbative result (4.10). Even the elimination of the DDS does not change the wrong behaviour. However in the ZML gauge (with additional DDS suppression) the photon correlator is in a good agreement with the perturbative one [90, 91].

A detailed inspection of the influence the zero-momentum modes on the photon correlator (4.11) has been performed in [90, 91, 93]. Next two sections will be devoted to analogous investigation in case of the fermion observables.

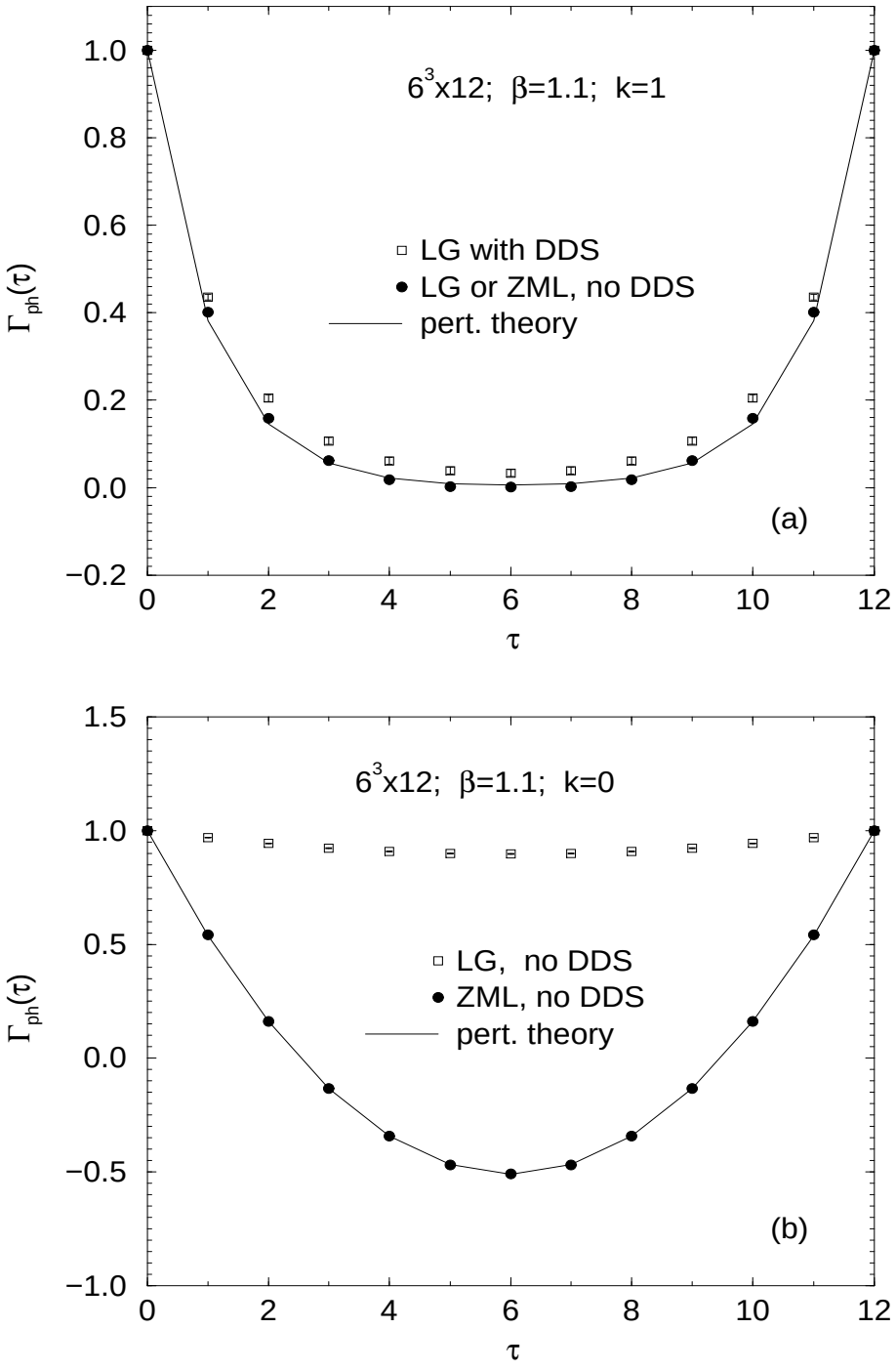

Figure 4.3: Transverse photon correlator at $\beta = 1.1$ on the $6^3 \times 12$ lattice for the nonzero momentum $k = 1$ (a) and for zero momentum $k = 0$ (b) cases.

4.3.2 Fermion correlator

The second gauge dependent observable in our investigation is the fermion zero-momentum correlator. For a given gauge field U we have:

$$\Gamma(\tau) = \frac{1}{V}\sum_{x,\vec{y}} \mathcal{M}^{-1}_{xy}[U], \qquad x = (\vec{x}, x_4), \quad y = (\vec{y}, x_4 + \tau). \tag{4.11}$$

For simplicity, we restrict ourselves to the scalar and vector parts of the fermion correlator, respectively:

$$\Gamma_S(\tau) = \frac{1}{4}\mathrm{Re}\,\mathrm{tr}\,\Gamma(\tau), \qquad \Gamma_V(\tau) = \frac{1}{4}\mathrm{Re}\,\mathrm{tr}\,\gamma_4\Gamma(\tau), \tag{4.12}$$

where the trace is taken with respect to the spinor indices. For antiperiodic in x_4 (or time-antiperiodic) b.c., the vector (scalar) part becomes an even (odd) function in τ around $\tau = N_4/2$, for periodic b.c. vice versa.

In quenched QED, the fermion correlator (4.11) has to be averaged with respect to the gauge field U distributed with the weight $\exp(-S_G[U])$. We will also compare the quantum averages within the zero-momentum mode approximation where only background gauge fields being constant in space-time are taken into account (it corresponds to the case $\beta \to \infty$). Therefore, we construct analytically the correlator for a uniform gauge configuration given by:

$$A_{x,\mu} = \phi_\mu, \qquad -\pi < \phi_\mu \leq \pi, \qquad \mu = 1, \ldots, 4.$$

One obtains the following finite size results for the scalar and vector parts, respectively:

$$\begin{aligned}
\Gamma_S(\tau;\phi) &= \frac{\delta_{\tau,0}}{2(1+\mathcal{W})} - \frac{1+\mathcal{E}^2-2\mathcal{E}(1+\mathcal{W})}{1-\mathcal{E}^2} \times \\
&\times \frac{[\mathcal{E}^\tau - \mathcal{E}^{2N_4-\tau}]\cos(\phi_4\tau) - c[\mathcal{E}^{N_4+\tau} - \mathcal{E}^{N_4-\tau}]\cos[\phi_4(N_4-\tau)]}{1+\mathcal{E}^{2N_4} - 2c\mathcal{E}^{N_4}\cos(\phi_4 N_4)},
\end{aligned} \tag{4.13}$$

$$\begin{aligned}
\Gamma_V(\tau;\phi) &= \frac{1-\delta_{\tau,0}}{2(1+\mathcal{W})} \times \\
&\times \frac{[\mathcal{E}^\tau + \mathcal{E}^{2N_4-\tau}]\cos(\phi_4\tau) - c[\mathcal{E}^{N_4+\tau} + \mathcal{E}^{N_4-\tau}]\cos[\phi_4(N_4-\tau)]}{1+\mathcal{E}^{2N_4} - 2c\mathcal{E}^{N_4}\cos(\phi_4 N_4)},
\end{aligned} \tag{4.14}$$

where $c = +1$ and $c = -1$ holds for periodic and time-antiperiodic boundary conditions, respectively, and

$$\mathcal{E} = 1 + \frac{\mathcal{W}^2+\mathcal{K}^2}{2(1+\mathcal{W})} + \frac{\sqrt{\mathcal{W}^2+\mathcal{K}^2}\sqrt{(\mathcal{W}+2)^2+\mathcal{K}^2}}{2(1+\mathcal{W})};$$

$$\mathcal{W} = m_0 + \sum_{l=1}^{3}(1-\cos\phi_l), \qquad \mathcal{K} = \sqrt{\sum_{l=1}^{3}\sin^2\phi_l}, \qquad m_0 > 0,$$

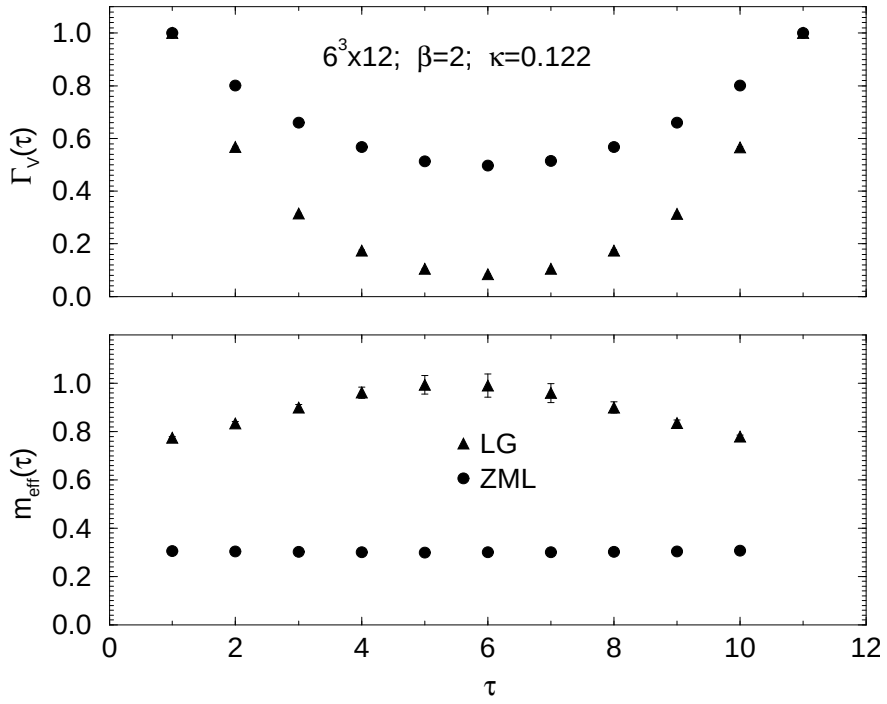

Figure 4.4: The fermionic vector correlator Γ_V and the effective mass $m_{\rm eff}$ at $\beta = 2$ and $\kappa = 0.122$ on a $6^3 \times 12$ lattice for LG and ZML gauges.

where the bare fermion mass m_0 is related to the hopping-parameter κ according to formula (2.17). If we put all $\phi_\mu = 0$, the equations (4.13), (4.14) reproduce the results for the standard free fermion correlator [97]. The formulas analogous to equations (4.13), (4.14) were obtained also in the case of staggered fermions [14].

The renormalized fermion masses are extracted in the following way. We consider an effective mass $m_{\rm eff}(\tau)$ determined from the correspondence of the vector part (4.12) of the ordinary correlator with the vector part of the free fermion correlator (4.14) at $\phi_\mu = 0$ in case of time-antiperiodic b.c. (or scalar parts (4.12) and (4.13) for periodic b.c.) according to the recipe:

$$\frac{\langle\Gamma(\tau+1)\rangle}{\langle\Gamma(\tau)\rangle} = \frac{\cosh\left[E(\tau)(\tau+1-N_4/2)\right]}{\cosh\left[E(\tau)(\tau-N_4/2)\right]}, \qquad E(\tau) = \ln(m_{\rm eff}(\tau)+1). \tag{4.15}$$

Then one searches for a plateau of the function $m_{\rm eff}(\tau)$ in order to identify the value of fermion mass.

Let us consider quenched QED within the Coulomb phase at β values between 2 and 10 for κ parameters not too close to $\kappa_c(\beta)$. In order to extract the pure ZMM effect, we first apply the standard Lorentz gauge procedure (3.3), (3.4) modified by initial random gauges in order to suppress DDS. Let us abbreviate the notation for

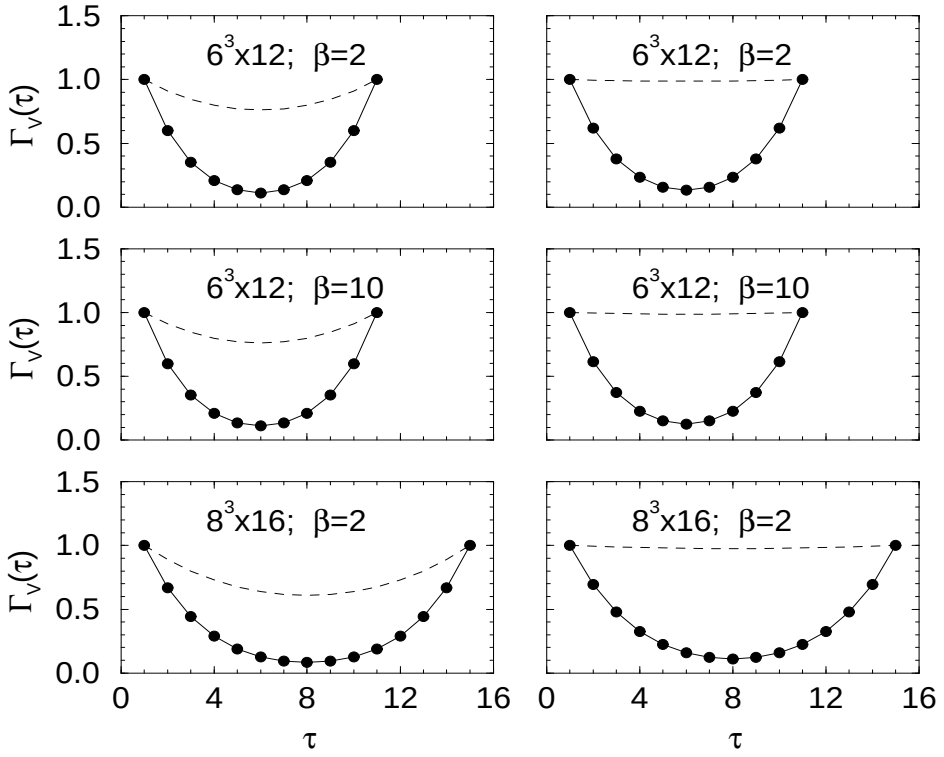

Figure 4.5: Free fermionic vector correlator (dashed line) and averaged constant mode correlator (full line) for two β-values and lattice sizes $6^3 \times 12$, $8^3 \times 16$.

this modified Lorentz gauge procedure by LG. We compare the result with that for the ZML gauge described above. For definiteness, we choose the time-antiperiodic boundary conditions for Fermi-fields and study the vector part Γ_V (4.12) of the fermion correlator.

For both these gauges we have computed the averaged fermion correlator (4.11) as defined in equations (4.12) and normalized to unity at $\tau = 1$. In the upper part of Figure 4.4 we have plotted the vector part $\langle \Gamma_V(\tau) \rangle$ for $\beta = 2$, $\kappa = 0.122$ and lattice size $6^3 \times 12$. The situation seen is typical for a wide range of parameter values within the Coulomb phase. Obviously, there is a strong dependence of the fermion correlator on the gauge copies differing by the different amount of ZMM. If ZMM are present, the correlator decays much stronger, than when they become suppressed.

In the lower part of Figure 4.4 the corresponding numerical results for the effective masses $m_{\rm eff}(\tau)$ (4.15) are shown. In the standard LG case no real plateau is visible, whereas the ZML case provides a very stable one. Thus, the ZML gauge

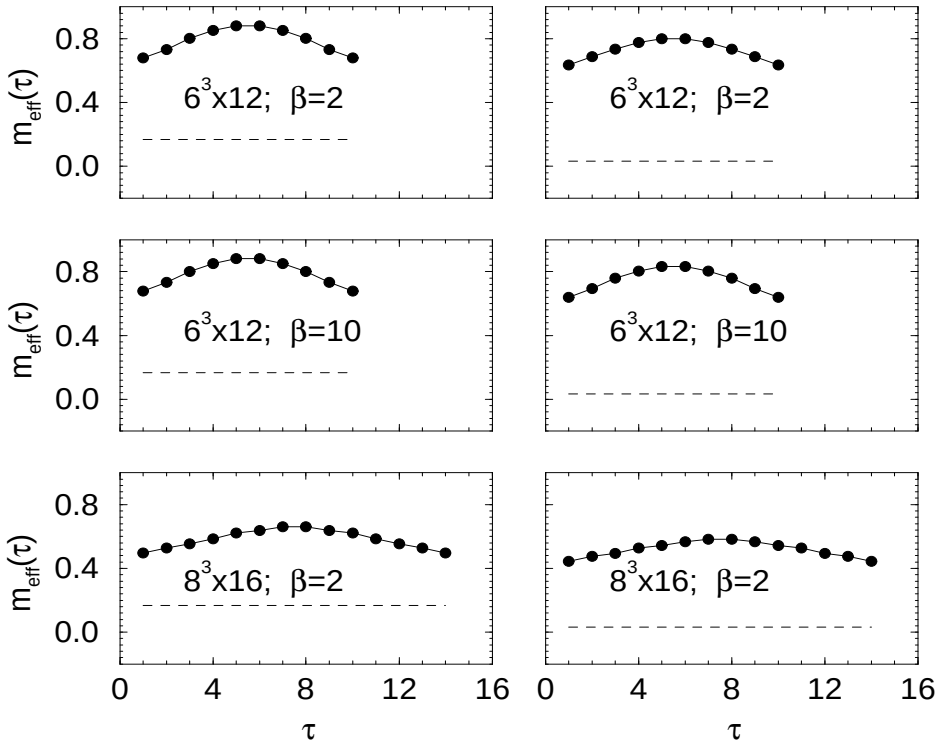

Figure 4.6: Effective masses corresponding to the fermion correlator results shown in Figure 4.5.

yields a reliable mass estimate, whereas the LG fails here. Naively, when only considering the LG method, one would be tempted to relate a 'bad plateau' to finite-size effects and to believe that the given LG effective mass result is already near to the real mass. Such a point of view obviously fails. Taking now the ZML mass estimate as the reliable one, the LG estimate fails by a factor ~ 3 in our case.

In order to estimate roughly the effect of the ZMM on the fermion correlator for various β and lattice size, we consider the zero-momentum mode approximation as follows. According to equations (4.13), (4.14) we compute the fermion correlator only within the constant background modes extracted from the quantum gauge fields in the LG case with the distribution $P(\phi)$:

$$\langle\Gamma\rangle_\phi = \int_{-\pi}^{\pi} \frac{\mathrm{d}^4\phi}{(2\pi)^4} P(\phi)\Gamma(\phi) \Big/ \int_{-\pi}^{\pi} \frac{\mathrm{d}^4\phi}{(2\pi)^4} P(\phi). \tag{4.16}$$

The results of this calculation for the vector part of the fermion correlator in the LG case are presented in Figure 4.5 together with the corresponding free, i.e.

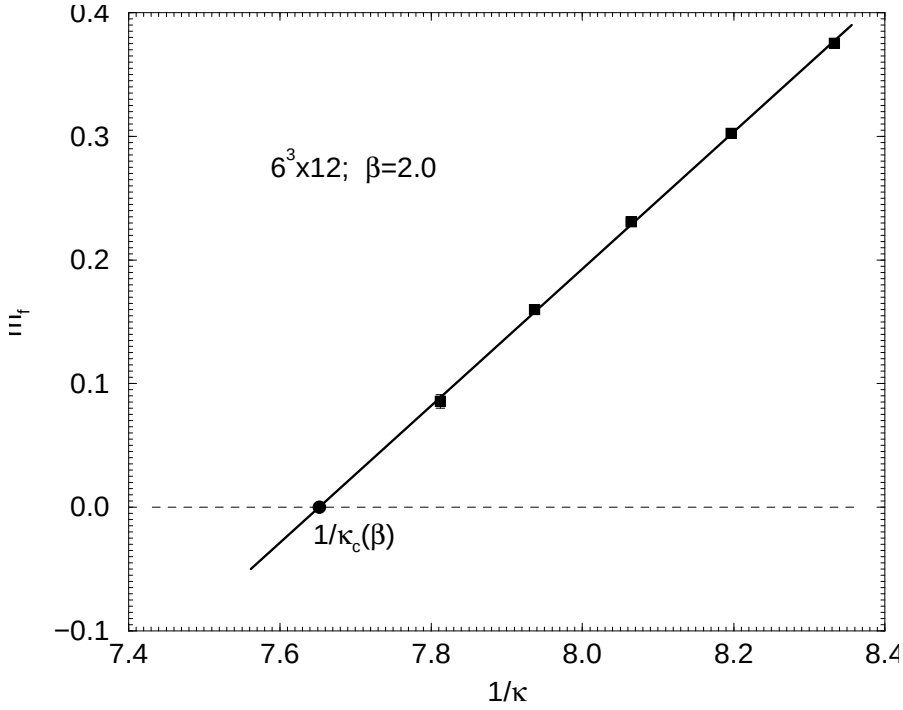

Figure 4.7: Fermion mass as a function of inverse κ obtained within the ZML gauge for $\beta = 2.0$ on a $6^3 \times 12$ lattice. The solid line represents a linear fit providing $\kappa_c(\beta) = 0.1307(1)$.

$\phi_\mu = 0$, correlator (dashed lines). One can see that the effect of the ZMM does not weaken with increasing β and lattice size, respectively. Having the estimate (4.2) for $\langle|\phi_\mu|\rangle$ one finds from (4.13), (4.14) and (4.16) that the ZMM effect does not disappear even in the limit $N_\mu \to \infty$.

The computations of the fermion correlator (4.11) within the full gauge field background confirm these observations.

We can take the pure zero-momentum mode approximation described above in order to check, how the corresponding effective fermion mass would behave. This result is shown in Figure 4.6. We clearly see, that for the LG case providing the ZMM background field configurations we do not find a plateau (full lines). The effective mass values strongly differ from the real ones, i.e. m_0 of the free correlator (dashed lines).

And at the end, in Figure 4.7 we present the renormalized fermion mass $m_{\rm f}$ extracted from the vector fermion correlator by use of (4.15) within the ZML gauge for $\beta = 2.0$ and various κ values. We see a nice linear behaviour $m_{\rm f} \propto m_q$ where m_q defined in (2.34), from which by extrapolating (solid line) to zero

mass $m_{\rm f} = 0$ (dashed line) one estimates the critical hopping-parameter value $\kappa_c = 0.1307(1)$. This value coincides with κ_c obtained by studying of the gauge invariant observables: the pion norm variance [33] and the PCAC-like fermion mass [98].

4.4 Gauge invariant fermion observables

Now we consider the influence of the zero-momentum modes on gauge invariant fermion observable. For this investigation we choose the scalar condensate (2.27) and the pion norm (2.28) values. We are not interested at the moment in the pure gauge observables like mean gauge energy (2.26) since their operators are invariant under the constant gauge transformations (2.12).

Remember the definition of the scalar condensate and pion norm average values:

$$\langle\overline{\psi}\psi\rangle \equiv \langle\frac{1}{4V}\,\mathrm{Tr}\,\mathcal{M}^{-1}\rangle = \langle\frac{1}{4V}\sum_j\frac{1}{\mu_j}\rangle, \tag{4.17}$$

$$\langle\Pi\rangle \equiv \langle\frac{1}{4V}\,\mathrm{Tr}\,\gamma_5\mathcal{M}^{-1}\gamma_5\mathcal{M}^{-1}\rangle = \langle\frac{1}{4V}\sum_j\frac{1}{\lambda_j^2}\rangle, \tag{4.18}$$

where the averaging $\langle\ldots\rangle$ is performed according to the equation (2.24), and μ_j, λ_j are the eigenvalues of $\mathcal{M}$ and $\gamma_5\mathcal{M}$ matrices, respectively. We remind that these values (4.17) and (4.18) are independent of the choice of the boundary conditions for fermion fields. One expects $\langle\overline{\psi}\psi\rangle$ and $\langle\Pi\rangle$ values (especially the latter one) to be good indicators of the chiral limit at $\kappa \to \kappa_c(\beta)$ as some of the μ_j and λ_j are expected to become very small [33].

However, the numerical study of fermionic observables like $\langle\Pi\rangle$ near the chiral limit does not reveal the critical properties as expected from lowest order and finite lattice size perturbation theory. This can be seen from the κ-dependence of the pion norm numerically computed at low β-values within the Coulomb phase [70] (see Figure 4.8). Its behaviour is very smooth and no sign of any critical behaviour is observed. The volume dependence of $\langle\Pi\rangle$ is rather weak, and there is no significant difference between the quenched and the dynamical case.

It is interesting to compare these results for $\langle\Pi\rangle$ with the standard perturbative free fermion case given by the expression:

$$\langle\Pi\rangle_0 = \frac{1}{V}\sum_p\left\{4\kappa^2\sum_\mu\sin^2\frac{2\pi p_\mu}{N_\mu} + \Big(1 - 2\kappa\sum_\mu\cos\frac{2\pi p_\mu}{N_\mu}\Big)^2\right\}^{-1}, \tag{4.19}$$

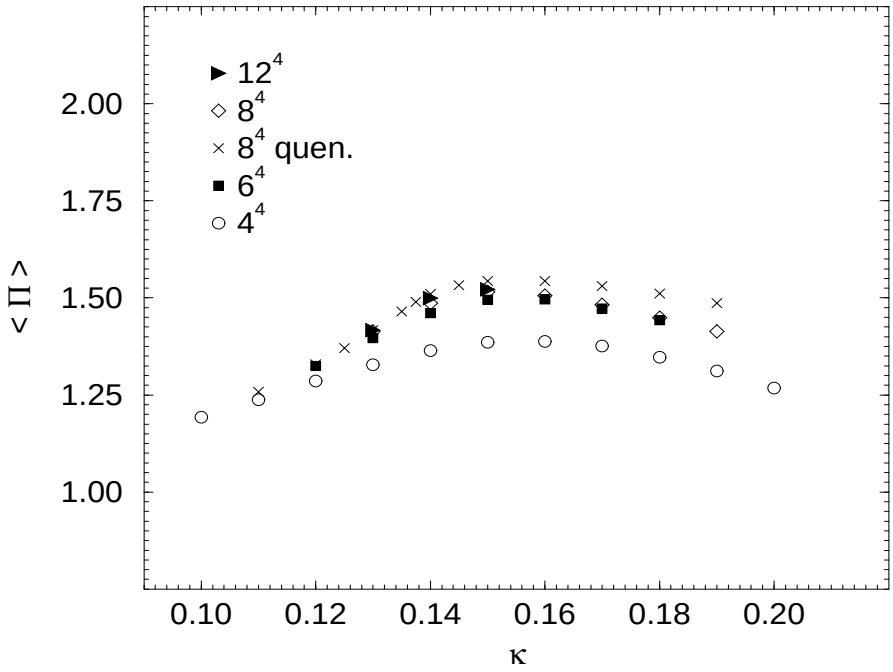

Figure 4.8: Pion norm as function of κ for full (and quenched) compact QED with Wilson action at $\beta = 1.1$ for various lattice sizes (data taken from [70]).

where the p_μ, $\mu = 1, \ldots, 4$ are integers except for time-antiperiodic b.c. causing p_4 to take half-integer values. In Figure 4.9 one can see the κ-dependence of $\langle\Pi\rangle_0$ calculated on a symmetric lattice ($N_4 = N_s = 6$) for periodic and time-antiperiodic b.c. For periodic b.c. $\langle\Pi\rangle_0$ obviously becomes singular at $\kappa = 1/8$, whereas for time-antiperiodic b.c. the κ-dependence of $\langle\Pi\rangle_0$ becomes smooth for symmetric lattices. However, note that in the latter b.c. case $\langle\Pi\rangle_0$ develops a peak for strongly elongated lattices ($N_4 \to \infty$ with N_s=fixed), too.

This behaviour can be explained by a rough analytical estimation of the free pion norm value from equation (4.19) near the critical point $\kappa_c = 1/8$. For periodic b.c. owing to the contribution of the $p = 0$ term one has:

$$\langle\Pi\rangle_0 \propto \frac{1}{V(1-8\kappa)^2}, \qquad \kappa \to \kappa_c = 1/8. \tag{4.20}$$

But in case of time-antiperiodic boundary conditions, $\langle\Pi\rangle_0 \propto N_4^2/V$, and there is no critical behaviour for the symmetric lattice $N_s = N_4$. However if $N_4 \gg N_s$, the critical effect is restored that is confirmed by our numerical observations.

We are going to demonstrate that this drastic difference between $\langle\Pi\rangle$ in the finite β (Figure 4.8) and free (Figure 4.9) cases is due to influence of constant or

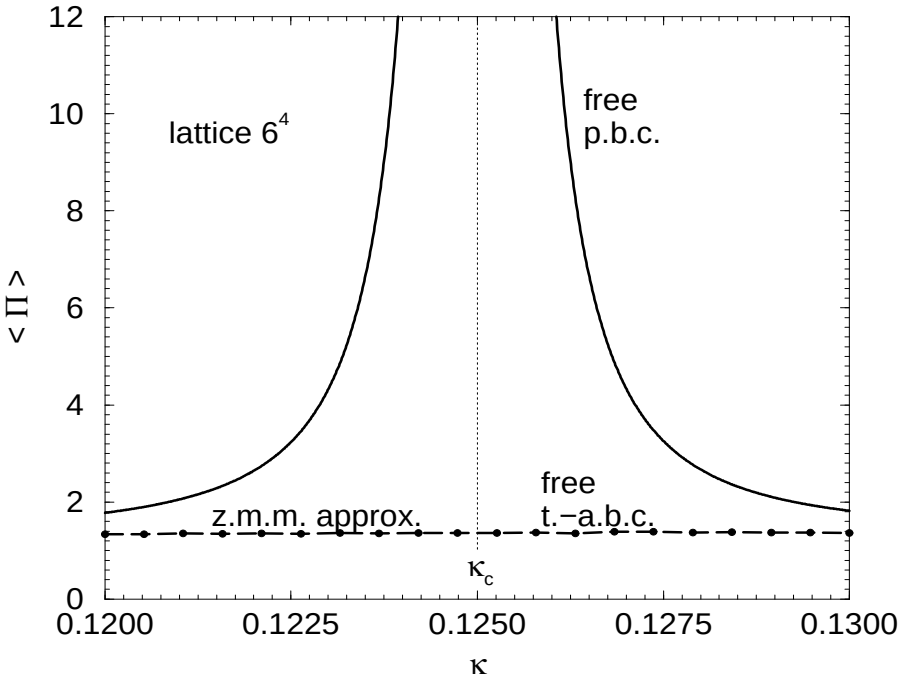

Figure 4.9: Pion norm in the free fermion case without zero-momentum modes and in the zero-momentum mode approximation, lattice size 6^4, periodic (p.b.c.), as well as time-antiperiodic (t-a.b.c.) boundary conditions.

zero-momentum modes of the gauge fields $\phi_\mu[U]$ as defined in equation (4.1).

Within the zero-momentum mode approximation this can be easily demonstrated by averaging $\langle\Pi\rangle$ over constant modes with uniform distribution. It yields the following expression independent of the b.c.:

$$\langle\Pi\rangle_\phi = \int_{-\pi}^{\pi} \frac{\mathrm{d}^4\phi}{(2\pi)^4} \left\{ 4\kappa^2 \sum_\mu \sin^2\phi_\mu + \Big(1 - 2\kappa \sum_\mu \cos\phi_\mu\Big)^2 \right\}^{-1}, \tag{4.21}$$

which is completely smooth in κ and agrees with the former time-antiperiodic, free result for symmetric lattices (see Figure 4.9).

Now let us consider the gauge interacting case, i.e. the finite β-values. We compute the pion norm in the ZML gauge according to the integral (4.8) when the zero-momentum modes in the observable become eliminated. Since the fermion operator (2.18) is not invariant under constant gauge transformations (2.12), the new average $\langle\Pi\rangle$ differs from the ordinary one averaged according to (2.24). In the following we choose periodic boundary conditions, because owing to (4.20) in the free case we expect that they lead to a more pronounced chiral behaviour than the

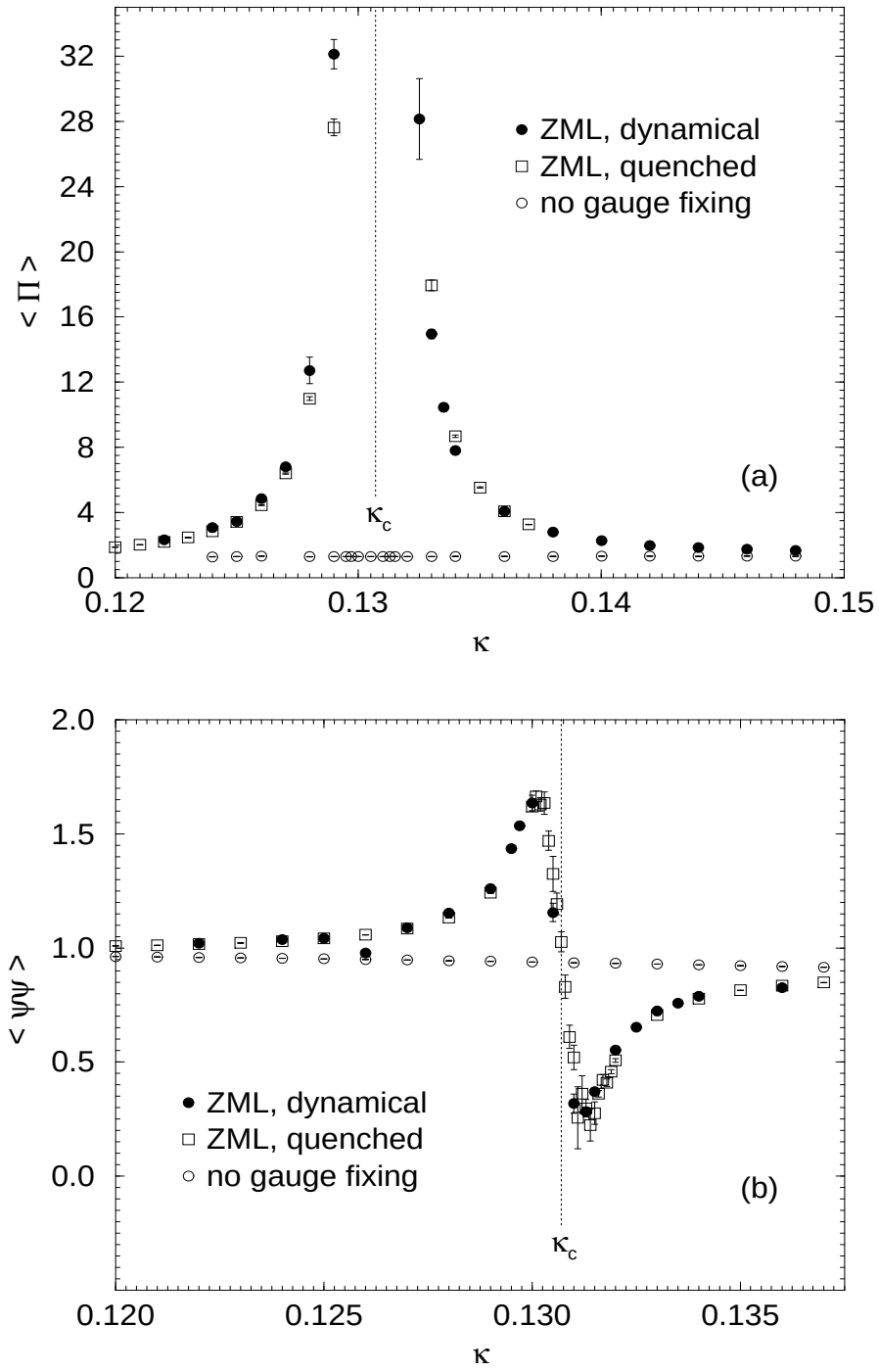

Figure 4.10: Pion norm $\langle \Pi \rangle$ (a) and scalar condensate $\langle \overline{\psi}\psi \rangle$ (b) as functions of κ in the ZML gauge for full and quenched QED, as well as without any gauge fixing for full QED; all data for $\beta = 2.0$, lattice size 4^4, periodic b.c.

time-antiperiodic ones.

In Figure 4.10a we show the dependence of the pion norm $\langle\Pi\rangle$ on κ. One can see that for dynamical fermions (full circles) as well as for quenched fermions (boxes) the ZML observable $\langle\Pi\rangle$ has a sharp singularity near the point $\kappa_c = 0.1307(1)$ for $\beta = 2.0$ (compare with Figure 4.7). In contrast, the standard definition of the pion norm demonstrates a completely smooth behaviour (open circles). We checked these results for $\langle\Pi\rangle$ also on larger lattices. For κ approaching κ_c the same critical behaviour is observed, whereas very close to and slightly above κ_c the influence of an increasing number of very small fermionic eigenmodes leads to stronger fluctuations ('exceptional configurations'). The dynamical and quenched results resemble each other. This can be interpreted as the zero-momentum modes which are removed from the observable $\langle\Pi\rangle$ evaluated by (4.8), continue to dominate the fermion determinant.

What about the scalar condensate $\langle\overline{\psi}\psi\rangle$ (4.17)? It also demonstrates the critical behaviour in the ZML gauge for both quenched and dynamical cases (see Figure 4.10b). As expected from (4.17), (4.18), its peak near the chiral limit line is not so pronounced as for the pion norm.

We have also studied the gauge invariant fermion observables in the Polyakov gauge (4.6). Our results have shown that this nonperiodic gauge fixing – without the necessity to employ the Lorentz gauge – leads to the singular chiral behaviour for both pion norm and scalar condensate values similar to the ZML gauge case.

At the end let us discuss the width of the critical behaviour in case of the periodic b.c. for fermions. As it follows from the asymptotic behaviour (4.20) for the free pion norm, the gap of the singularity shrinks to zero in the thermodynamic limit $V \to \infty$. Our numerical results confirm this statement. However, the singular behaviour of gauge invariant fermion observables without ZMM can serve in the finite lattice case for an evaluation of the critical hopping-parameter $\kappa_c(\beta)$.

4.5 Discussion

Within the physically interesting Coulomb phase we have studied the effect of different gauge copies of the gauge field on gauge dependent correlators, in particular on the fermion one, and also on the gauge invariant fermion observables.

We have convinced ourselves that the standard Lorentz gauge fixing prescription to maximize the functional (3.4) provides gauge copies with DDS and ZMM.

These modes disturb the photon and the fermion correlator behaviour in comparison with standard perturbation theory and consequently spoil the naive effective mass estimate. A Lorentz gauge employing non-periodic gauge transformations (2.12) in order to suppress the ZMM (4.1) (the ZML gauge) – additionally to DDS – allows us to reach the global maximum of the Lorentz gauge functional (3.4). Furthermore, it provides a reliable fermion mass determination, at least, if κ is chosen not too close to the chiral critical line $\kappa_c(\beta)$. A computation of the fermion correlator with constant background gauge fields taken from the ZMM of the quantum fields demonstrates the disturbing effect of these modes very clearly. Moreover, it shows the effect to be independent of the bare coupling and not to disappear for large volumes.

The ZMM configurations smooth out also the critical chiral behaviour expected from lowest order perturbation theory for gauge invariant fermion observables like the pion norm and the scalar condensate. This was proven in the free fermion case and confirmed in the finite β theory. But the elimination of ZMM by the use of ZML gauge fixing (3.4), (4.5) or the Polyakov line one (4.6) restores the critical behaviour in case of the periodic b.c for fermions. And the position of the chiral limit line $\kappa_c(\beta)$ appears to be coincident with that obtained from the gauge dependent fermion mass estimates. Although there is no singular behaviour in case of the time-antiperiodic b.c. for symmetric lattices, it becomes again visible for the pion norm if $N_4 \gg N_s$. And the width of the peak shrinks in the thermodynamic limit $V \to \infty$.

So far we have studied the gauge dependent observables in the framework of the quenched approximation of U(1) lattice gauge theory. The gauge action (2.11) is invariant under constant gauge transformations (2.12). Thus, we are allowed to use the ZML gauge for the evaluation of gauge dependent objects. Contrary to the gauge action, the fermion action (2.15) does depend on the ZMM. And these constant modes lead as shown (see Figure 4.10) to the smoothing of the fermion determinant in the integral (2.24) for lattice observables. In this case another way of dealing with the Gribov problem has to be searched for.

Rigorously speaking, the consistent study of the compact U(1) theory without zero-momentum modes requires also their elimination from the fermion determinant. However on the one hand, it strongly complicates the numerical calculations. And on the other hand, the ZMM suppression (4.5) owing to the gauge covariance (4.3) must be accompanied by the maximization of the Lorentz functional

(3.4), and gauge invariant observables will depend on the gauge fixing. Here, the Polyakov gauge (4.6) could be a good candidate of the gauge invariant constant modes suppression.

However, there is an important objection to use the elimination of the zero-momentum modes. As one sees from the Figure 4.10, the critical behaviour of gauge invariant fermion observables without ZMM near the chiral limit line seems to indicate a first order phase transition. But it is spurious because of its vanishing in the thermodynamic limit $V \to \infty$. At the same time, it could disturb the correct study of lattice observables in the continuum limit and the precise determination of critical points $(\beta^\star, \kappa^\star)$, if they exist. Hence, one should try to find alternatives to the ZMM suppression. One of such ways is to employ the C^*-boundary conditions [99] to both gauge and fermion fields, which *implicitly* suppress the ZMM and also Gribov copies like double Dirac sheets.

Another way nevertheless, could be considering standard Lorentz gauge with additional DDS suppression and taking the constant background modes properly into account in describing the perturbative finite volume fermion correlator (4.13), (4.14) and then identifying correspondingly the renormalized fermion mass [14]. And moreover, it is enough to use only LG in case of objects independent of the zero-momentum modes as the photon correlator (4.9) at $\vec{p} \neq 0$ [83, 90, 91].

The basic material of the chapter 4 was published in papers [34, 35].

Chapter 5

Algorithms for the lattice

5.1 Monte Carlo method

In practical numerical studies of average observables on the lattice one has to evaluate the integral (2.24). However computations of this integral by usual numerical methods are impossible because they require an exponentially large number of computer operations. For instance even in case of the simplest discrete group $\mathbf{Z}_2 = \{+1, -1\}$ for 4d gauge theory, such number is equal to 2^{4V} which can never be reached by present computing devices.

It means that one has to use qualitatively different, statistical way for the evaluation of the lattice integral (2.24) – *Monte Carlo* method (see e.g. [9, 10]). The idea of this technique is that one generates a series of gauge configurations $U^{(1)}$, $U^{(2)}$, etc. distributed with a weight $\mathbf{m}[U]$. The integral (2.24) for average observable $\mathcal{O} = \mathcal{O}[U]$ is then evaluated as follows:

$$\langle \mathcal{O} \rangle = \lim_{N\to\infty} \frac{\sum_{j=1}^{N} \mathcal{O}[U^{(j)}] \exp(-S_G[U^{(j)}]) \det{}^{N_f} \mathcal{M}[U^{(j)}]/\mathbf{m}[U^{(j)}]}{\sum_{j=1}^{N} \exp(-S_G[U^{(j)}]) \det{}^{N_f} \mathcal{M}[U^{(j)}]/\mathbf{m}[U^{(j)}]}. \tag{5.1}$$

It is obvious from this equation that in order to suppress strong fluctuations of the integral measure in (2.24), one should generate the gauge configurations distributed as:

$$\mathbf{m}[U] \propto \exp(-S_G[U]) \left| \det{}^{N_f} \mathcal{M}[U] \right|. \tag{5.2}$$

Then the expression (5.1) with the assumption $\det{}^{N_f} \mathcal{M} > 0$ is just the arithmetic

mean value for sampled observables $\mathcal{O}[U^{(j)}]$:

$$\langle \mathcal{O} \rangle = \lim_{N\to\infty} \frac{1}{N} \sum_{j=1}^{N} \mathcal{O}[U^{(j)}]. \tag{5.3}$$

But usually the direct generation of the weight (5.2) is impossible. One may only perform a Markov process $U \to U'$ to get a new configuration U' from the previous one U, described by some transition probability $p[U', U]$. However if the weight $\mathbf{m}[U]$ satisfies the equilibrium relation:

$$\mathbf{m}[U] = \int [\mathrm{d}U'] p[U, U'] \mathbf{m}[U'], \tag{5.4}$$

then the transition process $p[U', U]$ will converge to the distribution proportional to the function $\mathbf{m}[U]$.

A sufficient condition for the equilibrium equation (5.4) is the detailed balance relation:

$$p[U', U]\mathbf{m}[U] = p[U, U']\mathbf{m}[U']. \tag{5.5}$$

Indeed, integrating out the U' field in this relation and taking into account the normalization condition

$$\int [\mathrm{d}U'] p[U', U] = 1,$$

one comes to the equation (5.4). Below we describe various methods generating the weight (5.2) for different fermion flavour N_f cases.

5.2 Quenched approximation: Metropolis and heatbath methods

Let us start with the quenched approximation case (2.29) when the weight has the following pure gauge distribution:

$$\mathbf{m}[U] \propto \exp(-S_G[U]), \tag{5.6}$$

Note that in contrast to the fermion determinant, the compact action $S_G[U]$ (2.11) can be computed almost immediately.

One of the well-known transition processes $U \to U'$ used in the lattice field theory is the *Metropolis* one [100]. In this process the new configuration U' is obtained by a uniform random distribution and accepted with probability

$$w_{\mathrm{acc}}[U', U] = \min\bigl(1, \exp(-S_G[U'] + S_G[U])\bigr). \tag{5.7}$$

It is obvious that the transition probability of this process $p[U', U] \propto w_{\rm acc}[U', U]$ satisfies the detailed balance relation (5.5) with (5.6). However in case of large β values, the acceptance rate of new configurations is very low. That is why one uses another transition dynamics algorithm called as *heatbath* method [101].

In this method, one performs successive updates known as sweeps of the gauge links $U_{x,\mu}$ for each site x and direction μ keeping remaining links fixed. The updating algorithm follows from the expression for the U(1) gauge action (2.11) which can be rewritten as follows:

$$S_G[U] = -\,\mathrm{Re}\,\left(U_{x,\mu}F^{(G)}_{x,\mu}\right) + (\text{terms, independent of } U_{x,\mu})\,, \tag{5.8}$$

with the so-called complex gauge force

$$F^{(G)}_{x,\mu} = \beta \sum_{\substack{\nu \\ \nu\neq\mu}} \left(U_{x+\hat{\mu},\nu}U^{\dagger}_{x+\hat{\nu},\mu}U^{\dagger}_{x,\nu} + U^{\dagger}_{x-\hat{\nu}+\hat{\mu},\nu}U^{\dagger}_{x-\hat{\nu},\mu}U_{x-\hat{\nu},\nu}\right). \tag{5.9}$$

Then the heatbath sweep $U_{x,\mu} \to U'_{x,\mu}$ for certain x and μ link point looks as

$$U'_{x,\mu} = \left(F^{(G)}_{x,\mu}/\left|F^{(G)}_{x,\mu}\right|\right)^{-1} \exp(\mathrm{i}\eta_{x,\mu}), \tag{5.10}$$

where the $\eta_{x,\mu}$ is real random number in the interval $(-\pi, \pi]$ distributed as

$$p_\eta \propto \exp\left(\left|F^{(G)}_{x,\mu}\right| \cos\eta_{x,\mu}\right). \tag{5.11}$$

Using the equations (5.8) – (5.11), one can convince himself that the heatbath transition probability function $p[U', U]$ is proportional to the pure gauge weight (5.6) for the new configuration U': $p[U', U] \propto \mathbf{m}[U']$. And therefore, it fulfills the detailed balance relation (5.5) with the pure gauge measure (5.6).

Since the heatbath method (5.10), (5.11) performs the sequential updates of gauge links without *total* rejection of the new gauge configuration, it usually converges faster than the Metropolis (5.7) one [9].

But now we must generate the random numbers $\varphi \in (-\pi, \pi]$ distributed as:

$$p(\varphi) = \mathcal{N}^{-1} \exp(|F| \cos\varphi). \tag{5.12}$$

There is no a fast direct way to obtain such a distribution. Hence one uses the following method known as *filtering* [10]. We generate the random numbers φ with another distribution density $p_{\rm filt}(\varphi)$ (called as filter) that can be done *exactly*, and this φ is accepted or rejected with the probability:

$$w_{\rm acc}(\varphi) = \frac{p(\varphi)/p_{\rm filt}(\varphi)}{\max\limits_{\varphi}(p/p_{\rm filt})}. \tag{5.13}$$

For an appropriate choice of the filter function p_{filt}, the filtering method controlled by probability (5.13) converges rapidly to the function (5.12) (see [10]). Indeed, the transition dynamics for such process of generating the $p(\varphi)$ function is described by the equation [10]:

$$p(\varphi', \varphi) = ap(\varphi') + (1 - a)\delta(\varphi', \varphi),$$

where the δ is the delta-function and the a is the average acceptance rate:

$$a = \int_{-\pi}^{\pi} \mathrm{d}\varphi w_{\text{acc}}(\varphi) p_{\text{filt}}(\varphi).$$

From these equations it follows that the filtering method converges to $p(\varphi)$ as fast as the acceptance probability (5.13) is close to 1 [10].

At the end let us present the filtering function p_{filt} which is used in our simulations [102]. It is equal to:

$$p_{\text{filt}}(\varphi) = \mathcal{N}_{\text{filt}}^{-1} \exp\left(-|F| \cdot |\phi|/\pi\right). \tag{5.14}$$

This function due to the concavity of $\cos\varphi$ leads to the target distribution (5.12) much faster than the uniform filter $p_{\text{filt}} = \text{const}$. However, if $|F| \gg 1$, one has to improve the filter (5.14). Moreover, in order to accelerate the covergence of the heatbath method (5.10), (5.11), it is worth in these cases to employ the overrelaxation procedure [84] $U \to U'$:

$$U'_{x,\mu} = \left(F^{(G)}_{x,\mu} / \left|F^{(G)}_{x,\mu}\right|\right)^{-2} U^{\dagger}_{x,\mu}, \tag{5.15}$$

which leaves the gauge action (5.8) unchanged. Such overrelaxation is used in the case of the dynamical fermion two-step multiboson algorithm (see section 5.5).

5.3 Evaluation of fermion observables

5.3.1 Noisy estimator and point-like source methods

As we know from the chapter 2, fermion observables can be expressed via matrix elements of the inverse fermion operator $\mathcal{M}^{-1}$. To calculate all these elements, one needs to perform at least $\mathrm{O}(V^3)$ operations which occupies much computer time.

However, one can simplify the treatment of the inverse fermion matrix by employing a statistical method – Gaussian *noisy estimator* [60, 103]. In this method, we generate the random complex spinor vector η distributed with probability

$$p_\eta \propto \exp\left(-\eta^\dagger \eta\right). \tag{5.16}$$

Then we compute the vector ξ:

$$\xi = \mathcal{M}^{-1}\eta, \tag{5.17}$$

assuming that the matrix inversion can be done exactly. And denoting for convenience by letters a, b, etc. the common indices (x, r) where r (and also s) stand for spinor labels, one estimates the following expression:

$$\langle \xi_{a_1} \dots \xi_{a_n} \eta^\dagger_{b_1} \dots \eta^\dagger_{b_n} \rangle_\eta = \lim_{N\to\infty} \sum_{j=1}^{N} \xi^{(j)}_{a_1} \dots \xi^{(j)}_{a_n} {\eta^{(j)}_{b_1}}^\dagger \dots {\eta^{(j)}_{b_n}}^\dagger. \tag{5.18}$$

Here the $\eta^{(1)}$, $\eta^{(2)}$, etc. are statistically independent Gaussian vectors with distribution (5.16) and the average value $\langle \mathcal{O} \rangle_\eta$ of an operator $\mathcal{O} = \mathcal{O}[\eta^\dagger, \eta]$ is computed according to the equation:

$$\langle \mathcal{O} \rangle_\eta = \frac{\int \left[\mathrm{d}\eta^\dagger \mathrm{d}\eta\right] \mathcal{O}[\eta^\dagger, \eta] \exp\left(-\eta^\dagger \eta\right)}{\int \left[\mathrm{d}\eta^\dagger \mathrm{d}\eta\right] \exp\left(-\eta^\dagger \eta\right)}. \tag{5.19}$$

To evaluate the l.h.s. of equation (5.18), we use the fictitious sources method as in the case of integral (2.24) for fermionic observables. And finally we obtain:

$$\langle \xi_{a_1} \dots \xi_{a_n} \eta^\dagger_{b_1} \dots \eta^\dagger_{b_n} \rangle_\eta = \sum_\sigma \mathcal{M}^{-1}_{a_1 b_{\sigma(1)}} \dots \mathcal{M}^{-1}_{a_n b_{\sigma(n)}}, \tag{5.20}$$

where σ is a permutation of $1, \dots, n$ numbers and summation is done over all such permutations. Equations (5.16) – (5.20) constitute the noisy estimator method and allow us to compute fermion values in the integral (2.24).

The simulation of the vectors η with Gaussian distribution (5.16) is realized as follows (see also [10]). Consider the simplest one-dimensional case where one has to produce the complex numbers z distributed as $\exp(-C|z|^2)$. Their generation is based on the relation for an arbitrary function $\mathcal{O}[z^\dagger, z]$:

$$\int \left[\mathrm{d}z^\dagger \mathrm{d}z\right] \mathcal{O}[z^\dagger, z] \exp(-C|z|^2) \propto \int_{-\pi}^{\pi} \mathrm{d}\varphi \int_0^\infty \mathrm{d}\rho\rho \exp(-C\rho^2) \mathcal{O}[\rho \mathrm{e}^{-\mathrm{i}\varphi}, \rho \mathrm{e}^{\mathrm{i}\varphi}].$$

From this expression follows that the complex values $z = \sqrt{-C^{-1}\ln\xi}\mathrm{e}^{\mathrm{i}\varphi}$ are indeed distributed with the probability $\exp(-C|z|^2)$, if the real values ξ and φ are random numbers distributed uniformly on the intervals $[0,1]$ and $[-\pi,\pi]$, respectively. Now the generalization to the multidimensional case of η vectors is trivial.

An alternative to the noisy estimator method for the calculation of fermion values is the so-called *point-like source* method [104]. Here instead of random Gaussian vectors, in the case of U(1) lattice theory one has to compute the $\xi^{(s)}$ vectors (5.17) for the following 4 $\eta^{(s)}$ sources:

$$\eta_a^{(s)} = \delta_{xx_0}\delta_{rs}, \qquad a = (x,r), \qquad s = 1,\ldots,4, \tag{5.21}$$

where x_0 is an arbitrary lattice point. Then the matrix elements of the $\mathcal{M}^{-1}$ operator are expressed as follows:

$$\mathcal{M}_{ab}^{-1} = \xi_a^{(s)}, \qquad a = (x,r), \quad b = (x_0,s), \tag{5.22}$$

and in the evaluation of average fermion observables one uses the translational invariance of the lattice theory (2.21).

The point-like source method (5.21), (5.22) appears to be more precise than the noisy estimator one (5.16) – (5.20) [104]. The former method is widely used by us for the investigation of the fermion observables such as the fermion correlator (4.11), the scalar condensate (2.27) and the pion norm (2.28).

5.3.2 Conjugate gradient and Lanczos methods

For both the noisy estimator and the point-like source methods, we have to compute the ξ vector (5.17). It means that one has to solve for a given vector $\mathbf{y}$ the following linear equations system:

$$\mathbf{A}\mathbf{x} = \mathbf{y}, \tag{5.23}$$

where $\mathbf{A} > \mathbf{0}$ is some Hermitean positively defined matrix. The expression (5.17) can be transformed to this system by multiplying both sides with the positive operator $\mathcal{M}^\dagger\mathcal{M}$. Note that such a multiplication requires the knowledge of only the nearest neighbouring lattice sites to each vector point. In other words, we have a *large sparse system*.

A very popular algorithm for the fast solution of such a system (5.23) is the *conjugate gradient* (CG) method (see e.g. [10, 105]). In this method, one computes

the series of vectors $\mathbf{x}_n$ approximate to $\mathbf{x}$ according to the following scheme:

$$\begin{aligned} \mathbf{x}_{n+1} &= \mathbf{x}_n + \alpha_n \mathbf{g}_n, & \mathbf{r}_n &= \mathbf{y} - \mathbf{A}\mathbf{x}_n, \\ \mathbf{r}_{n+1} &= \mathbf{r}_n - \alpha_n \mathbf{A}\mathbf{g}_n, & \alpha_n &= \frac{\|\mathbf{r}_n\|^2}{(\mathbf{g}_n, \mathbf{A}\mathbf{g}_n)}, \\ \mathbf{g}_{n+1} &= \mathbf{r}_{n+1} + \beta_n \mathbf{g}_n, & \beta_n &= \frac{\|\mathbf{r}_{n+1}\|^2}{\|\mathbf{r}_n\|^2}, \end{aligned} \tag{5.24}$$

where the vectors $\mathbf{g}_n$ and $\mathbf{r}_n$ are called respectively gradient and residual, $n = 0, 1, \ldots$. Here, the initial residual vector $\mathbf{r}_0$ is obtained from an initial approximation $\mathbf{x}_0$ (to $\mathbf{x}$) and the initial gradient vector $\mathbf{g}_0 = \mathbf{r}_0$. The stopping criterion for the algorithm (5.24) is:

$$\|\mathbf{r}_{n+1}\| < \delta, \tag{5.25}$$

for some small value δ. The CG algorithm is constructed in such a way that the residual vectors $\mathbf{r}_n$ are mutually orthogonal. It means that this method must converge for finite number of iterations restricted by the dimension of the matrix $\mathbf{A}$. However, for the residual vectors the following estimate is valid [105]:

$$\|\mathbf{r}_n\| \leq \frac{2\rho^n}{1+\rho^{2n}}\|\mathbf{r}_0\|, \qquad \rho = \frac{\sqrt{\zeta}-1}{\sqrt{\zeta}+1}, \qquad \zeta = \frac{\lambda_{\max}(\mathbf{A})}{\lambda_{\min}(\mathbf{A})}, \tag{5.26}$$

where the $\lambda_{\max}$ and $\lambda_{\min}$ are the maximal and minimal eigenvalues of the positive matrix $\mathbf{A}$, respectively, and we note that the ζ is called the condition number. In case of $\zeta \sim 1$, the CG method (5.24) converges almost immediately. But if the condition number $\zeta \gg 1$, the rough number of CG iterations $N^{(\mathrm{CG})}$ required to reach the terminating condition (5.25) according to the estimate (5.26) looks as follows:

$$N^{(\mathrm{CG})} \simeq \frac{\sqrt{\zeta}}{2}\ln(2/\delta). \tag{5.27}$$

Let us rewrite the updating scheme (5.24) in a more elegant form. Introducing the unit vectors $\mathbf{e}_n = \mathbf{r}_n/\|\mathbf{r}_n\|$, we have:

$$\mathbf{A}\mathbf{e}_n = \left(\frac{1}{\alpha_n} + \frac{\beta_{n-1}}{\alpha_{n-1}}\right)\mathbf{e}_n - \frac{\sqrt{\beta_{n-1}}}{\alpha_{n-1}}\mathbf{e}_{n-1} - \frac{\sqrt{\beta_n}}{\alpha_n}\mathbf{e}_{n+1}, \qquad n = 0, 1, \ldots, \tag{5.28}$$

$\mathbf{e}_{-1} = \mathbf{0}$, and other vectors $\mathbf{e}_n$ are mutually orthogonal: $(\mathbf{e}_m, \mathbf{e}_n) = 0, \quad m \neq n$. It means that the $\mathbf{A}$ matrix in the orthonormal basis $\mathbf{e}$ is tridiagonal. Such tridiagonal decomposition of Hermitean operator $\mathbf{A}$ is called *Lanczos* method (see e.g. [106]).

In the usual Hermitean case the Lanczos decomposition looks as follows [106]:

$$\mathbf{A}\mathbf{e}_n = \beta_n \mathbf{e}_{n+1} + \alpha_n \mathbf{e}_n + \beta_{n-1}\mathbf{e}_{n-1}, \qquad n = 0, 1, \ldots, \tag{5.29}$$

where α and β coefficients are determined by the equations:

$$\alpha_n = (\mathbf{e}_n, \mathbf{A}\mathbf{e}_n), \qquad \beta_n = \|\mathbf{A}\mathbf{e}_n - \alpha_n \mathbf{e}_n - \beta_{n-1}\mathbf{e}_{n-1}\|, \qquad n = 0, 1, \ldots,$$

for some initial $\mathbf{e}_0$ vector when $\mathbf{e}_{-1} = \mathbf{0}$. But contrary to the CG case, this decomposition does not produce correctly all vectors $\mathbf{e}$ owing to finite computer precision. One has either to use an additional reorthogonalization of the $\mathbf{e}$ vectors, or employ some restarting procedure when the new starting Lanczos vector is a linear combination of previous ones [106] – [109].

The Lanczos decomposition (5.29) can be used for the evaluation of the smallest and largest eigenvalues of Hermitean matrices. Let us present the so-called *explicitely restarted Lanczos method* [106, 108]:

1. Take for $n = 1$ an arbitrary vector $\mathbf{e}_0^{(n)}$:

$$\|\mathbf{e}_0^{(1)}\| = 1. \tag{5.30}$$

2. Construct a set of first M Lanczos vectors for $n = 1, 2, \ldots$ until convergence:

$$\mathbf{v}^{(n)} = (\mathbf{e}_0^{(n)}, \mathbf{e}_1^{(n)}, \ldots, \mathbf{e}_{M-1}^{(n)}) \tag{5.31}$$

3. Construct the tridiagonal $M \times M$ matrix $\mathbf{T}^{(n)}$:

$$\mathbf{T}^{(n)} = {\mathbf{v}^{(n)}}^{\dagger} \mathbf{A} \mathbf{v}^{(n)}. \tag{5.32}$$

4. Compute the extremal (minimal or maximal) eigenvalue $\lambda^{(n)}$ and corresponding eigenvector $\mathbf{s}^{(n)}$ of the matrix $\mathbf{T}^{(n)}$:

$$\mathbf{T}^{(n)}\mathbf{s}^{(n)} = \lambda^{(n)}\mathbf{s}^{(n)}. \tag{5.33}$$

5. Construct an approximate eigenvector $\mathbf{x}^{(n)}$ which is a new starting vector $\mathbf{e}_0^{(n+1)}$ for the Lanczos decomposition:

$$\mathbf{x}^{(n)} = \mathbf{e}_0^{(n+1)} = \mathbf{v}^{(n)}\mathbf{s}^{(n)}. \tag{5.34}$$

6. Go to step 2 with:

$$n := n + 1. \tag{5.35}$$

In the case of $M = 2$, this method coincides with the Ritz algorithm [105] for the evaluation of smallest and largest eigenvalues. The Ritz method can be also used for fast evaluation of extremal eigenvalues $\lambda^{(n)}$ and eigenvectors $\mathbf{s}^{(n)}$ of the tridiagonal (not very large) $M \times M$ matrix $\mathbf{T}^{(n)}$. The stopping criterion for prescription (5.30) – (5.35) can be taken to be either:

$$|\lambda^{(n+1)} - \lambda^{(n)}| \leq \delta,$$

or (which is more accurate):

$$\|\mathbf{A}\mathbf{x}^{(n)} - \lambda^{(n)}\mathbf{x}^{(n)}\| \leq \delta.$$

Let us mention other restarting methods which are widely used for the investigation of a small set of eigenvalues: the *complex gradient method* for Hermitean [107, 109] and the *implicitly restarted Arnoldi method* (IRAM) for arbitrary large sparse matrices [108].

5.3.3 Even-odd decomposition

We return to the problem of the fermion matrix inversion. One notes that for the matrix $\mathcal{M}$ only nearest-neighbour coordinates to x, i.e. $x \pm \hat{\mu}$ are necessary to perform the matrix-vector multiplication. Hence we can define for all x the signature function $c(x) = \pm 1$ with the following property:

$$c(x \pm \hat{\mu}) = -c(x), \qquad \forall x, \mu.$$

The unique up to a sign solution of such an equation is:

$$c(x) = (-1)^{\sum_\mu x_\mu}. \tag{5.36}$$

On a finite lattice, with the identification of the points x and $x \pm N_\mu \hat{\mu} \;\; \forall \mu$, one requires that all N_μ must be *even* numbers. This explains why we take even lattice sizes N_s and N_4. After the definition of the function $c(x)$ we will call x an *even* point if $c(x) = 1$ and *odd* otherwise [110].

Using such a definition of even-odd sites, one can represent the Wilson matrix $\mathcal{M}$ (2.18) in the following way:

$$\mathcal{M} = \begin{bmatrix} \mathbf{1}_{\mathrm{e}} & \mathcal{M}_{\mathrm{eo}} \\ \mathcal{M}_{\mathrm{oe}} & \mathbf{1}_{\mathrm{e}} \end{bmatrix}, \tag{5.37}$$

where $\mathbf{1}_{\mathrm{e}}$ is unity in the even or odd subspace, and $\mathcal{M}_{\mathrm{eo}}$ and $\mathcal{M}_{\mathrm{oe}}$ are even and odd parts of (2.18) matrix, respectively. Note that from this decomposition and γ_5-Hermiticity (2.20) of the Wilson fermion matrix it follows that:

$$\mathcal{M}_{\mathrm{eo}} = \gamma_5 \mathcal{M}_{\mathrm{oe}}^{\dagger} \gamma_5. \tag{5.38}$$

And the linear equation for the ξ vector (5.17) can be written as follows:

$$\left\{ \begin{array}{rcl} \xi_{\mathrm{e}} + \mathcal{M}_{\mathrm{eo}} \xi_{\mathrm{o}} & = & \eta_{\mathrm{e}} \\ \mathcal{M}_{\mathrm{oe}} \xi_{\mathrm{e}} + \xi_{\mathrm{o}} & = & \eta_{\mathrm{o}} \end{array} \right. . \tag{5.39}$$

where we decompose vectors ξ and η onto even and odd parts. This means that one can solve the equivalent system:

$$\left\{ \begin{array}{rcl} \mathbf{Q}^{\dagger}\mathbf{Q}\xi_{\mathrm{o}} & = & \mathbf{Q}^{\dagger}(\eta_{\mathrm{o}} - \mathcal{M}_{\mathrm{oe}}\eta_{\mathrm{e}}) \\ \xi_{\mathrm{e}} & = & \eta_{\mathrm{e}} - \mathcal{M}_{\mathrm{eo}}\xi_{\mathrm{o}} \end{array} \right. , \tag{5.40}$$

where we have denoted

$$\mathbf{Q} = \mathbf{1}_{\mathrm{e}} - \mathcal{M}_{\mathrm{oe}}\mathcal{M}_{\mathrm{eo}}. \tag{5.41}$$

Let us note that for the even-odd represented matrix $\mathcal{M}$ (5.37)

$$\det \mathcal{M} = \det \mathbf{Q}. \tag{5.42}$$

It turns out to be better to work with the $\mathbf{Q}^{\dagger}\mathbf{Q}$ matrix rather than with $\mathcal{M}^{\dagger}\mathcal{M}$ [111]. Indeed, suppose that λ is an eigenvalue of $\mathcal{M}$ i.e. for some nonzero complex spinor vector Ψ:

$$\mathcal{M}\Psi = \lambda\Psi.$$

Then in terms of even-odd decomposition:

$$\left\{ \begin{array}{rcl} \Psi_{\mathrm{e}} + \mathcal{M}_{\mathrm{eo}}\Psi_{\mathrm{o}} & = & \lambda\Psi_{\mathrm{e}} \\ \Psi_{\mathrm{o}} + \mathcal{M}_{\mathrm{oe}}\Psi_{\mathrm{e}} & = & \lambda\Psi_{\mathrm{o}} \end{array} \right. ,$$

or using the matrix $\mathbf{Q}$:

$$\left\{ \begin{array}{rcl} \mathbf{Q}\Psi_{\mathrm{o}} & = & 2\lambda(1-\lambda/2)\Psi_{\mathrm{o}} \\ \Psi_{\mathrm{e}} & = & (\lambda-1)^{-1}\mathcal{M}_{\mathrm{eo}}\Psi_{\mathrm{o}} \end{array} \right. .$$

Hence the matrix $\mathbf{Q}$ has the corresponding eigenvalue $2\lambda(1-\lambda/2)$. Thus, if λ is the smallest eigenvalue (by magnitude) then the respective eigenvalue for $\mathbf{Q}$ is approximately twice larger. In case of $\kappa \sim 1/8$, the largest eigenvalue $\lambda \sim 1$.

Hence, the condition number ζ for the $\mathbf{Q}^\dagger\mathbf{Q}$ matrix is ~ 2 times smaller than that for the $\mathcal{M}^\dagger\mathcal{M}$ operator. And according to the estimate (5.27), the CG algorithm for $\mathbf{Q}^\dagger\mathbf{Q}$ converges $\sim\sqrt{2}$ faster than for the $\mathcal{M}^\dagger\mathcal{M}$ matrix.

Thus, to obtain the inverse vector ξ (5.17), we apply the CG method to get the odd part $\xi_{\rm o}$ of vector ξ in the upper equation of the system (5.40). Then it is not difficult to find the even part $\xi_{\rm e}$.

5.4 Dynamical fermions: the hybrid Monte Carlo method

5.4.1 Formulation of the method

In the dynamical fermion case with $N_f = 2$ fermion flavours, one has to generate gauge configurations U distributed with weight

$$\mathbf{m}[U] \propto \exp(-S_G[U])\det{}^2\mathcal{M}[U]. \tag{5.43}$$

The most popular algorithm for simulations of this weight is the *hybrid Monte Carlo* (HMC) method [39, 40]. Below we describe its main constituents.

First of all one notes, that due to the γ_5-Hermiticity property (2.20) of the Wilson fermion matrix $\mathcal{M}$, the determinant $\det{}^2\mathcal{M}$ can be factorized as follows [60, 103]:

$$\det{}^2\mathcal{M} = \det\left(\mathcal{M}^\dagger\mathcal{M}\right) \propto \int[\mathrm{d}\chi^\dagger\mathrm{d}\chi]\exp\left\{-\chi^\dagger\left(\mathcal{M}^\dagger\mathcal{M}\right)^{-1}\chi\right\}, \tag{5.44}$$

where the auxiliary complex spinor variables $\chi^\dagger$, χ are called pseudofermions.

Plugging the l.h.s. of equation (5.44) into the integral (2.24) for average observables in case of $N_f = 2$ flavours, one can represent this integral in the following form [112, 113]:

$$\langle\mathcal{O}\rangle = \frac{1}{Z}\int[\mathrm{d}U][\mathrm{d}\Pi][\mathrm{d}\chi^\dagger\mathrm{d}\chi]\mathcal{O}[U]\exp(-H[U,\Pi,\chi^\dagger,\chi]), \tag{5.45}$$

where the functional

$$H[U,\Pi,\chi^\dagger,\chi] = \frac{1}{2}\Pi^2 + S_G[U] + \chi^\dagger\left(\mathcal{M}^\dagger[U]\mathcal{M}[U]\right)^{-1}\chi \tag{5.46}$$

is called the Hamiltonian and we denote

$$\Pi^2 = \sum_{x,\mu}\Pi^2_{x,\mu},$$

where the auxiliary real field $\Pi = \{\Pi_{x,\mu}\}$ is called the adjoint momentum to the gauge field U.

The integral (5.45) is the core of the hybrid Monte Carlo algorithm. In this algorithm, one generates the series of sampled gauge configurations $U^{(1)}$, $U^{(2)}$, etc. distributed with the weight $\exp(-H)$. Here a new configuration U' is obtained from previous U one according to the following prescription.

We select the initial random momentum Π according to the Gaussian distribution:

$$p_\Pi \propto \exp\left(-\frac{1}{2}\Pi^2\right), \tag{5.47}$$

and choose the pseudofermion fields $\chi^\dagger, \chi$ randomly with respect to the weight:

$$p_\chi[U] \propto \det{}^{-2}\mathcal{M} \exp\left\{-\chi^\dagger \left(\mathcal{M}^\dagger\mathcal{M}\right)^{-1}\chi\right\}, \qquad \mathcal{M} = \mathcal{M}[U]. \tag{5.48}$$

The latter fields are taken merely as $\chi = \mathcal{M}^\dagger[U]\eta$, where η is the Gaussian vector distributed as (5.16). Then one performs the discrete Hamilton (or molecular, called also leapfrog) dynamics $\{U, \Pi\} \to \{U', \Pi'\}$ [112, 113, 40]. We solve for the compact U(1) gauge field $U = \exp(\mathrm{i}A)$ (2.7) and its adjoint momentum Π the following second order discrete equation of motion system with N_τ time steps where the time step size $\Delta\tau = \Delta t/N_\tau$ for some auxiliary time period Δt. First, one performs the initial step for the adjoint momentum:

$$\Pi_{1/2} = \Pi_0 + \frac{\Delta\tau}{2}F[A_0]. \tag{5.49}$$

For the next time steps with number $j = 1, \ldots, N_\tau - 1$, the gauge and adjoint momentum variables are updated via the following rule:

$$A_j = A_{j-1} + \Delta\tau\Pi_{j-1/2} \mod 2\pi, \qquad \Pi_{j+1/2} = \Pi_{j-1/2} + \Delta\tau F[A_j]. \tag{5.50}$$

And in the final step for the gauge and adjoint momentum:

$$A_{N_\tau} = A_{N_\tau-1} + \Delta\tau\Pi_{N_\tau-1/2} \mod 2\pi, \qquad \Pi_{N_\tau} = \Pi_{N_\tau-1/2} + \frac{\Delta\tau}{2}F[A_{N_\tau}], \tag{5.51}$$

Here we omitted for convenience the link number (x, μ) and denoted initial (at $j = 0$) and final (for $j = N_\tau$) variables as follows:

$$A_0, \Pi_0 = A, \Pi, \qquad A_{N_\tau}, \Pi_{N_\tau} = A', \Pi',$$

where the gauge force $F[A] = -\partial H/\partial A$ is determined by the expression:

$$F[A] = 2\,\mathrm{Re}\left\{X^\dagger \frac{\partial\mathcal{M}}{\partial A}Y\right\} - \frac{\partial S_G}{\partial A}, \qquad X = \left(\mathcal{M}^\dagger\right)^{-1}\chi, \qquad Y = \mathcal{M}^{-1}X, \tag{5.52}$$

and the pseudofermion fields $\chi^\dagger$, χ are kept fixed during this dynamics.

The discrete molecular dynamics (5.49) – (5.51) violates the energy conservation law for Hamiltonian (5.46):

$$H[U', \Pi', \chi^\dagger, \chi] \neq H[U, \Pi, \chi^\dagger, \chi].$$

This Hamiltonian is conserved only in the limit $\Delta\tau \to 0$. Then in order to maintain the desired weight $\exp(-H)$, one has to introduce the last, Metropolis accept-reject step for Hamiltonian. The new gauge configuration U' is accepted with the probability

$$w_{\rm acc}[U', \Pi'; U, \Pi] = \min\left(1, \mathrm{e}^{-\Delta H}\right), \tag{5.53}$$

where $\Delta H = H[U', \Pi', \chi^\dagger, \chi] - H[U, \Pi, \chi^\dagger, \chi]$.

The combination of successive steps (5.47) – (5.53) is called the hybrid Monte Carlo method. Let us show that it indeed generates the gauge configurations distributed according to weight (5.43) [10]. First of all, one notes that the forward and backward transition probabilities for the gauge variables are proportional to the corresponding adjoint momentum distribution weights (5.47):

$$\tilde{p}[U', U] \propto \exp\left(-\frac{1}{2}\Pi^2\right)\left|\det\frac{\partial\Pi}{\partial A'}\right|, \quad \tilde{p}[U, U'] \propto \exp\left(-\frac{1}{2}\Pi'^2\right)\left|\det\frac{\partial\Pi'}{\partial A}\right|. \tag{5.54}$$

Further, we must prove that the leapfrog scheme (5.49) – (5.51) satisfies the area preserving law:

$$\det\begin{pmatrix} \frac{\partial A'}{\partial A} & \frac{\partial A'}{\partial \Pi} \\ \frac{\partial \Pi'}{\partial A} & \frac{\partial \Pi'}{\partial \Pi} \end{pmatrix} = 1, \tag{5.55}$$

from which follows the reversibility relation:

$$\left|\det\frac{\partial\Pi}{\partial A'}\right| = \left|\det\frac{\partial\Pi'}{\partial A}\right|. \tag{5.56}$$

The definition of the adjoint momentum at the time step with number j:

$$\Pi_j = \frac{1}{2}\Big\{\Pi_{j+1/2} + \Pi_{j-1/2}\Big\},$$

where $j = 1, \ldots, N_\tau - 1$, allows us to rewrite the equations (5.49) – (5.51) in the following compact form:

$$\begin{aligned} A_{j+1} &= A_j + \Delta\tau\Pi_j + \frac{1}{2}(\Delta\tau)^2 F[A_j] \mod 2\pi, \\ \Pi_{j+1} &= \Pi_j + \frac{1}{2}\Delta\tau\left(F[A_j] + F[A_{j+1}]\right), \qquad j = 0, \ldots, N_\tau - 1. \end{aligned} \tag{5.57}$$

Direct calculations based of the equations (5.57) show that for elementary discrete steps the area preserving law is fulfilled:

$$\det \begin{pmatrix} \frac{\partial A_{j+1}}{\partial A_j} & \frac{\partial A_{j+1}}{\partial \Pi_j} \\ \frac{\partial \Pi_{j+1}}{\partial A_j} & \frac{\partial \Pi_{j+1}}{\partial \Pi_j} \end{pmatrix} = 1. \tag{5.58}$$

Multiplying the equations (5.58) for each time steps $j = 0, \ldots, N_\tau - 1$, one gets the relation (5.55) for the total transition dynamics $\{U, \Pi\} \to \{U', \Pi'\}$.

Now using equations (5.48) for the pseudofermion distribution, (5.54) for the molecular dynamics transition probabilities, (5.56) for reversibility relation and (5.53) for the accept-reject step, we can convince ourselves that the total transition probability of the hybrid Monte Carlo algorithm, $p = w_{\mathrm{acc}} \tilde{p} p_\chi$ satisfies the detailed balance relation (5.5) with $N_f = 2$ dynamical fermion weight (5.43). This completes the proof.

So far in the description of the hybrid Monte Carlo algorithm we have tacitly assumed that the inverse fermion matrix $\mathcal{M}^{-1}$ is known in advance. However since the exact matrix inversion is time consuming, one uses fast but approximate inversion methods e.g. conjugate gradient one (5.24) applied to even-odd decomposed system (5.39) for the evaluation of the X and Y vectors in the HMC force (5.52) and also for the $(\mathcal{M}^\dagger[U'])^{-1}\chi$ vector in the updated Hamiltonian $H[U', \Pi', \chi^\dagger, \chi]$ in the accept-reject step (5.53). This means that the hybrid Monte Carlo method is *approximate* owing to the lack of exactness in the inversion of the fermion matrix. Nevertheless, the accuracy of the hybrid Monte Carlo algorithm using the CG method can be controlled by an appropriate selection of the δ parameters in the stopping criteria (5.25): δ_{md} for molecular dynamics process (5.49) – (5.51) and δ_{acc} for accept-reject step (5.53). Later on we present a recipe for choosing such parameters [114, 115].

5.4.2 Acceptance rate

Let us now consider the problem of new configuration acceptance in the discrete hybrid Monte Carlo dymamics [116]. For the leapfrog dynamics (5.49) – (5.51), the variation of Hamiltonian ΔH in (5.53) satisfies the following relation:

$$\left\langle \mathrm{e}^{-\Delta H} \right\rangle = 1, \tag{5.59}$$

where the averaging $\langle \ldots \rangle$ is performed according to the equation (5.45). To prove it, one uses the area preserving law (5.55). Then owing to the convexity of the exponent function,

$$\left\langle \mathrm{e}^{-\Delta H} \right\rangle \geq \mathrm{e}^{-\langle \Delta H \rangle}.$$

The latter inequality together with (5.59) means that the average Hamiltonian variance $\langle \Delta H \rangle$ in the hybrid Monte Carlo dynamics is always non-negative: $\langle \Delta H \rangle \geq 0$. Equality can be achieved only in case of exact Hamilton dynamics.

For very small time step size $\Delta\tau$ in the leapfrog dynamics, one may use the Taylor expansion of the exponent in the equation (5.59). In the leading order one gets:

$$\langle \Delta H \rangle = \frac{1}{2} \left\langle (\Delta H - \langle \Delta H \rangle)^2 \right\rangle + \mathrm{O}\left(\langle |\Delta H| \rangle^3 \right). \tag{5.60}$$

Hence in the $\Delta\tau \to 0$ limit, the probability distribution of ΔH value can be well approximated by the Gaussian function:

$$p_{\Delta H}(x) \simeq \frac{1}{4\pi \langle \Delta H \rangle} \mathrm{e}^{-(x - \langle \Delta H \rangle)^2 / 4 \langle \Delta H \rangle}.$$

And the average value of acceptance rate (5.53) $\langle w_{\mathrm{acc}} \rangle$ is approximately equal to [116]:

$$\langle w_{\mathrm{acc}} \rangle \simeq \int \mathrm{d}x p_{\Delta H}(x) \min\left(1, \mathrm{e}^{-x}\right) = \mathrm{erfc}\left(\sqrt{\langle \Delta H \rangle}/2\right) \approx 1 - \sqrt{\langle \Delta H \rangle / \pi}. \tag{5.61}$$

At the same time, in the 2nd order discrete molecular dynamics scheme (5.49) – (5.51) the sampling variance $\Delta H \propto (\Delta\tau)^2$ [40]. Therefore, in order to keep the acceptance rate (5.61) close to 1, one would require owing to (5.60) that $V(\Delta\tau)^4 \propto 1$ [116]. But it is also necessary to take into account the magnitude of the gauge force (5.52) which is not small in the case of large condition number ζ (2.30). We will return to this question at the investigation of performance of the HMC algorithm.

5.4.3 Advantages and shortcomings

There are several merits of the HMC algorithm. First of all, it requires the knowledge of only a few parameters. Namely, we must set $\Delta\tau$, N_τ, and the conjugate gradient stopping criteria (5.25) δ_{md} and δ_{acc} for the fermion matrix inversions in the leapfrog dynamics steps (5.49) – (5.51) and in the Metropolis accept-reject one (5.53), respectively. It does not need to find all elements of the inverse fermion

matrix $\mathcal{M}^{-1}$ since the CG (5.24) performs this indirectly and fast enough. And the convergence of the HMC, controlled mainly by acceptance rate (5.61), can be tuned by plausible choice of the molecular dynamics parameters $\Delta\tau$, N_τ [114, 115].

However, the precision of the equation of motion in case of very large lattices may get lost which leads to false generated gauge configurations [117, 118]. Further, the CG method owing to the computer precision limitation does not work properly in case of a large condition number ζ (see e.g. [117, 118]). This happens e.g. for the above mentioned confinement phase near the chiral limit line and for the Aoki phase in case of compact QED theory [77]. The main disadvantage of the HMC algorithm is that it can be used due to the pseudofermion factorization (5.44) only for an even number of fermion flavours in spite of various proposals to implement it for odd N_f values (see e.g. [40, 119, 120]).

That is why one requires an alternative to the hybrid Monte Carlo method, which allows us to simulate the gauge configurations for odd (and possibly for *arbitrary*) N_f fermion flavours.

5.5 Dynamical fermions: the two-step multiboson algorithm

5.5.1 First step: the multiboson method

One of the alternatives to the HMC method is the two-step multiboson (TSMB) algorithm [36] – [38]. It consists of two basic parts. Its first part is the *multiboson* method proposed by M. Lüscher [121] (see also [122]). The idea of the method is to approximate the fermion determinant by the inverse determinant of a local positive polynomial operator which can be easily factorized by a set of complex spinor fields called multibosons. To do this, one has to approximate the $x^{-N_f/2}$ function by an appropriate polynomial $P_1(x)$ for $x > 0$:

$$x^{-N_f/2} \simeq P_1(x) = c_{n_1} \prod_{j=1}^{n_1/2} (x - r_j)(x - r_j^\dagger), \qquad \mathrm{Im}\, r_j > 0, \qquad n_1 \text{ is even.} \quad (5.62)$$

Using this starting approximation, one can evaluate the x^{-N_f} function by the following polynomial:

$$x^{-N_f} \simeq P_1(x^2) = c_{n_1} \prod_{j=1}^{n_1} (x - \rho_j)(x - \rho_j^\dagger), \qquad x > 0, \quad (5.63)$$

where $\quad \rho_j^2 = r_j, \quad \rho_{j+n_1/2} = -\rho_j^\dagger, \quad \mathrm{Im}\,\rho_j \geq 0, \quad j = 1, \ldots, n_1/2.$

We know from section 5.3 that in order to improve the efficiency of a simulation method involving a fermion determinant it is worthwhile to work with a preconditioned fermion matrix [110, 111]. Taking into account the equality (5.42) for the determinant of even-odd decomposed matrix $\mathbf{Q}$ (5.41) and the polynomial approximation (5.63), one approximates the modulus of the fermion determinant power as follows [123]:

$$\left|\det{}^{N_f}\mathcal{M}\right| \propto \left\{\det P_1(\mathbf{Q}^\dagger\mathbf{Q})\right\}^{-1} \propto \left\{\prod_{j=1}^{n_1} \det\left(\gamma_5\mathbf{Q} - \rho_j\right)^\dagger \det\left(\gamma_5\mathbf{Q} - \rho_j\right)\right\}^{-1}. \tag{5.64}$$

Remembering the equation for the block matrix determinant, one notes that

$$\det\left(\gamma_5\mathbf{Q} - \rho_j\right) = \det\hat{\mathcal{M}}_j, \tag{5.65}$$

where the matrix $\hat{\mathcal{M}}_j$ looks as:

$$\hat{\mathcal{M}}_j = \begin{bmatrix} \mathbf{1}_\mathrm{e} & \mathcal{M}_\mathrm{eo} \\ \gamma_5\mathcal{M}_\mathrm{oe} & (\gamma_5 - \rho_j)\,\mathbf{1}_\mathrm{e} \end{bmatrix}. \tag{5.66}$$

Substituting (5.65) into the r.h.s. of equation (5.64), one factorizes the determinant power as follows [123]:

$$\left|\det{}^{N_f}\mathcal{M}[U]\right| \propto \left\{\det P_1(\mathbf{Q}^\dagger\mathbf{Q})\right\}^{-1} \propto \int \left[\mathrm{d}\Phi^\dagger\mathrm{d}\Phi\right] \exp\left(-S_B[\Phi, U]\right). \tag{5.67}$$

Here S_B is the multiboson field action:

$$S_B[\Phi, U] = \sum_{j=1}^{n_1} \Phi_j^\dagger(\hat{\mathcal{M}}_j^\dagger\hat{\mathcal{M}}_j)\Phi_j, \qquad \hat{\mathcal{M}}_j = \hat{\mathcal{M}}_j[U], \tag{5.68}$$

and the fields Φ_j are complex spinor variables called as multibosons.

Using this representation one can define the integral for average observables in the multiboson method:

$$\langle\mathcal{O}\rangle_1 = \frac{1}{Z}\int \left[\mathrm{d}U\right]\left[\mathrm{d}\Phi^\dagger\mathrm{d}\Phi\right] \mathcal{O}[U] \exp(-S[\Phi, U]), \tag{5.69}$$

where the total action of multiboson and gauge fields [121, 122]:

$$S[\Phi, U] = S_B[\Phi, U] + S_G[U]. \tag{5.70}$$

One has to reduce the matrix $\hat{\mathcal{M}}_j$ in (5.68) to an analysable form. Let us introduce first the even-odd subspace projectors:

$$\mathbf{\Pi}_+ = \begin{bmatrix} \mathbf{1}_{\mathrm{e}} & \mathbf{0} \\ \mathbf{0} & \mathbf{0} \end{bmatrix}, \qquad \mathbf{\Pi}_- = \begin{bmatrix} \mathbf{0} & \mathbf{0} \\ \mathbf{0} & \mathbf{1}_{\mathrm{e}} \end{bmatrix}. \tag{5.71}$$

These projectors in the lattice coordinate representation according to (5.36) look like

$$(\mathbf{\Pi}_\pm)_{xy} = \frac{1 \pm (-1)^{\sum_\mu x_\mu}}{2} \delta_{xy}. \tag{5.72}$$

The projectors (5.71) have the following properties:

$$\mathbf{\Pi}_\pm^2 = \mathbf{\Pi}_\pm, \qquad \mathbf{\Pi}_\pm \mathbf{\Pi}_\mp = \mathbf{0}, \qquad \mathbf{\Pi}_+ + \mathbf{\Pi}_- = \mathbf{1}, \qquad \mathbf{\Pi}_\pm (\mathbf{1} - \mathcal{M}) = (\mathbf{1} - \mathcal{M}) \mathbf{\Pi}_\mp,$$

Using (5.71) we find a representation for $\hat{\mathcal{M}}_j$ defined by equation (5.66):

$$\hat{\mathcal{M}}_j = \mathbf{\Pi}_+ \mathcal{M} + \mathbf{\Pi}_- \gamma_5 \mathcal{M} - \rho_j \mathbf{\Pi}_-. \tag{5.73}$$

Taking into account expression (5.73), the coordinate representation (5.72) and the properties of projectors (5.71), one can write down an algorithm of local scalar and gauge fields updates. To do this, we must first extract terms related to the element Φ_{jxr} for each j, x, r coordinate (r and also s denote spinor indices), then to each $U_{x,\mu}$ component of the U set. For the former case we have:

$$S_B[\Phi, U] = A_{jxr} \left| \Phi_{jxr} + \frac{V_{jxr}}{A_{jxr}} \right|^2 + (\text{terms, independent of } \Phi_{jxr}). \tag{5.74}$$

Here we denote A_{jxr} and V_{jxr} as follows:

$$V_{jxr} = \kappa \sum_{\mu,s} \Big\{ U^\dagger_{x-\hat{\mu},\mu} \Big(\left[\rho_{jx} \gamma_5 (1+\gamma_\mu) - 2\right]_{rs} \Phi_{j,x-\hat{\mu},s} + \left[\gamma_5 (1+\gamma_\mu)\right]_{rs} \chi_{j,x-\hat{\mu},\mu s} \Big) +$$
$$+ U_{x,\mu} \Big(\left[\rho_{jx} \gamma_5 (1-\gamma_\mu) - 2\right]_{rs} \Phi_{j,x+\hat{\mu},s} + \left[\gamma_5 (1-\gamma_\mu)\right]_{rs} \chi_{j,x+\hat{\mu},\mu s} \Big) \Big\},$$
$$A_{jxr} = 1 + 4 \times 4\kappa^2 + \frac{1 - (-1)^{\sum_\mu x_\mu}}{2} \Big\{ |\rho_j|^2 - 2 \left[\gamma_5\right]_{rr} \operatorname{Re} \rho_j \Big\},$$

where

$$\chi_{jx\mu r} = \kappa \sum_{\substack{\nu,s \\ \nu \neq \mu}} \Big\{ \left[\gamma_5 (1-\gamma_\nu)\right]_{rs} U_{x,\nu} \Phi_{j,x+\hat{\nu},s} + \left[\gamma_5 (1+\gamma_\nu)\right]_{rs} U^\dagger_{x-\hat{\nu},\nu} \Phi_{j,x-\hat{\nu},s} \Big\},$$
$$\rho_{jx} = \frac{1 + (-1)^{\sum_\mu x_\mu}}{2} \rho_j + \frac{1 - (-1)^{\sum_\mu x_\mu}}{2} \rho_j^\dagger.$$

We use such a representation of Dirac matrices in which the γ_5 matrix is diagonal i.e. it has the only nonzero components $[\gamma_5]_{rr} = \pm 1$.

For the latter case, one gets:

$$S_B[\Phi, U] = -\,\mathrm{Re}\,\left(U_{x,\mu} F^{(B)}_{x,\mu}\right) + (\text{terms, independent of } U_{x,\mu})\,, \tag{5.75}$$

where we denoted the complex multiboson force by

$$F^{(B)}_{x,\mu} = -2\kappa \sum_{jrs} \Big\{ \left[\gamma_5 \left(1 - \gamma_\mu\right)\right]_{rs} \Big(\rho_{jx} \Phi^\dagger_{jxr} \Phi_{j,x+\hat{\mu},s} + \Phi^\dagger_{jxr} \chi_{j,x+\hat{\mu},\mu s} + \\ + \chi^\dagger_{jx\mu r} \Phi_{j,x+\hat{\mu},s} \Big) - 2\delta_{rs} \Phi^\dagger_{jxr} \Phi_{j,x+\hat{\mu},s} \Big\}.$$

Remembering the expression for the gauge action (5.8) and for the gauge force $F^{(G)}_{x,\mu}$ (5.9) in the pure gauge heatbath update (5.10), (5.11), one can present the total multiboson action (5.70) as follows:

$$S[\Phi, U] = -\,\mathrm{Re}\,\left(U_{x,\mu} F_{x,\mu}\right) + (\text{terms, independent of } U_{x,\mu})\,, \tag{5.76}$$

where the total force $F_{x,\mu} = F^{(B)}_{x,\mu} + F^{(G)}_{x,\mu}$.

Equations (5.74) and (5.76) allow us to use the following updating algorithm for scalar Φ and for gauge U fields, respectively. We perform first the multiboson field updates at the fixed U field configuration:

– N_{BH} multiboson field heatbath sweeps for each point (jxr):

$$\Phi'_{jxr} = -\frac{V_{jxr}}{A_{jxr}} + \xi_{jxr}, \tag{5.77}$$

where ξ_{jxr} is a complex Gaussian random number distributed according to:

$$p_\xi \propto \exp\left(-A_{jxr}\,|\xi_{jxr}|^2\right).$$

– N_{BO} multiboson field overrelaxation sweeps:

$$\Phi'_{jxr} = -\Phi_{jxr} - 2\frac{V_{jxr}}{A_{jxr}}. \tag{5.78}$$

Now perform for fixed multiboson fields Φ the gauge field updates which resemble to the pure gauge ones (5.10), (5.15):

– N_{GH} gauge field heatbath sweeps for each link (x, μ):

$$U'_{x,\mu} = \left(F_{x,\mu}/|F_{x,\mu}|\right)^{-1} \exp(\mathrm{i}\eta_{x,\mu}), \tag{5.79}$$

where $\eta_{x,\mu}$ is a real random number in the interval $(-\pi, \pi]$ distributed as

$$p_\eta \propto \exp\left(|F_{x,\mu}| \cos \eta_{x,\mu}\right),$$

and for the generating such numbers we use the filtering method (5.13) with the filter (5.14).

– N_{GO} gauge field overrelaxation sweeps:

$$U'_{x,\mu} = U^\dagger_{x,\mu} \left(F_{x,\mu}/|F_{x,\mu}|\right)^{-2}. \tag{5.80}$$

Using arguments similar to the quenched heatbath case one can prove that each of the steps (5.77) – (5.80) $\{\Phi, U\} \to \{\Phi', U'\}$ with a transition density $p_1[\Phi', U', \Phi, U]$ satisfies the detailed balance relation:

$$p_1[\Phi', U', \Phi, U] \exp(-S[\Phi, U]) = p_1[\Phi, U, \Phi', U'] \exp(-S[\Phi', U']). \tag{5.81}$$

Hence, the updating algorithm (5.77) – (5.80) (called also multiboson method) indeed generates both the gauge and the multiboson field configurations with the weight $\exp(-S_B[\Phi, U])$ in integral (5.69).

All these steps require nearest-neighbouring indices to certain (jxr) or $(x\mu)$ point, hence the multiboson method belongs to a class of *local* algorithms. It allows us to provide efficient vector or parallel simulation with the appropriate ordering of the above indices. In our realization, each component of the coordinate indices x for the multiboson updating steps (5.77), (5.78) is split into even and odd constituents. One performs first even coordinate projection sweeps then odd ones, at certain polynomial j and spinor r indices [124]. Such sweeps are *independent*, because due to (5.74) the updated multiboson field Φ at the certain index x depends only on the fixed fields Φ at coordinates $x \pm \hat{\mu}$ and $x \pm \hat{\mu} \pm \hat{\nu}$, where $\mu \neq \nu$. Moreover, one can perform *independent* polynomial index sweeps. For *independent* gauge updating sweeps (5.79), (5.80) we widely use the even-odd decomposition (5.36) due to the representation (5.76) with notations in (5.9), (5.74) and (5.75) and perform first even then odd coordinate gauge updates at the fixed μ direction.

5.5.2 Second step: noisy correction

The algorithm (5.77) – (5.80) assumes a very good approximation (5.62) of the x^{-N_f} function. In practice however, this requires very large polynomial orders n_1 which strongly increase the computational efforts [123, 125, 126]. In order to

cure the problem, one uses a second step after the multiboson method – the noisy correction accept-reject step [36, 127, 128].

To realize this idea, first of all, let us approximate the $x^{-N_f/2}$ function by the product of *two* polynomials but not one as earlier:

$$x^{-N_f/2} \approx P_1(x)P_2(x), \tag{5.82}$$

where the first polynomial $P_1(x)$ appoximates the $x^{-N_f/2}$ function but with *not* very high accuracy. However, the second polynomial $P_2(x)$ of order $n_2 \gg n_1$ improves the approximation by the first polynomial of the $x^{-N_f/2}$ function. At the same time, it is assumed to take values which are not very different from 1.

Using the approximation (5.82) and adopting the multiboson realization (5.64), (5.68) of the fermion determinant power with respect to the P_1 polynomial where one takes into account the equality (5.42) for even-odd decomposed fermion matrix $\mathbf{Q}$, we can correct the measure in the integral (5.69) as follows [36, 127, 128]:

$$\langle \mathcal{O} \rangle_{12} = \frac{1}{Z} \int \left[\mathrm{d}U \right] \left[\mathrm{d}\Phi^\dagger \mathrm{d}\Phi \right] \mathcal{O}[U] \exp(-S[\Phi, U]) \det{}^{-1} P_2(\mathbf{Q}^\dagger \mathbf{Q}[U]). \tag{5.83}$$

In order to generate the gauge configurations with the measure in the integral (5.83), one performs first the multiboson updates $\{\Phi, U\} \to \{\Phi', U'\}$ according to the prescription (5.77) – (5.80), then the new gauge configuration U' accepted with some probability $w_{\mathrm{acc}}[U', U]$. The total transition probability $p_{12} = w_{\mathrm{acc}} p_1$, where p_1 is a multiboson transition function, has to satisfy the detailed balance condition:

$$\begin{aligned} p_{12}[\Phi', U', \Phi, U] \exp(-S[\Phi, U]) \det{}^{-1} P_2(\mathbf{Q}^\dagger \mathbf{Q}[U]) = \\ = p_{12}[\Phi, U, \Phi', U'] \exp(-S[\Phi', U']) \det{}^{-1} P_2(\mathbf{Q}^\dagger \mathbf{Q}[U']). \end{aligned} \tag{5.84}$$

Owing to the detailed balance equation (5.81) for the multiboson transition density p_1, the acceptance probability function w_{acc} must obey the relation:

$$w_{\mathrm{acc}}[U', U] \det{}^{-1} P_2(\mathbf{Q}^\dagger \mathbf{Q}[U]) = w_{\mathrm{acc}}[U, U'] \det{}^{-1} P_2(\mathbf{Q}^\dagger \mathbf{Q}[U']). \tag{5.85}$$

A usual choice for such a function is the Metropolis one [36, 127, 128]:

$$w_{\mathrm{acc}}[U', U] = \min \left(1, \frac{\det P_2(\mathbf{Q}^\dagger \mathbf{Q}[U])}{\det P_2(\mathbf{Q}^\dagger \mathbf{Q}[U'])} \right). \tag{5.86}$$

It is not difficult to check that the acceptance probability (5.86) fulfills the relation (5.85) and therefore the total transition density p_{12} satisfies detailed balance (5.84), indeed.

We have to compute the determinant ratio in the equation (5.86). For this purpose, one can use the noisy estimator technique [60, 103] for the inverse determinant of any positive matrix. Thus we can write [36, 127, 128]

$$\frac{\det P_2(\mathbf{Q}^\dagger\mathbf{Q}[U])}{\det P_2(\mathbf{Q}^\dagger\mathbf{Q}[U'])} = \frac{\int[\mathrm{d}\eta^\dagger\mathrm{d}\eta]\exp(-\eta^\dagger P_2(\mathbf{Q}^\dagger\mathbf{Q}[U'])\eta)}{\int[\mathrm{d}\eta^\dagger\mathrm{d}\eta]\exp(-\eta^\dagger P_2(\mathbf{Q}^\dagger\mathbf{Q}[U])\eta)},$$

where η is an arbitrary complex spinor vector in the even (odd) subspace. Making the following substitution of integration variables for both numerator and denominator integrals [36]:

$$\eta \to \xi = P_2^{-1/2}(\mathbf{Q}^\dagger\mathbf{Q}[U])\eta \tag{5.87}$$

we get the final expression for the determinant ratio:

$$\frac{\det P_2(\mathbf{Q}^\dagger\mathbf{Q}[U])}{\det P_2(\mathbf{Q}^\dagger\mathbf{Q}[U'])} = \left\langle \exp\left(-\xi^\dagger P_2(\mathbf{Q}^\dagger\mathbf{Q}[U'])\xi + \eta^\dagger\eta\right)\right\rangle_\eta, \tag{5.88}$$

where the noisy estimator averaging is defined according to equation (5.19).

For practical evaluations of ξ vectors defined in (5.87), one can approximate the $P_2^{-1/2}(x)$ function by some polynomial $P_3(x)$ with order n_3 [36]:

$$P_3(x) \approx P_2^{-1/2}(x). \tag{5.89}$$

Then one can use the equation (5.88) presuming that the approximation (5.89) is fulfilled with high accuracy.

The second, additional to multiboson updates (5.77) – (5.80) step described by equations (5.86) – (5.89) is called *noisy correction accept-reject* step, and the combination of both steps is called the (Hermitean) *two-step multiboson* (TSMB) algorithm. Note that for the noisy correction step, the deviation of the $P_2(x)$ from 1 should not be very large.

In another (non-Hermitean) scheme proposed in [127, 128], the choice of the ξ vectors for the estimate (5.88) differs from the (5.87), (5.89) one. Moreover, their scheme together with multiboson method (5.77) – (5.80) was claimed [127, 128] to be an *exact* algorithm. We will not describe this alternative approach. Let us only note that the noisy correction step in the form (5.86) – (5.89) on the one hand, can be implemented to *arbitrary* number of fermion flavours N_f and on the other hand, the precision of this second step is tunable by an appropriate choice of the approximating polynomials [36]. Another problem, related to the approximation of $x^{-N_f/2}$ function by the first polynomial $P_1(x)$ in both approaches, will be considered later (see also [37]).

5.5.3 Reweighting

If the approximation (5.82) of $x^{-N_f/2}$ function by a product of two polynomials is still not very accurate, one can improve the approximation by means of a choice of an auxiliary polynomial $P_4(x)$ with order $n_4 \geq n_2$ in a such way that the approximation [38]:

$$x^{-N_f/2} \approx P_1(x)P_2(x)P_4(x). \tag{5.90}$$

is much better than the (5.82) one. But the P_4 polynomial should deviate from 1 less than the P_2 one.

As in the case of the second step, the use of the approximation (5.90) to represent the fermion determinant power and also taking into account the sign of the fermion determinant lead to an integral for average observables analogous to (5.83) (see [38, 129, 130]):

$$\begin{aligned} \langle \mathcal{O} \rangle_{\rm rew} &= \frac{1}{Z} \int \left[{\rm d}U \right] \left[{\rm d}\Phi^\dagger {\rm d}\Phi \right] \mathcal{O}[U] \exp(-S[\Phi, U]) \times \\ &\times \det{}^{-1} P_2(\mathbf{Q}^\dagger \mathbf{Q}) \det{}^{-1} P_4(\mathbf{Q}^\dagger \mathbf{Q}) \left(\frac{\det \mathbf{Q}}{|\det \mathbf{Q}|} \right)^{N_f}, \end{aligned} \tag{5.91}$$

where we have employed the identity (5.42) for the determinant of the even-odd decomposed matrix $\mathbf{Q}$. Here, in case of not very large deviation of $\det{}^{-1} P_4(\mathbf{Q}^\dagger \mathbf{Q})$ from 1, one may use the two-step multiboson algorithm (5.77) – (5.80), (5.86) – (5.89) for generating the weight function in the integral (5.83). Hence, the last two multipliers related to P_4 polynomial determinant and to the determinant phase, play the role of the *reweighting* factor.

Realizing this idea, we rewrite the expression (5.91) as follows:

$$\langle \mathcal{O} \rangle_{\rm rew} = \frac{\left\langle \mathcal{O} \det{}^{-1} P_4(\mathbf{Q}^\dagger \mathbf{Q}) (\det \mathbf{Q}/|\det \mathbf{Q}|)^{N_f} \right\rangle_{12}}{\left\langle \det{}^{-1} P_4(\mathbf{Q}^\dagger \mathbf{Q}) (\det \mathbf{Q}/|\det \mathbf{Q}|)^{N_f} \right\rangle_{12}}, \tag{5.92}$$

where the averaging $\langle \ldots \rangle_{12}$ is performed according to equation (5.83).

For practical simulations of the inverse determinant in the expression (5.92), one uses the noisy estimator representation like (5.88) in case of the noisy correction step [38, 129, 130]:

$$\det{}^{-1} P_4(\mathbf{Q}^\dagger \mathbf{Q}) \propto \left\langle \exp\left(-\eta^\dagger P_4(\mathbf{Q}^\dagger \mathbf{Q}) \eta + \eta^\dagger \eta \right) \right\rangle_\eta . \tag{5.93}$$

This auxiliary step for improvement of measured observables described by equations (5.92), (5.93) is known as *reweighting* step. Its use assumes a small deviation of P_4 polynomial from 1.

5.5.4 Polynomials

All these polynomials $P_k(x)$, $k = 1, \ldots, 4$ approximating the $x^{-N_f/2}$ function are obtained according to the following prescription [37]. First of all, one selects the approximation interval $[\epsilon, \lambda]$ in a such way that it contains the average minimal $\langle\lambda_{\min}\rangle$ and maximal $\langle\lambda_{\max}\rangle$ eigenvalues of the preconditioned fermion matrix $\mathbf{Q}^\dagger\mathbf{Q}$:

$$[\langle\lambda_{\min}\rangle, \langle\lambda_{\max}\rangle] \subset [\epsilon, \lambda]. \tag{5.94}$$

The averaging of eigenvalues is done according to the equation (5.92).

Then one applies the least squares method for mean integral polynomial deviation to the successive evaluation of 1st then 2nd and 4th (reweighting) polynomials:

$$\begin{aligned}
&\int_\epsilon^\lambda \mathrm{d}x \left|x^{-N_f/2} P_1(x) - 1\right|^2 \xrightarrow{P_1} \min, \\
&\int_\epsilon^\lambda \mathrm{d}x \left|x^{-N_f/2} P_1(x) P_2(x) - 1\right|^2 \xrightarrow{P_2} \min, \qquad P_1 \text{ fixed}, \\
&\int_\epsilon^\lambda \mathrm{d}x \left|x^{-N_f/2} P_1(x) P_2(x) P_4(x) - 1\right|^2 \xrightarrow{P_4} \min, \qquad P_1, P_2 \text{ fixed},
\end{aligned} \tag{5.95}$$

where the minimization is performed with respect to the coefficients of a polynomial $P_k(x)$ at the *fixed* order n_k.

For the 3rd polynomial P_3 we employ the Newton tangential method with the appropriate least squares polynomial approximation of the $(P_2P_3)^{-1}$ function:

$$\begin{aligned}
&P_3^{(j+1)}(x) = \frac{1}{2}\left(P_3^{(j)}(x) + \tilde{P}_3^{(j)}(x)\right), \qquad j = 0, 1, \ldots, \\
&\int_\epsilon^\lambda \mathrm{d}x \left|P_2(x) P_3^{(j)}(x) \tilde{P}_3^{(j)}(x) - 1\right|^2 \xrightarrow{\tilde{P}_3^{(j)}} \min, \qquad P_2, P_3^{(j)} \text{ fixed}.
\end{aligned} \tag{5.96}$$

and

$$P_3(x) = \lim_{j\to\infty} P_3^{(j)}(x).$$

Here the $P_3^{(j)}$ and $\tilde{P}_3^{(j)}$ are polynomials of order n_3, and the P_2, $P_3^{(j)}$ polynomials are kept fixed during the least squares integral minimization with respect to the coefficients of $\tilde{P}_3^{(j)}$.

In this way we evaluate the coefficients of all these polynomials. To obtain the complex roots of the first polynomial P_1, one applies the Legendre method [105].

All such calculations require very large computer precision. Therefore, for this purpose we use codes for the MAPLE or Mathematica software. But in case of ordinary (low precision) computations, to reconstruct the polynomials with reasonable accuracy, one should employ the orthogonal polynomial basis decomposition:

$$P_k(x) = \sum_{j=0}^{n_k} c_j^{(k)} O_j^{(k)}(x), \qquad O_{j+1}^{(k)}(x) = (x + \beta_j^{(k)}) O_j^{(k)}(x) + \gamma_{j-1}^{(k)} O_{j-1}^{(k)}(x), \quad (5.97)$$

where $k = 1, \ldots, 4$, polynomials $O_j(x)$ have the order j, $O_0(x) = 1$, $\gamma_{-1} = 0$ and the orthogonality condition for polynomials looks as follows:

$$\int_{\epsilon}^{\lambda} \mathrm{d}x \rho^{(k)}(x) O_i^{(k)}(x) O_j^{(k)}(x) = 0, \qquad i \neq j. \quad (5.98)$$

The integral weights $\rho^{(k)}(x)$ are taken in the following way:

$$\begin{aligned} \rho^{(1)}(x) = x^{N_f}, \qquad & \rho^{(2)}(x) = x^{N_f} P_1^2(x), \\ \rho^{(3)}(x) = P_2^2(x) P_3^2(x), \qquad & \rho^{(4)}(x) = x^{N_f} P_1^2(x) P_2^2(x). \end{aligned} \quad (5.99)$$

Our numerical studies of the polynomials obtained according to the recipe (5.94) – (5.99) have shown that they indeed can be reproduced with high enough accuracy by usual (e.g. FORTRAN) codes.

5.5.5 Acceptance rate

Let us discuss now the acceptance rate of the two-step multiboson algorithm. From the detailed balance relation (5.84) follows the equality [127, 128]

$$\langle \exp(-\Delta E) \rangle_{\eta, \{U,\Phi\}, \{U',\Phi'\}} = 1, \qquad \Delta E = \xi^\dagger P_2(\mathbf{Q}^\dagger \mathbf{Q}[U'])\xi - \eta^\dagger \eta.$$

Here the ξ vector is defined according to (5.87) and averaging over $\{U, \Phi\}$ and $\{U', \Phi'\}$ fields is peformed with respect to the weight $p_{12} \exp(-S)$:

$$\begin{aligned} \langle \mathcal{O} \rangle_{\{U,\Phi\}, \{U',\Phi'\}} &= \frac{1}{Z} \int [\mathrm{d}U][\mathrm{d}\Phi^\dagger \mathrm{d}\Phi][\mathrm{d}U'][\mathrm{d}\Phi'^\dagger \mathrm{d}\Phi'] \times \\ &\times \mathcal{O} \exp(-S[\Phi, U]) p_{12}[\Phi', U', \Phi, U], \end{aligned} \quad (5.100)$$

where p_{12} is a transition probability of the TSMB algorithm. The same arguments as for the acceptance rate of the HMC method lead to the expression (5.61) for

$\langle w_{\rm acc}\rangle$, averaged according to (5.100). Where ΔE substitutes the ΔH and satisfies the relation (5.60). Hence, for the $\langle\Delta E\rangle$ the following estimate [127, 128] is valid:

$$\langle\Delta E\rangle \propto V\|P_2 - 1\|^2. \tag{5.101}$$

Here the $\|\ldots\|$ is a norm in the polynomial space corresponding to a maximal deviation absolute value.

5.5.6 Technical notes

In contrast to the hybrid Monte Carlo method, the two-step multiboson algorithm is bulky in computer memory owing to the auxiliary multiboson fields. An approporiate choice of its technical parameters is complicate. Moreover, it needs an information about the minimal and maximal average eigenvalues of the matrix $\mathbf{Q}^\dagger\mathbf{Q}$. Their correct values can be obtained either by means of self-consistent checks and correspondent tunings of approximation interval margins or from preliminary HMC runs (in case of even flavours N_f and when the hybrid Monte Carlo works normally). And at the end, the algorithm requires the polynomial roots and coefficients data which can be found by use of separate high precision calculations.

However, one should mention the stability of the TSMB algorithm in case of large lattices owing to use of local update cycles. It can work also in case of very large condition numbers. And the most important advantage of the algorithm is that it can be used for simulations with any number N_f of dynamical fermion flavours (see [36] – [38]).

The two-step multiboson algorithm (5.77) – (5.80), (5.86) – (5.89) and also the reweighting step (5.92), (5.93) which use the recursive polynomial evaluation (5.97), were implemented by us for investigations of the U(1) lattice model with an even number N_f of dynamical fermion flavours, where it is not necessary to evaluate the sign of the determinant $\det\mathbf{Q}$. As far as the application of the TSMB has been successful in the supersymmetric case [36] – [38], it is natural to ask the question, how this algorithm is efficient in comparison with HMC in our case of compact QED with $N_f = 2$ Wilson fermions. Next section will be devoted to the answer to this question.

5.6 Performance of the dynamical fermion algorithms

5.6.1 Autocorrelation time

Let us now study the performance of both the HMC and TSMB methods. The performance of an algorithm means the average number of total operations between statistically independent measurements.

Statistically independent measurements can be identified as follows [10, 131]. Let us first consider the Markov chain of sampled observables: $\mathcal{O}_1, \mathcal{O}_2, \ldots$ with the mean average $\langle \mathcal{O}_j \rangle = \langle \mathcal{O} \rangle$ and the autocorrelation function which depends only on the difference $j - k$:

$$\Big\langle \big(\mathcal{O}_j - \langle \mathcal{O} \rangle\big)\big(\mathcal{O}_k - \langle \mathcal{O} \rangle\big) \Big\rangle = \Gamma_{\mathcal{O}}(j-k) = \Gamma_{\mathcal{O}}(k-j).$$

Then the squared deviation for the sampled mean value:

$$\mathbf{M}_N(\mathcal{O}) = \frac{1}{N}\sum_{j=1}^{N} \mathcal{O}_j, \tag{5.102}$$

looks as follows:

$$\Big\langle \big(\mathbf{M}_N(\mathcal{O}) - \mathcal{O}\big)^2 \Big\rangle \simeq \frac{2\tau_{\rm int}}{N}\Gamma_{\mathcal{O}}(0), \tag{5.103}$$

where $\tau_{\rm int}$ is the so-called *integrated autocorrelation time*:

$$\tau_{\rm int} = \lim_{N\to\infty} \frac{1}{2N} \sum_{j,k=1}^{N} \frac{\Gamma_{\mathcal{O}}(j-k)}{\Gamma_{\mathcal{O}}(0)}. \tag{5.104}$$

In case of an exponentially decreasing autocorrelation function $\Gamma_{\mathcal{O}}(j) \propto \exp(-|j|/\tau^\star)$ (which is usually not realized), $\tau_{\rm int} \simeq \tau^\star$ holds. The $\tau_{\rm int}$ can be represented as follows:

$$\tau_{\rm int} = \frac{1}{2} + \lim_{N\to\infty} \sum_{j=1}^{N} \frac{\Gamma_{\mathcal{O}}(j)}{\Gamma_{\mathcal{O}}(0)}. \tag{5.105}$$

For the mutually independent sampled observables $\Gamma_{\mathcal{O}}(j) = 0$, $j \neq 0$, the integrated autocorrelation time is $\tau_{\rm int} = 1/2$. Hence, the expression (5.103) means that an effective number of statistically independent measurements is equal to $N/2\tau_{\rm int}$. And $\tau_{\rm int}$ can be treated as an effective distance between the nearest independent measurements.

The integrated autocorrelation time $\tau_{\rm int}$ can be evaluated by means of the equation (5.105), where the approximated autocorrelation functions are evaluated as follows:

$$\Gamma_{\mathcal{O}}(j) \approx \frac{1}{N-j}\sum_{i=1}^{N-j}\left(\mathcal{O}_i - \frac{1}{N-j}\sum_{k=1}^{N-j}\mathcal{O}_k\right)\left(\mathcal{O}_{i+j} - \frac{1}{N-j}\sum_{k=j+1}^{N}\mathcal{O}_k\right).$$

The sum in (5.105) is taken (instead of the total number of measurements N) up to some cut-off value W called the window [131]:

$$\tau_{\rm int} \approx \frac{1}{2} + \frac{1}{W}\sum_{j=1}^{W}\frac{\Gamma_{\mathcal{O}}(j)}{\Gamma_{\mathcal{O}}(0)}. \tag{5.106}$$

The relative accuracy of such method is the follows [131]:

$$\frac{\sqrt{\langle(\Delta\tau_{\rm int})^2\rangle}}{\tau_{\rm int}} \approx \sqrt{\frac{2(2W+1)}{N}}.$$

In an alternative method of evaluating $\tau_{\rm int}$ called *binning* (see e.g. [10, 132]) the total set of N measurements is divided into N/B blocks with length B: $N \gg B \gg 1$. For each block one computes the sampled mean value (5.102) denoted as $[\mathcal{O}]_B$. Then, according to (5.103) and to the original definition (5.104) of the autocorrelation time one evaluates $\tau_{\rm int}$ as follows:

$$\tau_{\rm int} \approx \frac{B\big\langle\big(\mathbf{M}_N(\mathcal{O}) - [\mathcal{O}]_B\big)^2\big\rangle}{2\Gamma_{\mathcal{O}}(0)}. \tag{5.107}$$

Errors of the binning method are estimated by the formula [133]:

$$\frac{\sqrt{\langle(\Delta\tau_{\rm int})^2\rangle}}{\tau_{\rm int}} \approx \max\left(\frac{\tau_{\rm int}}{B}, \sqrt{\frac{B}{N}}\right).$$

In our simulations, we used mostly the binning method (5.107) since it can be easily accustomized to the evaluation of errors for the functions of mean measured values by the *jack-knife* method [134, 132]. However, the summation method (5.106) appears to be more precise than the binning (5.107). The best window size is $W \propto \ln N$ since the systematic error of the expression (5.106) decreases as $\exp(-W/\tau_{\rm int})$ [133].

5.6.2 Theoretical estimates

Summarizing, one can define the performance value $\mathbf{P}$ of an algorithm by the equation:

$$\mathbf{P} = \mathbf{N}_{\rm oper}\tau_{\rm int}, \tag{5.108}$$

where $\mathbf{N}_{\rm oper}$ is a total number of operations per 1 update.

Before studying the values (5.108), one should also know how to choose the technical parameters in an appropriate way. In case of HMC we use the arguments [117, 118] of the harmonic oscillator Hamiltonian approximation:

$$H_{(\rm eff)} = \frac{1}{2}\Pi^2 + \frac{1}{2}A^\dagger \Omega A.$$

Here the matrix Ω is roughly estimated as:

$$\Omega = \frac{\partial F}{\partial A},$$

where the HMC force F is defined according to equation (5.52). In order to keep the average acceptance rate $\langle w_{\rm acc}\rangle \approx 1$, one chooses the time step size $\Delta\tau$ and number of time steps N_τ in such a way that:

$$V\|\Omega\|^2(\Delta\tau)^4 \propto 1, \qquad \sqrt{\|\Omega\|}N_\tau\Delta\tau \propto 1. \tag{5.109}$$

Here, owing to the pseudofermion distribution (5.48),

$$\|\Omega\| \propto \langle\frac{1}{V}\,\mathrm{Tr}\,\frac{1}{\mathcal{M}^\dagger\mathcal{M}}\rangle \propto \langle\frac{1}{V}\sum_j \frac{1}{\lambda_j(\mathcal{M}^\dagger\mathcal{M})}\rangle \propto \sqrt{\zeta}, \qquad \zeta = \frac{\langle\lambda_{\max}(\mathbf{Q}^\dagger\mathbf{Q})\rangle}{\langle\lambda_{\min}(\mathbf{Q}^\dagger\mathbf{Q})\rangle}.$$

Further, the CG precision δ in (5.25) should not spoil both the molecular dynamics and the precise Hamiltonian accept-reject step. The $\delta_{\rm md}$ for molecular dynamics and $\delta_{\rm acc}$ for accept-reject step must obey the following estimates [114, 115]:

$$\delta_{\rm md} \propto \frac{1}{V}, \qquad \delta_{\rm acc} \propto \frac{1}{V^2}. \tag{5.110}$$

According to (5.27) this gives the estimate for the average number of corresponding iterations of the CG method applied to even-odd decomposed systems (5.40):

$$\langle N^{(\rm CG)}\rangle \propto \sqrt{\zeta}\ln V. \tag{5.111}$$

The parameters for the TSMB in case of $N_f = 2$ should be choosen in the best way as follows [135]. The interval margins ϵ and λ are selected as:

$$\epsilon = 0.5\langle\lambda_{\min}\rangle, \qquad \lambda = (1.2\,—1.4)\langle\lambda_{\max}\rangle. \tag{5.112}$$

Here one takes into account the statistical fluctuations of the minimal eigenvalue $\lambda_{\min}$. But the value for the upper interval margin λ can be selected closer to the

average maximal eigenvalue $\langle\lambda_{\max}\rangle$ due to the possibility of finding an exact upper limit $\|\mathbf{Q}^\dagger\mathbf{Q}\|$ depending on the hopping-parameter κ.

And again in order to keep the acceptance rate $\langle w_{\rm acc}\rangle \sim 1$ and to deal with the reweighting determinant values $\det P_4\left(\mathbf{Q}^\dagger\mathbf{Q}\right) \sim 1$, the deviations of the second and reweighting polynomials $P_2(x)$ and $P_4(x)$, respectively, should satisfy the following conditions according to (5.101) and (5.93):

$$\|P_2 - 1\| \propto \frac{1}{\sqrt{V}}, \qquad \|P_4 - 1\| \propto \frac{1}{V}, \tag{5.113}$$

which give rough estimates for orders of the first and second polynomials:

$$n_1 \propto \zeta^{1/4} \ln V, \qquad n_2 \simeq \langle N^{(\rm CG)}\rangle. \tag{5.114}$$

Here we take into account the effective square root decreasing of the condition number $\zeta \to \sqrt{\zeta}$ for the approximation of $1/x$ by the least squares first polynomial $P_1(x)$ [37] which has been established by empirical observations.

Indeed, in an alternative to the least squares polynomial approach in the case of $N_f = 2$, the Chebyshev polynomial approximation [121, 122]:

$$P_1(x) = \frac{1}{x}\left(1 - \frac{T_{n_1+1}(\frac{2x-(\lambda+\epsilon)}{\lambda-\epsilon})}{T_{n_1+1}(-\frac{\lambda+\epsilon}{\lambda-\epsilon})}\right), \qquad T_n(x) = \cos\left(n \arccos x\right),$$

the choice of the same approximation interval leads to much worse interpolation of $1/x$ for the Chebyshev polynomial than for the least squares one (see Figure 5.1a). But if one increases the lowest interval margin for the Chebyshev method as follows:

$$\epsilon \to \sqrt{\zeta}\epsilon,$$

one reaches almost the same approximation of the $1/x$ function as in the case of the least squares method (Figure 5.1b).

At the same time, the deviation of the least squares polynomial $P_1(x)$ from $1/x$ function in the vicinity of the $x = \epsilon$ margin is larger than for the Chebyshev one (see Figure 5.2) [37]. This means that in order to reach a good approximation of $1/x$ in the whole interval $x \in [\epsilon, \lambda]$, the correcting least squares polynomial $P_2(x)$ must deviate large from 1 when x is close to ϵ, and our numerical observations confirm this statement. And the contribution of lowest eigenmodes of the operator $\mathbf{Q}^\dagger\mathbf{Q}$, owing to such discrepancy decreases the acceptance rate (5.86) of TSMB algorithm, especially when the condition number ζ is very large. A reasonable

TSMB acceptance is maintained, seems, due to a good closeness to 1 of the second polynomial $P_2(x)$ for the remaining eigenmodes of the fermion operator.

The deviations for the approximate square root polynomial inversion as well as a good enough approximation of the $1/x$ function:

$$\|P_2(x)P_3^2(x) - 1\| \propto \frac{1}{V^2}, \qquad \|xP_1(x)P_2(x)P_4(x) - 1\| \propto \frac{1}{V^2}, \tag{5.115}$$

require the following estimates of the orders of third and reweighting polynomials:

$$n_3 = (1.2 \text{—} 1.4)n_2, \qquad n_4 \geq n_2. \tag{5.116}$$

Before presenting numerical results, let us speculate about the theoretical performance estimate according to the formula (5.108). In the case of HMC, the number of operations per update is

$$\mathbf{N}_{\text{oper}}^{\text{HMC}} \propto V\langle N^{(\text{CG})}\rangle N_\tau. \tag{5.117}$$

For the TSMB in case of very large order of the correcting polynomial P_2, the number of operations per sweep is determined mostly by the number of operations in the noisy correction step:

$$\mathbf{N}_{\text{oper}}^{\text{TSMB}} \propto Vn_2, \qquad n_2 \gg n_1. \tag{5.118}$$

The autocorrelation time in the HMC case for almost total acceptance for the oscillator dynamics [117, 118, 136] is

$$\tau_{\text{int}}^{\text{HMC}} \propto (\Delta t)^{-2}, \qquad \Delta t = N_\tau \Delta\tau. \tag{5.119}$$

In the case of TSMB for an acceptance rate near to 1, the autocorrelation time is proportional to the inverse imaginary part of the polynomial roots $\operatorname{Im} r_j$ in (5.62) [137] (see also [125, 126]). Therefore by use of Chebyshev polynomial arguments to the least squares polynomial case, this time is proportional to the expression:

$$\tau_{\text{int}}^{\text{TSMB}} \propto n_1\zeta^{1/4}. \tag{5.120}$$

Taking into account the estimates (5.109), (5.111), (5.114) and (5.117) – (5.120), one can find roughly the theoretical gain $\mathbf{G}_{\text{TSMB/HMC}}$ of TSMB over HMC algorithm:

$$\mathbf{G}_{\text{TSMB/HMC}} = \frac{\mathbf{P}_{\text{HMC}}}{\mathbf{P}_{\text{TSMB}}} \propto \frac{V^{1/4}}{\ln V}. \tag{5.121}$$

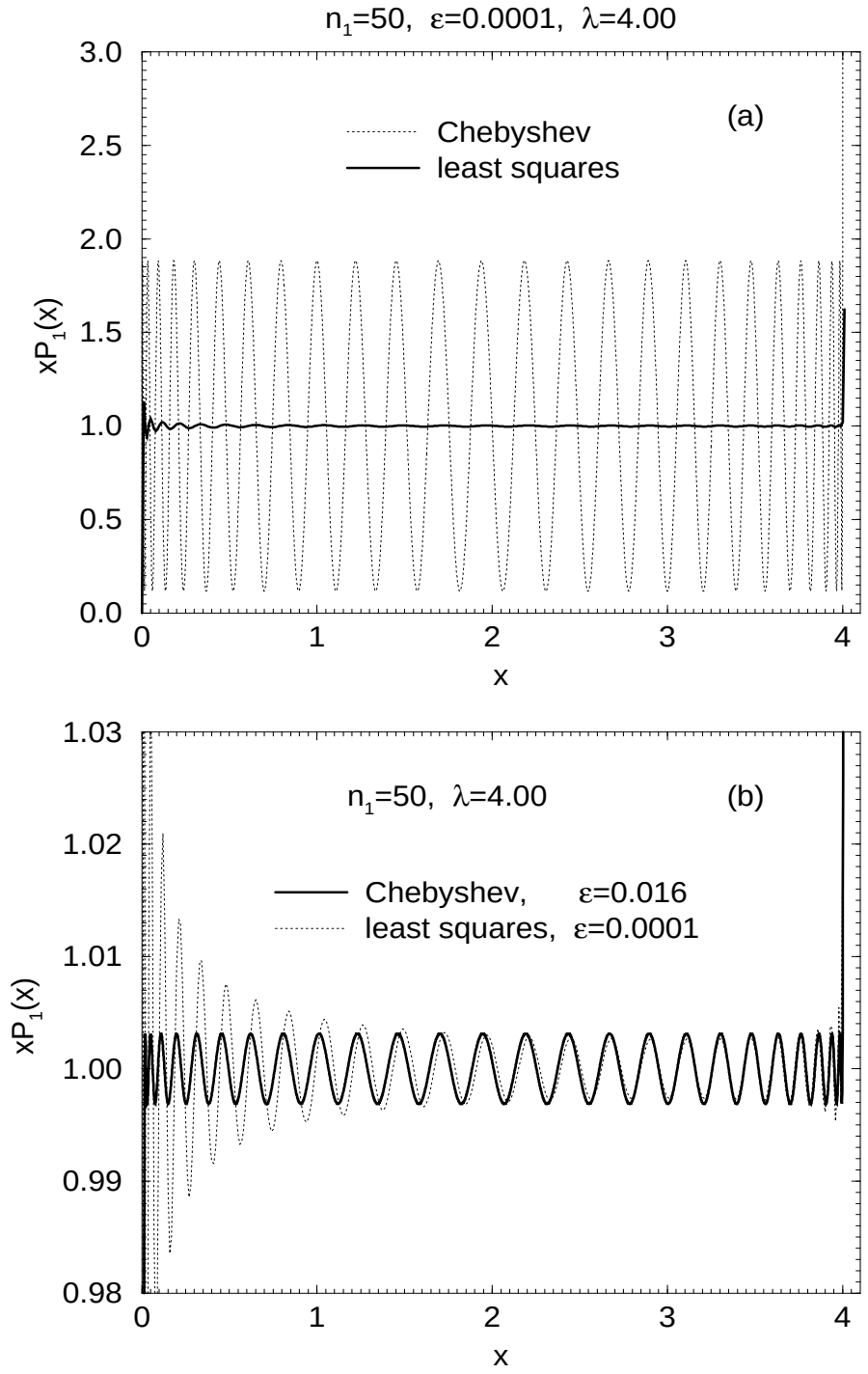

Figure 5.1: Approximation of $1/x$ function by Chebyshev and least squares polynomials, $n_1 = 50$, $\lambda = 4.0$: (a) $\epsilon = 0.0001$ for both polynomials and (b) $\epsilon = 0.016$ for Chebyshev and $\epsilon = 0.0001$ for least squares polynomials.

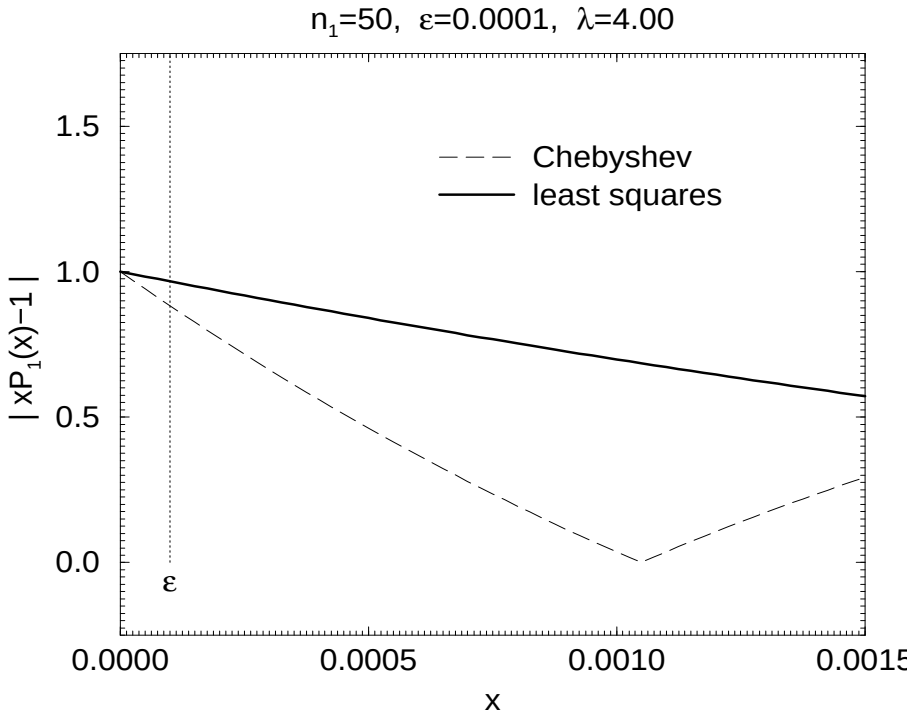

Figure 5.2: Deviation $|xP_1(x) - 1|$ for the $1/x$ approximation by Chebyshev and least squares polynomials in the vicinity of $x = \epsilon$. Polynomial order $n_1 = 50$, interval margins $\epsilon = 0.0001$ and $\lambda = 4.0$.

5.6.3 Numerical studies

Now we turn to the numerical investigation of the performance of dynamical fermion algorithms in the case of $N_f = 2$ for both Coulomb and confinement phases. The lattice size in our case is $6^3 \times 12$ and time-antiperiodic boundary conditions for Fermi-fields are employed. In the Coulomb phase, we choose the parameters $\beta = 2$, $\kappa = 0.130$ but in the confinement phase $\beta = 0$, $\kappa = 0.238$. The κ parameters lie quite near the critical chiral limit line $\kappa_c(\beta)$ (see section 2.5 and chapter 4). Due to the prescription (5.109), (5.110), we took the parameters N_τ, $\Delta\tau$, $\delta_{\rm md}$, $\delta_{\rm acc}$ for HMC as in Table 5.1. Then we are able to evaluate numerically an average number of CG iterations in leapfrog dynamics $\langle N_{\rm md}^{\rm (CG)} \rangle$ (see this Table). In the TSMB case, the corresponding polynomial parameters n_1, n_2, n_3, n_4 and interval margins ϵ, λ selected according to (5.114), (5.116) and (5.112) are given in the Table 5.2.

Almost all these parameters require a knowledge of the average lowest $\langle \lambda_{\rm min} \rangle$ and largest $\langle \lambda_{\rm max} \rangle$ eigenvalues of even-odd decomposed fermion matrix $\mathbf{Q}^\dagger \mathbf{Q}$. They

phase	β	κ	N_τ	$\Delta\tau$	δ_{md}	δ_{acc}	$\langle N_{\mathrm{md}}^{(\mathrm{CG})} \rangle$
Coulomb	2	0.130	40	1/40	10^{-3}	10^{-7}	36.0(2)
confinement	0	0.238	10	0.01	10^{-3}	10^{-7}	500(2)

Table 5.1: Parameters for simulation by HMC algorithm in both Coulomb and confinement phases on a $6^3 \times 12$ lattice.

phase	β	κ	n_1	n_2	n_3	n_4	ϵ	λ
Coulomb	2	0.130	6	36	48	200	0.025	2.5
confinement	0	0.238	50	360	450	500	0.000225	9

Table 5.2: Parameters for simulation by TSMB $N_f = 2$ algorithm in both Coulomb and confinement phases on a $6^3 \times 12$ lattice.

			quenched		dynamical	
phase	β	κ	$\langle \lambda_{\mathrm{min}} \rangle$	$\langle \lambda_{\mathrm{max}} \rangle$	$\langle \lambda_{\mathrm{min}} \rangle$	$\langle \lambda_{\mathrm{max}} \rangle$
Coulomb	2	0.130	0.065(1)	1.60(1)	0.13(1)	1.63(1)
confinement	0	0.238	0.0010(1)	6.78(1)	0.0005(1)	6.59(1)

Table 5.3: Minimal $\langle \lambda_{\mathrm{min}} \rangle$ and maximal $\langle \lambda_{\mathrm{max}} \rangle$ average eigenvalues of even-odd decomposed Wilson fermion matrix $\mathbf{Q}^\dagger \mathbf{Q}$ for both Coulomb and confinement phases in quenched and dynamical $N_f = 2$ fermion models on a $6^3 \times 12$ lattice.

were evaluated by the explicitely restarted Lanczos method (5.30) – (5.35). Initially they were taken from the quenched gauge configurations and then tuned to the dynamical $N_f = 2$ case (Table 5.3). It is worthwhile noting that if in the Coulomb phase the condition number decreases by the factor ~ 2 with the incorporation of the fermion loops, in the confinement phase the situation is quite different.

Our numerical results have shown that the choice of polynomial orders (5.114) and (5.116) confirms the conditions (5.113) and (5.115). As an example, in Figure 5.3 we show the behaviour of the second $P_2(x)$ (Figure 5.3a) and fourth $P_4(x)$ (Figure 5.3b) polynomials for the approximation of $1/x$ function (for the confinement case). One sees that maximal deviation of these polynomials from 1 indeed satisfies the estimate (5.113) required for the lattice $6^3 \times 12$. Also measurements of the reweighting factors $\det{}^{-1} P_4(\mathbf{Q}^\dagger \mathbf{Q})$ according to (5.93) indicate for both Coulomb and confinement phases (see Figure 5.4 for confinement phase) that such factors are commensurable with 1.

Let us present the numerical results for comparison of the performance for both the HMC and TSMB algorithms. We investigated the following mean gauge invariant observables $\langle \mathcal{O} \rangle$: mean gauge energy $\langle E_G \rangle$ (2.26), scalar condensate $\langle \overline{\psi}\psi \rangle$ (2.27) and pion norm $\langle \Pi \rangle$ (2.28). The statistics in our case (10000 measurements) was enough to evaluate the integrated autocorrelation time $\tau_{\rm int}$ by use of the binning method (5.107). To compute observables in the case of the TSMB algorithm, we used also the reweighting step (5.92), (5.93). At the end we measured the gain of the TSMB algorithm over HMC method $\mathbf{G}_{\rm TSMB/HMC}$ according to the equations (5.121) and (5.108), where instead of the measurement of the number of operations $\mathbf{N}_{\rm oper}$ we took the measured CPU time for one update $t_{\rm CPU}$ since, as one expects,

$$\mathbf{N}_{\rm oper} \propto t_{\rm CPU}.$$

Results of the comparison for the Coulomb phase are presented in the Table 5.4. The acceptance rate in case of HMC method was $\langle w_{\rm acc}^{\rm HMC} \rangle = 0.94(1)$, in the case of TSMB algorithm $\langle w_{\rm acc}^{\rm TSMB} \rangle = 0.48(1)$. Numbers of heatbath and overrelaxation updating sweeps in the multiboson method (5.77) – (5.80) are the follows: $N_{BH} = 1$, $N_{BO} = 9$, $N_{GH} = 1$, $N_{GO} = 0$. The observables obtained from simulations of TSMB algorithm agrees with those from HMC runs. The autocorrelation time for the pion norm is an order larger than that for mean gauge energy and

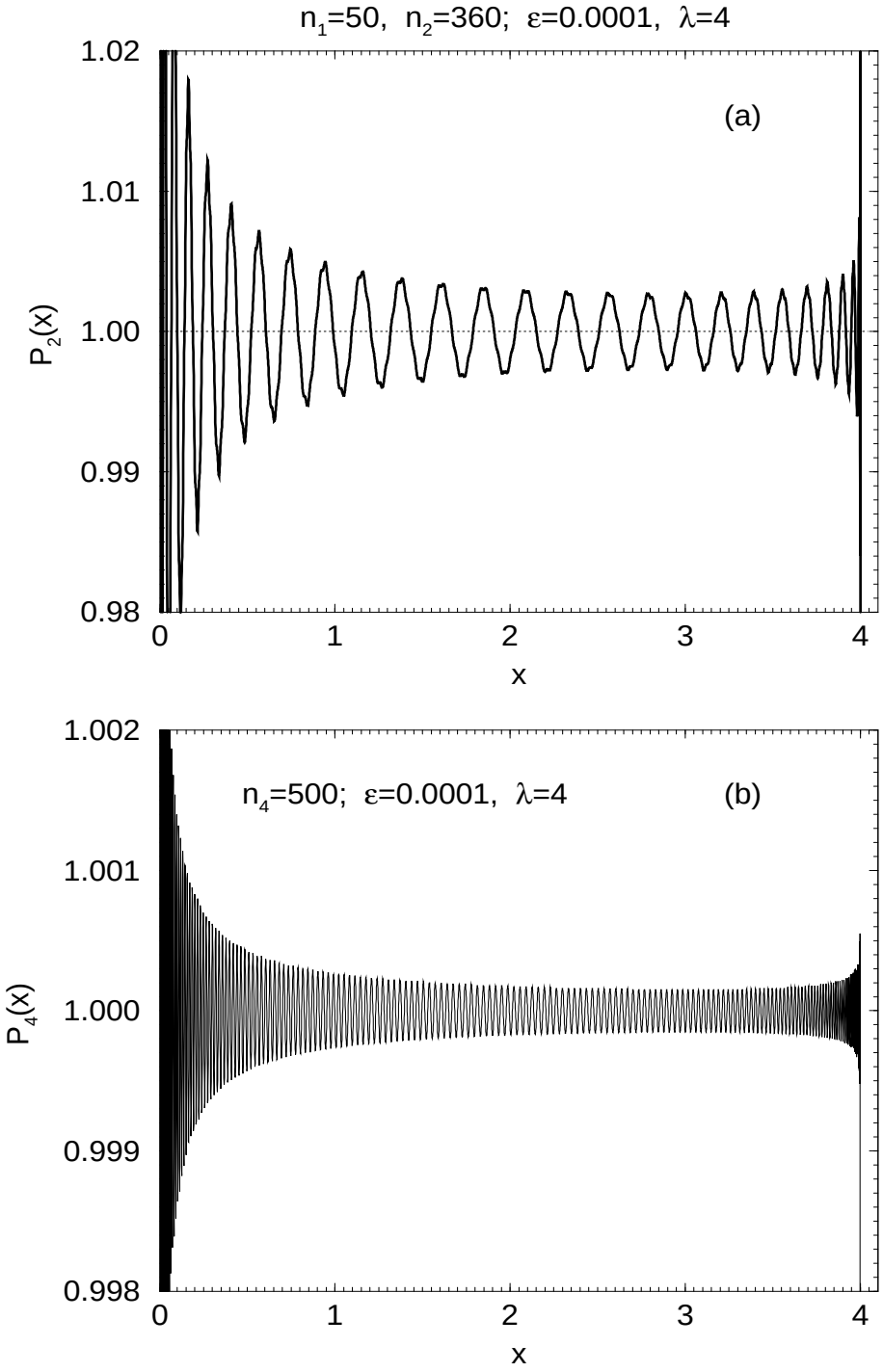

Figure 5.3: Least squares polynomials $P_2(x)$ (a) and $P_4(x)$ (b) to the polynomial approximation of the $1/x$. Polynomial orders $n_1 = 50$, $n_2 = 360$, $n_4 = 500$. Interval margins $\epsilon = 0.0001$, $\lambda = 4.0$.

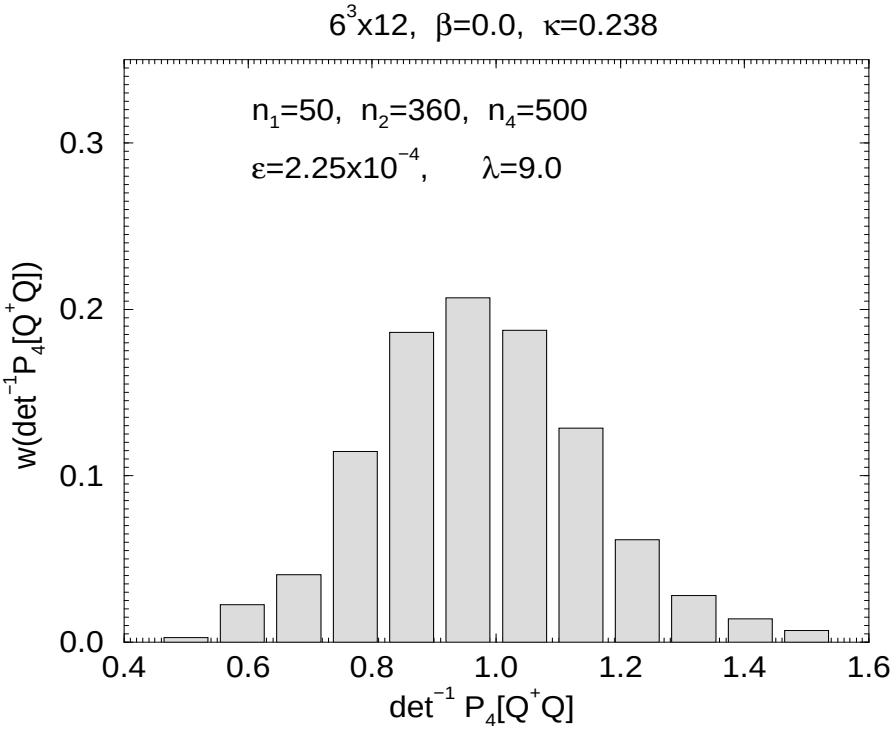

Figure 5.4: Distribution of reweighting factors $\det{}^{-1} P_4(\mathbf{Q}^\dagger\mathbf{Q})$ in the TSMB simulations on a $6^3 \times 12$ lattice, confinement phase.

scalar condensate. CPU times per update for HMC and TSMB algorithms look as $t_{\rm CPU}^{\rm HMC} = 15.1(2)$ sec and $t_{\rm CPU}^{\rm TSMB} = 8.96(2)$ sec. One sees a little gain for plaquette and scalar condensate, and no win of performance for the pion norm.

The situation is rather different in the confinement case (Table 5.5). The autocorrelation time for the pion norm is smaller than for the mean gauge energy and scalar condensate. In spite of agreement of the measured observables, there is no visible win of TSMB performance over HMC one. The acceptance rates $\langle w_{\rm acc}^{\rm HMC}\rangle = 0.72(1)$ and $\langle w_{\rm acc}^{\rm TSMB}\rangle = 0.68(1)$ are comparable. CPU times in this case are $t_{\rm CPU}^{\rm HMC} = 76(1)$ sec and $t_{\rm CPU}^{\rm TSMB} = 69(1)$ sec. The numbers of local update sweeps in the multiboson algorithm were taken as follows: $N_{BH} = 2$, $N_{BO} = 2$, $N_{GH} = 2$, $N_{GO} = 2$.

It is worth to note also that measured average reweighting factors:

$$\langle \det{}^{-1} P_4(\mathbf{Q}^\dagger\mathbf{Q})\rangle \approx 1$$

for both Coulomb and confinement phase cases. And therefore, the reweighting step (5.92), (5.93) in our $N_f = 2$ case brings only subtle corrections to the observables evaluated according to the ordinary two-step multiboson averaging (5.83).

	$\langle E_G \rangle$	$\langle \overline{\psi}\psi \rangle$	$\langle \Pi \rangle$
$\langle \mathcal{O}^{\mathrm{HMC}} \rangle$	0.1332(1)	0.9381(1)	1.378(1)
$\langle \mathcal{O}^{\mathrm{TSMB}} \rangle$	0.1331(1)	0.9379(1)	1.376(1)
$\tau_{\mathrm{int}}^{\mathrm{HMC}}$	3.2(3)	2.0(2)	25(4)
$\tau_{\mathrm{int}}^{\mathrm{TSMB}}$	3.0(3)	2.8(2)	50(8)
$\mathbf{G}_{\mathrm{TSMB/HMC}}$	1.7(2)	1.2(2)	0.8(2)

Table 5.4: Performance of HMC and TSMB $N_f = 2$ algorithms in the Coulomb phase ($\beta = 2$, $\kappa = 0.130$). Lattice size $6^3 \times 12$.

	$\langle E_G \rangle$	$\langle \overline{\psi}\psi \rangle$	$\langle \Pi \rangle$
$\langle \mathcal{O}^{\mathrm{HMC}} \rangle$	0.939(1)	0.95(1)	13.9(2)
$\langle \mathcal{O}^{\mathrm{TSMB}} \rangle$	0.938(1)	0.96(1)	13.7(2)
$\tau_{\mathrm{int}}^{\mathrm{HMC}}$	65(7)	60(7)	35(5)
$\tau_{\mathrm{int}}^{\mathrm{TSMB}}$	120(20)	125(15)	45(5)
$\mathbf{G}_{\mathrm{TSMB/HMC}}$	0.5(1)	0.5(1)	0.7(1)

Table 5.5: Performance of HMC and TSMB $N_f = 2$ algorithms in the confinement phase ($\beta = 0$, $\kappa = 0.238$). Lattice size $6^3 \times 12$.

5.6.4 Methods to improve TSMB performance

The numerical results for both Coulomb and confinement phases presented above mean nevertheless, that the TSMB algorithm is *competitive* with the HMC one. And moreover, the theoretical gain expected from the rough estimate (5.121) is not very large for $6^3 \times 12$ lattice:

$$\mathbf{G}_{\mathrm{TSMB/HMC}} = 0.90(1).$$

In order to improve the gain of TSMB algorithm over HMC one, it is necessary to use more local update sweeps (5.77) – (5.80). Indeed, the autocorrelation time $\tau_{\mathrm{int}}^{\mathrm{TSMB}}$ can be decreased to values of order 1 by applying a number of gauge sweeps commensurable with the initial autocorrelation time (5.120):

$$N_{GH} + N_{GO} \propto \tau_{\mathrm{int}}^{\mathrm{TSMB}}.$$

where according to estimates (5.111) and (5.114), $\tau_{\mathrm{int}}^{\mathrm{TSMB}} \propto n_2$. However, the number of operations in the TSMB algorithm remains the same magnitude as earlier in (5.118) due to the correspondent choice (5.114), (5.116) of polynomial orders:

$$\mathbf{N}_{\mathrm{oper}}^{\mathrm{TSMB}} \propto V n_2, \qquad n_2 \gg n_1.$$

This increases the gain (5.121):

$$\mathbf{G}_{\mathrm{TSMB/HMC}} \propto (V\zeta^2)^{1/4}.$$

Another way to improve the TSMB performance follows from the estimates (5.120), (5.118) and also from the numerical observation that the TSMB measurements required use only the first and the second steps of the algorithm (for $N_f = 2$) without necessity to employ the reweighting procedure (5.92), (5.93). To enlarge the TSMB gain, one should decrease the n_1 and n_2 polynomial orders. And then the reweighting step will be very important for the correct evaluation of average lattice observables.

5.7 Discussion

We have studied the performance of the two-step multiboson algorithm in the I. Montvay version [36] – [38] and compared it with the well-established hybrid Monte Carlo method [39, 40] for compact lattice QED with $N_f = 2$ dynamical

Wilson fermions within both Coulomb and confinement phases. Results of our investigation have shown that on the one hand, the TSMB algorithm is a robust alternative to the HMC method and on the other hand, the former algorithm is competitive with the latter one. It can be used for the investigation of the Aoki phase in the compact Wilson fermion QED (see Figure 2.1b) without auxiliary twisted mass term (2.35) and also for the study of the QED with odd fermion flavours N_f.

Nevertheless, we can further improve the performance of the TSMB method by increasing the number of local update sweeps e.g. for gauge fields. One should take the number of operations commensurable with that for the noisy correction accept-reject step.

The gain can be enlarged also by decreasing the orders of the first and the second polynomials. It needs to revise the role of the reweighting step correcting for the average observable values. One should note nevertheless, that this way requires a very careful choice of the approximating polynomials especially the $P_4(x)$ one in order to avoid the pathologically huge reweighting factors $|\det{}^{-1} P_4(\mathbf{Q}^\dagger\mathbf{Q})| \gg 1$.

Let us now discuss the application of the TSMB algorithm to a study of the U(1) lattice theory with an odd number of dynamical Wilson fermions. In principle, this algorithm is suitable for simulations with arbitrary N_f number but in the reweighting procedure (5.92), (5.93) one has to take into account the fermion determinant phase (or sign, in case of integer odd N_f). Fortunately studying the Coulomb phase, one may not think about the sign problem. It was shown (see e.g. [62, 10]) that owing to reflection symmetry:

$$\det \mathcal{M} > 0, \qquad |\kappa| < 1/6.$$

And since the critical $\kappa^\star$ parameter lies on the chiral limit line $\kappa_c(\beta)$ such as $\kappa_c(\infty) = 1/8$ (see Figure 2.1), for evaluation of a large critical $\beta^\star$ it is not necessary to compute the sign of fermion determinant.

This sign might be taken into account only in case of confinement or Aoki phase investigation. Unfortunately, the sign can not be found by means of pseudofermion factorization (5.44) as in the squared fermion determinant case. The straightforward method to obtain information about the determinant sign – direct evaluation of the fermion determinant – is enormously slow for large lattice sizes and is very expensive in computer memory. One can, however, bypass the problem using the complex gradient method [107, 109] for evaluation of lowest eigenvalues

of even-odd decomposed matrix $\mathbf{Q}^\dagger\mathbf{Q}$ (5.41) at different κ' values: $\kappa' \in [\kappa_0, \kappa]$. Here κ_0 is such a hopping-parameter when exactly $\det \mathcal{M} > 0$ and κ is the studied value. Then corresponding eigenvectors of $\mathbf{Q}^\dagger\mathbf{Q}$ will be eigenvectors of the operator $\gamma_5\mathbf{Q}$ which is Hermitean according to the property (5.38). If one of the lowest eigenvalues of the latter matrix crosses 0 in the interval $[\kappa_0, \kappa]$, it means that contribution of this eigenvalue to the target determinant is negative. And the determinant sign will be equal to the -1 value in the power of the number of such crosses.

Such a method of determinant sign evaluation is still not very fast. A possible alternative to the lowest eigenvalue study could look as follows. Let us consider the Hermitean unitary operator:

$$\mathbf{U} = \gamma_5\mathbf{Q}\left(\mathbf{Q}^\dagger\mathbf{Q}\right)^{-1/2}. \tag{5.122}$$

One can write the following expressions:

$$\frac{\det \mathbf{Q}}{|\det \mathbf{Q}|} = \det \mathbf{U} = (-1)^{n_-}, \qquad n_- = 2V - \operatorname{Tr}\mathbf{U} = 2V - \langle \eta^\dagger \mathbf{U} \eta \rangle_\eta, \tag{5.123}$$

where n_- is the number of -1 eigenvalues of the $\mathbf{U}$ matrix and the η is the Gaussian noise (5.16), (5.19). The unitary operator (5.122) requires the knowledge of the $\left(\mathbf{Q}^\dagger\mathbf{Q}\right)^{-1/2}$ matrix. To compute it, one can use the polynomial approximation [138] of the $x^{-1/2}$ function, e.g. (5.90), when $N_f = 1$:

$$\left(\mathbf{Q}^\dagger\mathbf{Q}\right)^{-1/2} \approx P_1(\mathbf{Q}^\dagger\mathbf{Q})P_2(\mathbf{Q}^\dagger\mathbf{Q})P_4(\mathbf{Q}^\dagger\mathbf{Q}). \tag{5.124}$$

The equations (5.122) – (5.124) allow to evaluate the sign of the determinant $\det \mathbf{Q}$ in the equation (5.92) for reweighted average observables. The disadvantage of this method is the low precision for the n_- value. Other ways to study the fermion determinant sign are now under investigation (see e.g. [139]).

The basic content of the section 5.6 will be published in paper [41].

Chapter 6

Summary and outlook

In this thesis, we investigated numerically and partly analytically the compact lattice QED with Wilson fermions. We studied the particular tasks in compact lattice QED: the problem of the zero-momentum modes in the Coulomb phase and the performance of dynamical fermion algorithms for U(1) gauge theory. Results of our inspection look as follows:

- The influence of the constant or zero-momentum modes on the gauge dependent lattice observables like photon and fermion zero-momentum correlators within the Coulomb phase leads to a disagreement of these observables in comparison with standard lattice perturbation theory.
- These constant modes are responsible for the screening of the critical behaviour of the gauge invariant fermion values in the vicinity of the chiral limit.
- The elimination of these zero-momentum modes from gauge configurations leads to the expected perturbative behaviour of gauge dependent observables within the Coulomb phase.
- The critical behaviour of gauge invariant fermion observables in the Coulomb phase upon removing the zero-momentum modes is restored. The critical hopping parameter $\kappa_c(\beta)$ then coincides with that obtained from gauge dependent observables.
- The two-step multiboson algorithm in the version of I. Montvay was implemented for numerical investigations in the U(1) lattice model with even dynamical Wilson fermion flavours.

- A scheme of an appropriate choice of technical parameters for both the two-step multiboson and the hybrid Monte Carlo algorithms is proposed. Theoretical estimates of the performance of such simulation methods are obtained.

- The two-step multiboson algorithm appears to be a good alternative and is at least competitive with the hybrid Monte Carlo method. This was proven by numerical results and explained by a theoretical analysis.

- Further improvement of the performance of the two-step multiboson algorithm can be achieved by increasing the number of local update sweeps and also by decreasing the orders of first and second polynomials and by compensating the errors with a reweighting step.

Finally, let us give some recommendations to the future investigation of the compact U(1) Wilson fermion model:

- For the study of the Aoki phase without an extra mass term as well as of the phase structure of the model in case of odd N_f fermion flavours, it is recommended to use the two-step multiboson algorithm. Its local update cycles can be improved, the role of the reweighting step should be increased, and an algorithm for the evaluation of the fermion determinant sign must be implemented to U(1) theory. However, in the case of large β values the problem of the determinant sign does not occur.

- The investigation of gauge dependent operators is necessary to determine the constant physics lines, containing more physical information about QED. In order to evaluate correctly the critical parameters $\beta^\star$ and $\kappa^\star$ in the Coulomb phase for the resolution of the 'Landau pole' problem (or problem of triviality of U(1) theory), one can directly eliminate the disturbing zero-momentum modes, or one has to take them properly into account. An alternative to be investigated might be the use of C^*-boundary conditions for the lattice fields in order to get rid of the zero-momentum modes.

Bibliography

[1] J. Bjorken and S. Drell. *Relativistic quantum fields*. McGraw-Hill, New York, 1964.

[2] N. Bogolyubov and D. Shirkov. *Introduction to the theory of quantized fields*. Wiley, New York, 1980.

[3] L. Faddeev and A. Slavnov. *Gauge fields. Introduction to quantum theory*. Benjamin Cummings, USA, 1980.

[4] A. Abrikosov, L. Landau, and L. Khalatnikov. *On the quantum theory of fields*. Nuovo Cim. Suppl. 3, 80 (1956).

[5] L. Landau and I. Pomeranchuk. *On point interactions in quantum electrodynamics*. Dokl. Akad. Nauk 102, 489 (1955).

[6] A. Polyakov. *Gauge fields and strings*. Harwood Academic Publ., 1987.

[7] A. Polyakov. *Compact gauge fields and the infrared catastrophe*. Phys. Lett. B59, 82 (1975).

[8] K. Wilson. *Confinement of quarks*. Phys. Rev. D10, 2445 (1974).

[9] M. Creutz. *Quarks, gluons and lattices*. Cambridge University Press, 1983.

[10] I. Montvay and G. Münster. *Quantum fields on a lattice*. Cambridge University Press, 1994.

[11] V. Miransky. *Dynamics of spontaneous chiral symmetry breaking and continuum limit in quantum electro dynamics*. Nuovo Cim. 90A, 149 (1985).

[12] E. Dagotto, A. Kocic, and J. Kogut. *A new phase of quantum electrodynamics: a nonperturbative fixed point in four-dimensions*. Phys. Rev. Lett. 60, 772 (1988).

[13] M. Göckeler, R. Horsley, E. Laermann, P. Rakow, G. Schierholz, R. Sommer, and U. Wiese. *QED: a lattice investigation of the chiral phase transition and the nature of the continuum limit*. Nucl. Phys. B334, 527 (1990).

[14] M. Göckeler, R. Horsley, P. Rakow, G. Schierholz, and R. Sommer. *Scaling laws, renormalization group flow and the continuum limit in noncompact lattice QED*. Nucl. Phys. B371, 713 (1992).

[15] M. Göckeler, R. Horsley, V. Linke, P. Rakow, G. Schierholz, and H. Stüben. *Seeking the equation of state of noncompact lattice QED*. Nucl. Phys. B487, 313 (1997), `hep-lat/9605035`.

[16] M. Göckeler, R. Horsley, V. Linke, P. Rakow, G. Schierholz, and H. Stüben. *Is there a Landau pole problem in QED?* Phys. Rev. Lett. 80, 4119 (1998), `hep-th/9712244`.

[17] T. DeGrand and D. Toussaint. *Topological excitations and Monte Carlo simulation of Abelian gauge theory*. Phys. Rev. D22, 2478 (1980).

[18] A. Hoferichter, V. Mitrjushkin, M. Müller-Preussker, and T. Neuhaus. *Compact lattice QED with staggered fermions and chiral symmetry breaking*. Phys. Lett. B338, 325 (1994), `hep-lat/9407009`.

[19] K. Symanzik. *Schrödinger representation and Casimir effect in renormalizable quantum field theory*. Nucl. Phys. B190, 1 (1981).

[20] M. Lüscher, R. Narayanan, P. Weisz, and U. Wolff. *The Schrödinger functional: a renormalizable probe for non-Abelian gauge theories*. Nucl. Phys. B384, 168 (1992), `hep-lat/9207009`.

[21] S. Mandelstam. *Vortices and quark confinement in non-Abelian gauge theories*. Phys. Rept. 23, 245 (1976).

[22] G. 't Hooft. *Topology of the gauge condition and new confinement phases in non-Abelian gauge theories*. Nucl. Phys. B190, 455 (1981).

[23] G. 't Hooft. *The topological mechanism for permanent quark confinement in a non-Abelian gauge theory*. Phys. Scripta 25, 133 (1982).

[24] A. Kronfeld, G. Schierholz, and U. Wiese. *Topology and dynamics of the confinement mechanism*. Nucl. Phys. B293, 461 (1987).

[25] T. Suzuki and I. Yotsuyanagi. *A possible evidence for Abelian dominance in quark confinement.* Phys. Rev. D42, 4257 (1990).

[26] T. Suzuki. *Monopoles and confinement.* Nucl. Phys. Proc. Suppl. 30, 176 (1993).

[27] G. Bali, V. Bornyakov, M. Müller-Preussker, and K. Schilling. *Dual superconductor scenario of confinement: a systematic study of Gribov copy effects.* Phys. Rev. D54, 2863 (1996), `hep-lat/9603012`.

[28] G. 't Hooft. *Symmetry breaking through Bell-Jackiw anomalies.* Phys. Rev. Lett. 37, 8 (1976).

[29] S. Aoki. *New phase structure for lattice QCD with Wilson fermions.* Phys. Rev. D30, 2653 (1984).

[30] S. Aoki. *A solution to the U(1) problem on a lattice.* Phys. Rev. Lett. 57, 3136 (1986).

[31] R. Frezzotti, P. Grassi, S. Sint, and P. Weisz. *A local formulation of lattice QCD without unphysical fermion zero modes.* Nucl. Phys. Proc. Suppl. 83, 941 (2000), `hep-lat/9909003`.

[32] P. Peter et. al. *Private commun.*

[33] A. Hoferichter, V. Mitrjushkin, and M. Müller-Preussker. *On the chiral limit in lattice gauge theories with Wilson fermions.* Z. Phys. C74, 541 (1997), `hep-lat/9506006`.

[34] I. Bogolubsky, V. Mitrjushkin, M. Müller-Preussker, P. Peter, and N. Zverev. *Fermionic correlators and zero-momentum modes in quenched lattice QED.* Phys. Lett. B476, 448 (2000), `hep-lat/9912017`.

[35] I. Bogolubsky, V. Mitrjushkin, M. Müller-Preussker, and N. Zverev. *Zero-momentum modes and chiral limit in compact lattice QED.* Nucl. Phys. Proc. Suppl. 94, 661 (2001), `hep-lat/0011024`.

[36] I. Montvay. *An algorithm for gluinos on the lattice.* Nucl. Phys. B466, 259 (1996), `hep-lat/9510042`.

[37] I. Montvay. *Quadratically optimized polynomials for fermion simulations*. Comput. Phys. Commun. 109, 144 (1998), `hep-lat/9707005`.

[38] R. Kirchner, S. Luckmann, I. Montvay, K. Spanderen, and J. Westphalen. *Numerical simulation of dynamical gluinos: experience with a multi-bosonic algorithm and first results*. Nucl. Phys. Proc. Suppl. 73, 828 (1999), `hep-lat/9808024`.

[39] S. Duane, A. Kennedy, B. Pendleton, and D. Roweth. *Hybrid Monte Carlo*. Phys. Lett. B195, 216 (1987).

[40] S. Gottlieb, W. Liu, D. Toussaint, R. Renken, and R. Sugar. *Hybrid molecular dynamics algorithms for the numerical simulation of quantum chromodynamics*. Phys. Rev. D35, 2531 (1987).

[41] I. Bogolubsky, V. Mitrjushkin, I. Montvay, M. Müller-Preussker, and N. Zverev. *Performance studies of the two-step multiboson algorithm in compact lattice QED*. Nucl. Phys. Proc. Suppl. to be published (2001), `DESY-01-149, HU-EP-01-43, hep-lat/0111031`.

[42] S. Adler. *Axial vector vertex in spinor electrodynamics*. Phys. Rev. 177, 2426 (1969).

[43] J. Bell and R. Jackiw. *A PCAC puzzle: $\pi_0 \to \gamma\gamma$ in the σ model*. Nuovo Cim. A60, 47 (1969).

[44] N. Nielsen and M. Ninomiya. *Absence of neutrinos on a lattice. 1. Proof by homotopy theory*. Nucl. Phys. B185, 20 (1981).

[45] N. Nielsen and M. Ninomiya. *Absence of neutrinos on a lattice. 2. Intuitive topological proof*. Nucl. Phys. B193, 173 (1981).

[46] L. Karsten and J. Smit. *Lattice fermions: species doubling, chiral invariance, and the triangle anomaly*. Nucl. Phys. B183, 103 (1981).

[47] J. Kogut and L. Susskind. *Hamiltonian formulation of Wilson's lattice gauge theories*. Phys. Rev. D11, 395 (1975).

[48] K. Symanzik. *Continuum limit and improved action in lattice theories. 2. O(N) nonlinear σ model in perturbation theory*. Nucl. Phys. B226, 205 (1983).

[49] B. Sheikholeslami and R. Wohlert. *Improved continuum limit lattice action for QCD with Wilson fermions*. Nucl. Phys. B259, 572 (1985).

[50] D. Kaplan. *A method for simulating chiral fermions on the lattice*. Phys. Lett. B288, 342 (1992), `hep-lat/9206013`.

[51] R. Narayanan and H. Neuberger. *A construction of lattice chiral gauge theories*. Nucl. Phys. B443, 305 (1995), `hep-th/9411108`.

[52] H. Neuberger. *Exactly massless quarks on the lattice*. Phys. Lett. B417, 141 (1998), `hep-lat/9707022`.

[53] P. Ginsparg and K. Wilson. *A remnant of chiral symmetry on the lattice*. Phys. Rev. D25, 2649 (1982).

[54] U. Wiese. *Fixed point actions for Wilson fermions*. Phys. Lett. B315, 417 (1993), `hep-lat/9306003`.

[55] H. Neuberger. *More about exactly massless quarks on the lattice*. Phys. Lett. B427, 353 (1998), `hep-lat/9801031`.

[56] W. Bietenholz and I. Hip. *The scaling of exact and approximate Ginsparg-Wilson fermions*. Nucl. Phys. B570, 423 (2000), `hep-lat/9902019`.

[57] W. Bietenholz. *Approximate Ginsparg-Wilson fermions for QCD*. (2000), `hep-lat/0007017`.

[58] W. Bietenholz, N. Eicker, I. Hip, and K. Schilling. *Constructing improved overlap fermions in QCD*. Nucl. Phys. Proc. Suppl. 94, 603 (2001), `hep-lat/0011012`.

[59] E. Marinari, G. Parisi, and C. Rebbi. *Monte Carlo simulation of the massive Schwinger model*. Nucl. Phys. B190, 734 (1981).

[60] D. Petcher and D. Weingarten. *Monte Carlo integration for lattice gauge theories with fermions*. Phys. Lett. B99, 333 (1981).

[61] D. Weingarten. *Masses and decay constants in lattice QCD*. Nucl. Phys. B215, 1 (1983).

[62] M. Lüscher. *Construction of a selfadjoint, strictly positive transfer matrix for Euclidean lattice gauge theories*. Commun. Math. Phys. 54, 283 (1977).

[63] N. Kawamoto. *Towards the phase structure of Euclidean lattice gauge theories with fermions*. Nucl. Phys. B190, 617 (1981).

[64] M. Bochicchio, L. Maiani, G. Martinelli, G. Rossi, and M. Testa. *Chiral symmetry on the lattice with Wilson fermions*. Nucl. Phys. B262, 331 (1985).

[65] L. Maiani, G. Martinelli, G. Rossi, and M. Testa. *The octet nonleptonic Hamiltonian and current algebra on the lattice with Wilson fermions*. Nucl. Phys. B289, 505 (1987).

[66] T. Banks, J. Kogut, and R. Myerson. *Phase transitions in Abelian lattice gauge theories*. Nucl. Phys. B129, 493 (1977).

[67] J. Kogut, D. Sinclair, and L. Susskind. *A quantitative approach to low-energy quantum chromodynamics*. Nucl. Phys. B114, 199 (1976).

[68] B. Berg and C. Panagiotakopoulos. *The photon in U(1) lattice gauge theory*. Phys. Rev. Lett. 52, 94 (1984).

[69] K. Bitar, A. Kennedy, and P. Rossi. *The chiral limit and phase structure of QCD with Wilson fermions*. Phys. Lett. B234, 333 (1990).

[70] A. Hoferichter, V. Mitrjushkin, M. Müller-Preussker, T. Neuhaus, and H. Stüben. *Compact lattice QED with Wilson fermions*. Nucl. Phys. B434, 358 (1995), `hep-lat/9408014`.

[71] J. Jersak, T. Neuhaus, and P. Zerwas. *U(1) lattice gauge theory near the phase transition*. Phys. Lett. B133, 103 (1983).

[72] R. Cordery, R. Gupta, and M. Novotny. *The nature of the transition in d=4 U(1) lattice gauge theory*. Phys. Lett. B172, 86 (1986).

[73] E. Dagotto and J. Kogut. *First order phase transition in compact lattice QED with light fermions*. Phys. Rev. Lett. 59, 617 (1987).

[74] J. Jersak, C. Lang, and T. Neuhaus. *Non-Gaussian fixed point in four-dimensional pure compact U(1) gauge theory on the lattice*. Phys. Rev. Lett. 77, 1933 (1996), `hep-lat/9606010`.

[75] J. Cox, W. Franzki, J. Jersak, C. Lang, T. Neuhaus, and P. Stephenson. *Properties of the non-Gaussian fixed point in 4D compact U(1) lattice gauge theory*. Nucl. Phys. Proc. Suppl. 53, 696 (1997), `hep-lat/9608106`.

[76] W. Franzki and J. Jersak. *Strongly coupled U(1) lattice gauge theory as a microscopic model of Yukawa theory*. Phys. Rev. D58, 034509 (1998), `hep-lat/9711038`.

[77] A. Hoferichter, V. Mitrjushkin, M. Müller-Preussker, and H. Stüben. *Dynamical Wilson fermions and the problem of the chiral limit in compact lattice QED*. Phys. Rev. D58, 114505 (1998), `hep-lat/9608053`.

[78] A. Hoferichter, V. Mitrjushkin, and M. Müller-Preussker. *Pseudoscalar correlators and the problem of the chiral limit in the compact lattice QED with Wilson fermions*. Nucl. Phys. Proc. Suppl. 42, 669 (1995), `hep-lat/9412005`.

[79] L. Faddeev and V. Popov. *Feynman diagrams for the Yang-Mills field*. Phys. Lett. B25, 29 (1967).

[80] J. Mandula and M. Ogilvie. *The gluon is massive: a lattice calculation of the gluon propagator in the Landau gauge*. Phys. Lett. B185, 127 (1987).

[81] A. Nakamura and R. Sinclair. *Fermion propagators in U(1) lattice gauge theory*. Phys. Lett. B243, 396 (1990).

[82] J. Mandula and M. Ogilvie. *Efficient gauge fixing via overrelaxation*. Phys. Lett. B248, 156 (1990).

[83] V. Bornyakov, V. Mitrjushkin, M. Müller-Preussker, and F. Pahl. *Dirac sheets and gauge fixing in U(1) lattice gauge theory*. Phys. Lett. B317, 596 (1993), `hep-lat/9307010`.

[84] S. Adler. *An overrelaxation method for the Monte Carlo evaluation of the partition function for multiquadratic actions*. Phys. Rev. D23, 2901 (1981).

[85] J. Vink and U. Wiese. *Gauge fixing on the lattice without ambiguity*. Phys. Lett. B289, 122 (1992), `hep-lat/9206006`.

[86] V. Gribov. *Quantization of non-Abelian gauge theories*. Nucl. Phys. B139, 1 (1978).

[87] T. Killingback. *The Gribov ambiguity in gauge theories on the 4 torus*. Phys. Lett. B138, 87 (1984).

[88] A. Nakamura and M. Plewnia. *Gauge fixing ambiguity and photon propagators in compact U(1) lattice gauge theory*. Phys. Lett. B255, 274 (1991).

[89] P. de Forcrand and J. Hetrick. *The continuum limit of the lattice Gribov problem, and a solution based on Hodge decomposition*. Nucl. Phys. Proc. Suppl. 42, 861 (1995), `hep-lat/9412044`.

[90] I. Bogolubsky, V. Mitrjushkin, M. Müller-Preussker, and P. Peter. *Lorentz gauge and Gribov ambiguity in the compact lattice U(1) theory*. Phys. Lett. B458, 102 (1999), `hep-lat/9904001`.

[91] I. Bogolubsky, L. Del Debbio, and V. Mitrjushkin. *Gribov copies and gauge variant correlators in U(1) lattice gauge theory*. Phys. Lett. B463, 109 (1999), `hep-lat/9903015`.

[92] V. Mitrjushkin. *Classical solutions in lattice gauge theories*. Phys. Lett. B389, 713 (1996), `hep-lat/9607069`.

[93] V. Mitrjushkin. *Gauge fixing, zero-momentum modes and the calculation of masses on a lattice*. Phys. Lett. B390, 293 (1997), `hep-lat/9606014`.

[94] W. Kerler, C. Rebbi, and A. Weber. *Monopole currents and Dirac sheets in U(1) lattice gauge theory*. Phys. Lett. B348, 565 (1995), `hep-lat/9501023`.

[95] D. Zwanziger. *Vanishing of zero momentum lattice gluon propagator and color confinement*. Nucl. Phys. B364, 127 (1991).

[96] D. Zwanziger. *Critical limit of lattice gauge theory*. Nucl. Phys. B378, 525 (1992).

[97] C. Baillie and D. Carpenter. *Free fermion propagators and lattice finite size effects*. Nucl. Phys. B260, 103 (1985).

[98] A. Hoferichter. *Private commun.*

[99] U. Wiese. *C periodic and G periodic QCD at finite temperature*. Nucl. Phys. B375, 45 (1992).

[100] N. Metropolis, A. Rosenbluth, M. Rosenbluth, A. Teller, and E. Teller. *Equation of state calculations by fast computing machines*. J. Chem. Phys. 21, 1087 (1953).

[101] M. Creutz. *Monte Carlo study of quantized SU(2) gauge theory*. Phys. Rev. D21, 2308 (1980).

[102] A. Hoferichter. Master's thesis, Institut für Physik, Humboldt-Universität zu Berlin, 1996.

[103] G. Batrouni, G. Katz, A. Kronfeld, G. Lepage, B. Svetitsky, and K. Wilson. *Langevin simulations of lattice field theories*. Phys. Rev. D32, 2736 (1985).

[104] S. Güsken. *A study of smearing techniques for hadron correlation functions*. Nucl. Phys. Proc. Suppl. 17, 361 (1990).

[105] J. Wilkinson. *The algebraic eigenvalue problem*. Clarendon Press, Oxford, 1988.

[106] J. Cullum and R. Willoughby. *Lanczos algorithm for large symmetric eigenvalue computations*. Birkhauser, 1985.

[107] B. Bunk. *Computing the lowest eigenvalues of the fermion matrix by subspace iterations*. Nucl. Phys. Proc. Suppl. 53, 987 (1997), `hep-lat/9608109`.

[108] D. Sorensen. SIAM J. Matrix Anal. Appl. 13, 357 (1992).

[109] T. Kalkreuter and H. Simma. *An accelerated conjugate gradient algorithm to compute low lying eigenvalues: a study for the Dirac operator in SU(2) lattice QCD*. Comput. Phys. Commun. 93, 33 (1996), `hep-lat/9507023`.

[110] T. DeGrand. *A conditioning technique for matrix inversion for Wilson fermions*. Comput. Phys. Commun. 52, 161 (1988).

[111] T. DeGrand and P. Rossi. *Conditioning techniques for dynamical fermions*. Comput. Phys. Commun. 60, 211 (1990).

[112] D. Callaway and A. Rahman. *The microcanonical ensemble: a new formulation of lattice gauge theory*. Phys. Rev. Lett. 49, 613 (1982).

[113] J. Polonyi and H. Wyld. *Microcanonical simulation of fermionic systems.* Phys. Rev. Lett. 51, 2257 (1983).

[114] R. Gupta, G. Kilcup, and S. Sharpe. *Tuning the hybrid Monte Carlo algorithm.* Phys. Rev. D38, 1278 (1988).

[115] C. Baillie, R. Gupta, G. Guralnik, G. Kilcup, A. Patel, and S. Sharpe. *QCD with dynamical Wilson fermions.* Phys. Rev. D40, 2072 (1989).

[116] M. Creutz. *Global Monte Carlo algorithms for many fermion systems.* Phys. Rev. D38, 1228 (1988).

[117] R. Edwards, I. Horvath, and A. Kennedy. *Instabilities and non-reversibility of molecular dynamics trajectories.* Nucl. Phys. B484, 375 (1997), `hep-lat/9606004`.

[118] S. Booth, A. Irving, B. Joo, A. Kennedy, B. Pendleton, S. Pickles, and J. Sexton. *Instability in the molecular dynamics step of hybrid Monte Carlo in dynamical fermion lattice QCD simulations.* Phys. Rev. D62, 114501 (2000), `hep-lat/0005023`.

[119] A. Borici. *A Lanczos approach to the inverse square root of a large and sparse matrix.* J. Comput. Phys. 162, 123 (2000), `hep-lat/9910045`.

[120] T. Lippert. *One-flavor hybrid Monte Carlo with Wilson fermions.* Lect. Notes Comput. Sci. 15, 166 (2000), `hep-lat/0007029`.

[121] M. Lüscher. *A new approach to the problem of dynamical quarks in numerical simulations of lattice QCD.* Nucl. Phys. B418, 637 (1994), `hep-lat/9311007`.

[122] B. Bunk, K. Jansen, B. Jegerlehner, M. Lüscher, H. Simma, and R. Sommer. *A new simulation algorithm for lattice QCD with dynamical quarks.* Nucl. Phys. Proc. Suppl. 42, 49 (1995), `hep-lat/9411016`.

[123] B. Jegerlehner. *Improvements of Lüscher's local bosonic fermion algorithm.* Nucl. Phys. B465, 487 (1996), `hep-lat/9512001`.

[124] C. Alexandrou, A. Borrelli, P. de Forcrand, A. Galli, and F. Jegerlehner. *Full QCD with the Lüscher local bosonic action.* Nucl. Phys. B456, 296 (1995), `hep-lat/9506001`.

[125] M. Peardon. *Dynamical fermion simulations using Lüscher's local bosonic action algorithm*. Nucl. Phys. Proc. Suppl. 42, 891 (1995), `hep-lat/9412008`.

[126] K. Jansen. *Recent developments in fermion simulation algorithms*. Nucl. Phys. Proc. Suppl. 53, 127 (1997), `hep-lat/9607051`.

[127] A. Borrelli, P. de Forcrand, and A. Galli. *Non-Hermitian exact local bosonic algorithm for dynamical quarks*. Nucl. Phys. B477, 809 (1996), `hep-lat/9602016`.

[128] P. de Forcrand and A. Galli. *Exact local bosonic algorithm for dynamical quarks*. Nucl. Phys. Proc. Suppl. 53, 956 (1997), `hep-lat/9609013`.

[129] A. Borici and P. de Forcrand. *Systematic errors of Lüscher's fermion method and its extensions*. Nucl. Phys. B454, 645 (1995), `hep-lat/9505021`.

[130] R. Frezzotti and K. Jansen. *A polynomial hybrid Monte Carlo algorithm*. Phys. Lett. B402, 328 (1997), `hep-lat/9702016`.

[131] A. Sokal. *Monte Carlo methods in statistical mechanics*. Lectures at the Cargese Summer School, 1996.

[132] F. Knechtli. *The static potential in the SU(2) Higgs model*. PhD thesis, 1999. hep-lat/9910044.

[133] R. Frezzotti, M. Hasenbusch, J. Heitger, K. Jansen, and U. Wolff. *Comparative benchmarks of full QCD algorithms*. Comput. Phys. Commun. 136, 1 (2001), `hep-lat/0009027`.

[134] B. Efron. SIAM review 24, 460 (1979).

[135] S. Hands, I. Montvay, S. Morrison, M. Oevers, L. Scorzato, and J. Skullerud. *Numerical study of dense adjoint matter in two color QCD*. Eur. Phys. J. C17, 285 (2000), `hep-lat/0006018`.

[136] A. Kennedy and B. Pendleton. *Cost of the generalised hybrid Monte Carlo algorithm for free field theory*. Nucl. Phys. B607, 456 (2001), `hep-lat/0008020`.

[137] A. Borici. *Theoretical analysis of multi-boson algorithm with local and global update of bosonic fields*. (1996), `hep-lat/9602018`.

[138] P. Hernandez, K. Jansen, and L. Lellouch. *A numerical treatment of Neuberger's lattice Dirac operator*. (2000), `hep-lat/0001008`.

[139] S. Chandrasekharan, J. Cox, K. Holland, and U. Wiese. *Meron-cluster simulation of a chiral phase transition with staggered fermions*. Nucl. Phys. B576, 481 (2000), `hep-lat/9906021`.

Acknowledgements

First of all, I would like to express my special gratitude to my scientific supervisor and head of the research group 'Theory of Elementary Particles/Phenomenology' at Humboldt-University Berlin (HU), Prof. Michael Müller-Preussker for the constant advice and attention, great help in my scientific endeavor, active support, and very kind and friendly relations.

I am very greatful to the Graduate College at Humboldt-University GK-271 'The Standard Model of Particle Physics – Structure, Precision Tests and Extensions' especially to speaker Prof. Dieter Lüst and secretary Mrs. Susanne Preisser for the kind hospitality and aid in solving all administrative problems.

I express the best acknowledgements to our collaborators from JINR, Dubna (Russia), namely to Dr. Valentin Mitrjushkin whose ideas appeared to be very useful and to Dr. Igor Bogolubsky, and also to Prof. Istvan Montvay (DESY, Hamburg) whose algorithm is widely used in our investigations and whose consultations were very fruitful.

I am heavily indebted to Dr. Andreas Hoferichter (NIC computer laboratory, DESY Zeuthen), Pierre Peter (Humboldt-University, Berlin) and Dr. Hinnerk Stüben (Konrad-Zuse Center of Information Technology, Berlin) for helpful consultations on the simulation methods and algorithms.

My colleagues of the research group especially Mr. Andrea Barresi and Mr. Frank Hofheinz, who encouraged my scientific activity and aided me in my daily life, deserve great acknowledgements.

I am also grateful to the group 'QCD-SF' at DESY, Zeuthen, especially Prof. Gerrit Schierholz (head) and Dr. Roger Horsley, also to Prof. Werner Kerler and Dr. Wolfgang Bietenholz at HU, Berlin, and to the 'Computational Physics' group at HU, especially Prof. Ullrich Wolff (head), for important advices on theoretical and numerical methods in quantum field theory.

I express acknowledgements to system administrators at the Intitute of Physics,

HU, Dr. Olf Epler and Dr. Burkhard Bunk, for help in using computer facilities and the possibility to match all necessary numerical calculations, and also to the Konrad-Zuse Center for Information Technology, Berlin, which provided the necessary computer time on the supercomputer VPP-300 at the RZNN Computer Center at Hannover University.

This work was supported by the German Research Society (DFG) with the GK-271 funds.

Selbständigkeitserklärung

Hiermit erkläre ich, die vorliegende Arbeit selbständig ohne fremde Hilfe verfaßt zu haben und nur die angegebene Quellen und Hilfsmittel verwendet zu haben.

Berlin, 30. September 2001
Nikolai Zverev

Lebenslauf

Angaben zur Person

Name:	Nikolai Zverev
Geburtsdatum:	14. Dezember 1971
Geburtsort:	Moskau
Staatsangehörigkeit:	Rußland
Familienstand:	ledig
Dienstanschrift:	Institut für Physik, Humboldt-Universität zu Berlin, Invalidenstr., 110, Berlin D-10115 Tel. (+0049-030) 2093-7974 e-mail: zverev@physik.hu-berlin.de
Privatanschrift:	Ketscherskaja ul., 6/1-192, Moskau 111402, Rußland Tel. (+007-095) 375-82-11

Ausbildung

Sep. 1986 – Mai 1989: Studium an der Physikalischen und Mathematischen Schule Nr. 57, Moskau, Rußland.

Sep. 1989 – Jan. 1995: Studium an der Physikalischen Fakultät der Moskauer Staatlichen Lomonossow-Universität.

Jan. 1995: Diplom der Physik am Lehrstuhl für Theoretische Physik, Physikalische Fakultät, Lomonossow-Universität, Moskau.
Titel der Diplomarbeit:

Berechnung abelschen Anomalie im chiralen
SO(10) Modell auf dem Gitter

Betreuer: Prof. Dr. A.A. Slavnov.

Apr. 1995 – Apr. 1998: Aspirant am Lehrstuhl für Theoretische Physik, Physikalische Fakultät, Lomonossow-Universität, Moskau.

Feb. 1996 – Dez. 1996: Tätigkeit als Übungsassistent im Fach Theoretische Physik an der Mechanischen und Mathematischen Fakultät, Lomonossow-Universität, Moskau.

Jun. 1998: Verleihung des Grades Kandidat der Physikalischen und Mathematischen Wissenschaften.
Titel der Abschlußarbeit: *Chirale Fermionen auf dem Gitter*
Betreuer: Prof. Dr. A.A. Slavnov.

Sep. 1998 – Sep. 2001: Promotionsstudium an der Humboldt-Universität zu Berlin. Mitglied des Graduiertenkollegs GK-271 'Strukturuntersuchungen, Präzisionstests und Erweiterungen des Standardmodells der Elementarteilchenphysik'.
Titel der Dissertation:

Algorithmische Untersuchungen der Kompakten
Gitter QED mit Wilson Fermionen

Betreuer: Prof. Dr. M. Müller-Preussker.

Publikationsliste

Zum Dissertationsthema

1. I. Bogolubsky, V. Mitrjushkin, M. Müller-Preussker, P. Peter and N. Zverev, *Lorentz gauge fixing and the Gribov problem: the fermion correlator in lattice compact QED with Wilson fermions*, Nucl. Phys. (Proc. Suppl.) **B83** (2000) 962–964.

2. I. Bogolubsky, V. Mitrjushkin, M. Müller-Preussker, P. Peter and N. Zverev, *Fermionic correlators and zero-momentum modes in quenched lattice QED*, Phys. Lett. **B476** (2000) 448–454.

3. I. Bogolubsky, V. Mitrjushkin, M. Müller-Preussker, P. Peter and N. Zverev, *Lorentz gauge fixing and lattice QED*, hep-lat/0004001, Talk at NATO Advanced Research Workshop 'Lattice Fermions and Structure of the Vacuum', Dubna, Russia, October 5–9, 1999; Kluwer Academic Publishers, Netherlands, 2000, 257–267.

4. I. Bogolubsky, V. Mitrjushkin, M. Müller-Preussker and N. Zverev, *Zero-momentum modes and chiral limit in compact lattice QED*, Nucl. Phys. (Proc. Suppl.) **B94** (2001) 661–664.

5. I. Bogolubsky, V. Mitrjushkin, I. Montvay, M. Müller-Preussker and N. Zverev, *Performance studies of the two-step multiboson algorithm in compact lattice QED*, Talk at Lattice 2001, Berlin, To be published in Nucl. Phys. (Proc. Suppl.).

Sonstige Publikationen

1. A.A. Slavnov and N. Zverev, *Calculation of abelian anomaly in lattice chiral SO(10) model*, Theor. Math. Phys. **103** (1995) 496–501.

2. A.A. Slavnov and N. Zverev, *A partial resummation of diagrams in the two dimensional lattice fermion model with the Pauli – Villars regularization*, Theor. Math. Phys. **106** (1996) 328–332.

3. A.A. Slavnov and N. Zverev, *Fermion theories on a 2d torus with Wilson action improved by Pauli – Villars regularization*, Phys. Lett. **B420** (1998) 323–332.

4. A.A. Slavnov and N. Zverev, *Nonlocal lattice fermion models on the 2d torus*, Theor. Math. Phys. **115** (1998) 448–457.

5. N. Zverev, *Overview of the chiral fermions on 2d torus*, Talk at NATO Advanced Research Workshop 'Lattice Fermions and Structure of the Vacuum', Dubna, Russia, October 5–9, 1999; Kluwer Academic Publishers, Netherlands, 2000, 163–172.